RUNX2-GENETICALLY ENGINEERED DERMAL FIBROBLASTS FOR ORTHOPAEDIC TISSUE REPAIR

A Dissertation
Presented to
The Academic Faculty

by

Jennifer Elizabeth Phillips

In Partial Fulfillment
of the Requirements for the Degree
Doctor of Philosophy in Biomedical Engineering

Georgia Institute of Technology
December 2007

RUNX2-GENETICALLY ENGINEERED DERMAL FIBROBLASTS FOR ORTHOPAEDIC TISSUE REPAIR

Approved by:

Dr. Andrés J. García, Advisor
School of Mechanical Engineering
Georgia Institute of Technology

Dr. Barbara D. Boyan
School of Biomedical Engineering
Georgia Institute of Technology

Dr. Robert E. Guldberg
School of Mechanical Engineering
Georgia Institute of Technology

Dr. Joseph M. Le Doux
School of Biomedical Engineering
Georgia Institute of Technology

Dr. Todd C. McDevitt
School of Biomedical Engineering
Georgia Institute of Technology

Dr. Roberto Pacifici
Division of Endocrinology
Emory University School of Medicine

Date Approved: September 5, 2007

"Courage is the most important of all the virtues, because without courage you cannot practice any other virtue consistently."
--Maya Angelou

For my Father, who teaches me courage…

ACKNOWLEDGEMENTS

"OCKHAM'S RAZOR" over my shoulder with a Spanish-German accent. Thank you, Andrés, for your trust, (sometimes brutal) honesty, and for always believing in me. Working with you for the last five years has been a privilege and I am certain that I will continue to see the benefits of your mentorship for many years to come. Now, I am off, to start my own Mickey Mouse operation!

I would also like to thank my committee members for their guidance and support. Dr. Robert Guldberg has been a veritable co-advisor to me during my time at Georgia Tech. My first experience in academic research was as a rotation student in his lab and he is a co-author on almost all of my papers. Scientifically, he brought a great deal of expertise to the project in the area of *in vivo* testing and characterization of tissue engineered constructs. Beyond science, Bob has been an exceptional example of a person who has achieved the ever-elusive combination of academic excellence and work-life balance. Thank you, Bob, for always allowing me to crash the annual Guldberg Orthopaedic Research Society lab dinner, and for investing in me like one of your own! Dr. Barbara Boyan has brought expertise to the project associated with bone cell biology and hormone signaling. Beyond this knowledge, she has also been a behind-the-scenes mentor to me on many science- and non-science-related topics. Thank you, Dr. Boyan, for taking a specific interest in me and my work and for teaching me the importance of using rigorous scientific wording which doesn't over-promise on experiments that under-deliver. Dr. Joe Le Doux has brought a great deal of expertise to the Runx2 project in the area of gene therapy since its inception ten years ago. He has patiently endured an open, revolving door policy for all of Andrés' students….offering technical expertise, advice, and/or reagents at any time we have run into roadblocks on our projects. Dr. Todd

McDevitt is a relatively new faculty member at Georgia Tech, but in a very short time on my committee has offered fresh ideas and a candid perspective which has improved the quality of the work. Todd brought expertise to the project in the area of biomaterials and signaling gradients and I greatly appreciate the extra time he invested in reading/analyzing my thesis work. Beyond science, watch out for Todd on the golf course….he might just take your money. Dr. Roberto Pacifici is an M.D., Ph.D. and chair of the Endocrinology department at Emory. His background has brought both extensive expertise in hormone signaling and bone biology as well as a clinical perspective to this work. Dr. Pacifici taught me that there is "nothing new under the sun" and stressed the importance of reading the primary literature from orthogonal fields in order to find creative solutions to scientific problems. Overall, each of my committee members provide examples of rewarding careers in biomedical research and tangible proof that I can enjoy the process along the way.

I would also like to acknowledge a subset of faculty members who have indirectly contributed to the completion of this work. In particular, Dr. Robert Nerem and Dr. Don Giddens, who have committed the majority of their professional careers toward the development of the field of Biomedical Engineering as a whole and this specific interdisciplinary program in Atlanta. The extraordinary vision and pioneering leadership of these two men has provided opportunities for countless young scientists to pursue their dreams. I would also like to thank Dr. Stephen DeWeerth and Dr. Ajit Yoganathan for their leadership and extensive efforts toward developing the joint GT/Emory Biomedical Engineering program from scratch into what it is today. In particular, I would like to acknowledge Steve, as well as Dr. Lena Ting, Dr. Bob Lee, Dr. Michelle La Placa, and

Dr. Wendy Newstetter for their role in the program's early curriculum development and for patiently humoring my numerous questions and blazing intensity during the first two years of graduate school. Special thanks also goes out to Dr. Nael McCarty for taking an interest in my career development and for teaching my favorite class at Georgia Tech. Also, I would like to acknowledge Dr. Laura O'Farrell, the veterinary consultant on this project, and Aqua Asberry and Tracey Couse for helpful discussions and histological assistance. Finally, a special *thank you* goes out to Sally Garrish and Beth Bullock Spencer for administrative support and ensuring that I completed all of the logistical details in a timely fashion. I appreciate your patience, kindness, fun conversations, and gentle reminders about deadlines!

I would also like to thank past and present members of the García lab for creating a challenging, fun, and intellectually stimulating work environment. First and foremost, I want to acknowledge our lab manager, Kellie Burns. Kellie runs a tight ship and keeps all of the members of the García lab humble and on their toes. She also brings a great deal of expertise to our lab in the area of animal work and *in vivo* testing—an expertise that has bailed me out of numerous tumultuous situations over the years! Behind her tough exterior, Kellie is a one-of-a-kind friend with a heart of gold (ahem, transformer-decorated cake, ahem!). Who else would be willing to donate her future offspring to science? I daresay I will never again find another fellow scientist who can use rap lyrics to describe experimental results, who understands the neurotic drama of an Italian family, and who knows from first-hand experience just how cold it really *is* in upstate NY. So, Kellie, thank you, for your help, comic relief, and friendship. You are proof that everyone does indeed love an Italian girl.

On the flip side, our former lab manager, Lindsay Bryant, was my first officially "southern" friend. I will forever be indebted to Lindsay for teaching this rough-around-the-edges Northerner how to dress appropriately ("do we *THINK* these two colors go together?") and how to conduct oneself like a lady at a South Carolina plantation. Throughout the course of our friendship, I was introduced to palmetto trees, monograms, country line dancing, and the dreaded "boat shoe". Most importantly, I learned that blue eyeliner is NEVER a good idea and that the secret to insulting people is to deliver the message with a big smile and a sickeningly sweet voice tone ("bless her heart"). Thank you, LinZ, for your refreshing honesty, tremendous loyalty, and the eye-liner intervention which saved my social life. I look forward to many more years of tomfoolery….the black feather boa WILL be mine someday!

Over the years, many former members of the García lab have also grown to be friends whom I respect and admire. Dr. Nathan Gallant has undoubtedly humbled many a giant in his day with his razor sharp wit and remarkable intuition. Thanks, Nate, for your empathetic ear, your no-nonsense honesty, and for being my Peachtree Road Race cross-training sidekick. I am proud to call you my friend! I would also like to thank Dr. Catherine Reyes for our inseparable friendship during my early years of grad school. Catherine opened my eyes to the value of good grammar, sophisticated cuisine, reading (gasp!) fiction, and overpriced accessories. Thank you, Cathy, for commiserating with me while sliding down black diamonds in Lake Tahoe, tolerating my neurotic animal-phobias, and always having a camera ready to capture moments of poor judgment on film. I'd also like to give mad props to Dr. Ben Keselowsky and Dr. Jeff Capadona for keeping me humble during my first year in the García lab with relentless verbal torture.

Thanks Ben, for serving as a fellow rap lyric appreciator ("you got money in da' bank!"), GRC canoeing partner, and for a second shot at friendship. And thank you, Jeff, for enlightening me on the life-changing power of FTIR, a solid poker face, and country music lyrics. I look forward to many more years of Gordon Research conference debauchery with team García!

Importantly, I'd also like to thank my predecessors on the Runx2 project, Dr. Ben Byers and Dr. Charles Gersbach, for the many hours spent training me on gene therapy techniques and the numerous rigorous discussions that have improved the quality of this work. The progress that was made in my own project would not have been possible without the groundwork that was laid by these two outstanding scientists. Also, I'd like to give a shout-out to Amanda Walls and Abigail Wojtowicz, who worked with me during their rotations on the dexamethasone signaling project. Abbey is a co-author on the JCS paper and her experiments played a critical role in the publication of this work. Thank you, Abbey, for being an awesome office-mate…one of these days I will get up enough nerve to go salsa dancing with you. And how could I not thank Amanda for being my partner-n-crime and roommate at the GRC and for laughing at my neurotic tendencies (n=100) through the years. I admire her grit and courage…who else could survive an airplane crash without shedding a single tear or twitching a single facial muscle? Finally, I must give a major shout-out to my gym-buddies, Timothy Petrie and David Dumbauld (a.k.a. sweet-tips and cool-tips, respectively). It was a pleasure collaborating with Tim on the human mesenchymal stem cells project. He is a hard worker and a creative person who is willing to stay up to all hours of the night to get the job done. Dave is also a hard worker and a terrific problem solver and I greatly

appreciate all of the help he offered me on a side project involving molecular cloning. Thanks, T&D, for letting me tag along on your male-bonding golf expeditions. Don't forget to *always* give the lady a choice……and remember, if your game ain't tight, you gotta call it a night! Finally, I would like to wish all of the current members of the García lab, including the international man of mystery (Sean Coyer) and the new wave (Nduka, Ed, Rachel, Brandon, and Asha) the best of luck in finding your path, your purpose, and completing your own dissertation work.

I would be remiss without acknowledging several members of the Guldberg lab who have made my time in graduate school fun and meaningful. Beyond his brilliant business sense, Chris Gemmitti is also the best super-bowl-party-thrower and final-four-bracket-organizer that I know. Without question, some of my favorite grad school memories involve moments when the goose was loose! Most importantly, I will forever be indebted to Chris for offering me his whoppers box on the way to Muir Woods. Thank you, Chris, for pretending to enjoy the 1-inch-thick-brownies I made for your birthday and for making me laugh every day during our 2+ years in The Fort. Much respect also goes out to Blaise Porter, for showing me the ropes in tissue culture, guarding me like a man in basketball, pushing me to run my first Peachtree Road Race, and, ultimately, inspiring me to run the Chicago marathon. Thanks, Blaise, for keeping me in line ("you're so base"), keeping up on the dance floor ("it's all in the down beat"), and, most importantly, for stealing the mashed potatoes AND the foul towel in the same night. For you, I would actually visit our friend Galen in Porkopolis. And yes, I am still waiting on that email reply, G-rob! Finally, I would like to thank Rhima Coleman for showing me the ropes during my rotation in the Guldberg lab and for being a loyal,

(sometimes brutally) honest friend. I look forward to many silly conversations and philosophical debates over Thai food in the future.

I must thank Angela Lin and Dr. Srinidhi Nagaraja for making it fun to come into work everyday. Throughout the many years of helping me with micro-CT image analysis and mechanical testing, they have both also become lifelong friends. Srin, affectionately known as Na-ha-rah, is a naturally gifted teacher with a knack for making people smile and keeping the atmosphere light. In retrospect, I realize that the majority of the time he made people smile *at my expense* with his relentless hazing and politically-incorrect remarks. Perhaps the most important lesson that I learned from Srin is that the emotional damage from my stern Italian glances can be undone with key lime pie or an exceptionally large piece of strawberry shortcake ("Dang, dats a goooood biscuit!"). Thank you, Srin, for five years of laughter, theological musings, impromptu 6am waffle house trips, ORS abstract all-nighters, Indian buffet information sessions, double-book-challenges, hijacked myspace pages, and regrettable conference craziness. Remember, "Hell hath no fury like a woman scorned!". Perhaps I will indeed visit the Russian federation someday.

Angela Shue-ping Lin, what can I say, except that I am so happy we crossed paths in the Lair of Inefficiency! Over the years, I have grown to highly respect "Jeela" for her problem-solving skills, courage, unusual capacity for fairness, and overall world-class-athlete-ness. From Angela, I have learned that any person can be beautiful when they are just being themselves and the importance of never judging a man until you have walked a mile in his shoes. Nevertheless, it certainly has not been easy to endure five years of Jeela flaunting her perfectly straight and shiny hair, while my knappy-Italian-weave

turned "frizzled" at the slightest hint of rain. And, for the record, I never found the whole "tape-a-picture-of-Jenn's-head-in-the-plastic-fish-aquarium" prank to be all that clever. Thank you, Angela, for your friendship, for accepting me for who I am, and for eating my insane culinary concoctions with a smile.   I look forward to the day when we find out after all these years just exactly *why* the white regions really are *so extremely white*. For you, I might actually go to the Georgia aquarium.

I would also like to quickly acknowledge a handful of teachers whose influence during my formative years led me to pursue a career in science. First, I'd like to thank Mrs. Karen O'Connor for sparking my initial interest in math during high school and Mr. Bill Stevens for believing in me when no one else did.   I would also like to acknowledge my undergraduate advisor, Dr. Richard McCluskey, for encouraging me to pursue higher education and opening my eyes to careers in academia. Also, a special thank you goes out to Dr. F. James Boerio at the University of Cincinnati for providing me with a short-term research opportunity which ultimately convinced me to leave industry and go back to graduate school.   Finally, I offer appreciation to my former bosses and colleagues at Procter & Gamble for equipping me with skills (critical thinking, writing, public speaking) that enabled me to succeed in graduate school. Thank you, Tim Fowler, Chris Irwin, Steve Hicks, Paul Tanner, Rich Farris, Paul Cootes (and many others) for graciously letting me off the hook to pursue my dreams.

I would also like to acknowledge some refreshingly non-science friendships that have kept me sane, grounded, and smiling over the years.   First and foremost, I express my heartfelt gratitude to my Atlanta partners-n-crime, Greer Howard, Brooke Forsyth, Rachel Forrester, Courtney Littlefield, and Elizabeth David. These women have become

like family to me during my time here in Atlanta and I will not even attempt to recount the many ways that their friendship has enriched my life. I will say that, without a doubt, the completion of this thesis would feel empty and anticlimactic if I did not have these women walking alongside me and sharing in the journey, the struggles, and the occasional victorious moments. Thank you, Greer, Brooke, Rach, Court, and Lizzie, for your faithful friendship and for making me a better person by your willingness to speak truth into my life. I'd also like to give a long-distance shout-out to my Clarkson friends, Megan Leto, Krista Nielsen, and Erika Parsons, who have stuck by me for over ten years despite being scattered throughout the United States. Together, we have traversed through multiple life-stages, dramatic career changes, and numerous city relocations—it has been an adventure! I look forward to many email laughs and weekend reunions in the future! Finally, I would also like to give mad props to Mumta Patel for being a top-notch marathon-training buddy ("what happens during the Chicago marathon *stays* at the Chicago marathon") and Rekha Nair for being an exceptional grad school roommate and an even better friend.

I must acknowledge the Patierno family, Steve, Kim, Katie, Nicole, Brendon, and Justin, for the numerous ways they have invested into my life over the years. In particular, my uncle, Dr. Steven Patierno, has without a doubt been the most significant influence on my decision to pursue a scientific research career. My initial interest in biology was sparked as a child when he brought me to a cadaver museum at the George Washington University Medical School. He then provided many key opportunities for me to fan the flames of this spark; most notably, tolerating my insatiable questions during a summer undergraduate research project in his lab at GWU. Throughout my time in

grad school, Steve and Kim have been a steady source of guidance, encouragement, and perspective on topics ranging far beyond science. What's more, their children, my cousins, have become fabulous friends and bona-fide sisters/brothers over the years. Thank you, Patierno family, for opening up your home to me as though I were your very own and for filling my life with love and laughter. Our holiday caravans between D.C. and NY and the over-the-top Italian celebratory feasts are the highlight of my year!

Speaking of Italian feasts, I must take a moment to offer much love, respect, and admiration to my NY grandparents, Arlene and Dominick Patierno. Their little green house on Cardiff road has served as a safe-haven for our family throughout their 55+ years of marriage. Thank you, Gram, for showing me that there is no disappointment or broken heart that cannot be healed with a good bowl of escarole soup or a 15-layer piece of lasagna! You sure do know a "Fachagalupe" when you see one! Thank you, Gramp, for infusing our holidays with rich Italian traditions…who knew there were *so many* different ways to prepare fish!?! Words cannot express how much I appreciate the way you have tirelessly and selflessly supported me and my crazy ideas/projects over the years. I am proud of my Italian-heritage, but even "prouder" to be your granddaughter!

I would also like to extend much love and appreciation to my Grandmother Phillips, for serving as a role model of hard work and perseverance during my childhood summers on her farm in Virginia. Although I did not realize it at the time, she taught me the secret to completing a Ph.D. when I was only five-years-old…

"When a task is once begun
Never leave it till it's done.
Be the labor great or small,
Do it well, or not at all."

Thank you, grandmother, for fostering my work ethic, curiosity, and creativity; and for your late-night prayers which have undoubtedly bailed me out of many a sticky situation!

Finally, I would like to express my eternal gratitude to my parents, Charles and Linda Phillips. I cannot fathom the amount of patience that was required to turn this strong-willed, type-A, first-born child into someone who would not become a terror and menace to society! I think they both had a panic attack five years ago when I casually mentioned that I wanted to quit my industry job and forgo any semblance of financial savings/security in order to come back to graduate school. But, within the hour, they called me back and told me that they would support any risk I needed to take to pursue my dreams. I tell this story because it exemplifies the type of people they are…and the selfless way they seem to always put not only me, but just about everyone that they come into contact with, ahead of themselves. From a very young age, they prioritized the importance of finding my purpose in life, they taught me the secret to finding that purpose, and then served as role models for the character traits necessary to pursue that purpose with all of my heart, mind, and strength. Thank you, Mom and Dad, for the numerous intangible ways that you have contributed to the completion of this work. I look forward to our future trips to Central America!

Upon completion of this dissertation, I now realize that the most valuable lesson I learned in graduate school is the importance of developing and maintaining a curious, teachable mind. I entered Georgia Tech as an ambitious and overly confident student with the naïvely utopian goal of curing a fatal disease with my graduate work. I leave Georgia Tech humbled, with a greater appreciation for the complexities of life, and a more realistic sense for just how little control we truly have over certain outcomes. It

seems that the more I learn, the more I realize I don't know; and that answering one question oftentimes gives rise to ten more questions, each harder and more complex than the first. Oddly enough, it was by studying the foundational principals of life that I found faith; a faith which is diametrically opposed to man-made religion/ritual/rules. This faith has infused every aspect of my life with a newfound sense of meaning, purpose, and, most importantly, peace. I intend to test this God-hypothesis, and its co-existence with science, for the rest of my life. There is just *so much more* to learn…

"The important thing is not to stop questioning. Curiosity has its own reason for existing. One cannot help but be in awe when he contemplates the mysteries of eternity, of life, of the marvelous structure of reality. It is enough if one tries merely to comprehend a little of this mystery every day. Never lose a holy curiosity."
--Albert Einstein

"Ask and it will be given to you; seek and you will find; knock and the door will be opened to you. For everyone who asks receives; he who seeks finds; and to him who knocks, the door will be opened." --Matthew 7:7-8

TABLE OF CONTENTS

LIST OF TABLES

LIST OF FIGURES

Page

LIST OF SYMBOLS AND ABBREVIATIONS

ALP	alkaline phosphatase
ANOVA	analysis of variance
bFGF	basic fibroblast growth factor
BMP	bone morphogenetic protein
BSP	bone sialoprotein
Cbfa	core binding factor-alpha
COL	collagen
DEX	dexamethasone
eGFP	enhanced green fluorescent protein
ERK	extracellular signal regulated kinase
EVRV	empty vector retrovirus
FBS	fetal bovine serum
FTIR	Fourier transform infrared
GAPDH	glyceraldehyde-3-phosphate dehydrogenase
GC	glucocorticoid
Glu	glutamic acid
Gly	glycine
H&E	hematoxylin and eosin
IRES	internal ribosomal entry site
LMP	LIM-mineralization protein
LTR	long terminal repeat

MAPK	mitogen-activated protein kinase
Micro-CT	micro-computed tomography
MKP-1	mitogen activated protein kinase phosphatase-1
OCN	osteocalcin
OSX	osterix
PBS	phosphate-buffered saline
PCR	polymerase chain reaction
pERK	phospho-ERK
PLL	poly-L-lysine
PST	proline-serine-threonine
RT	reverse transcription
Runx	runt-related gene
R2RV	Runx2 retrovirus
SEM	standard error of the mean
Ser	serine
TGF-β	transforming growth factor-beta
3-D	three-dimensional
VEGF	vascular endothelial growth factor
WT	wild type
Zeo(r)	zeocin resistance

SUMMARY

Tissue engineering has emerged as a promising alternative to conventional orthopaedic grafting therapies. The general paradigm for this approach, in which phenotype-specific cells and/or bioactive growth factors are integrated into polymeric matrices, has been successfully applied in recent years toward the development of bone, ligament, and cartilage tissues *in vitro* and *in vivo*. Despite these advances, an optimal cell source for skeletal tissue repair and regeneration has not been identified. Furthermore, the lack of robust, functional orthpaedic tissue interfaces, such as the bone-ligament enthesis, severely limits the integration and biological performance of engineered tissue substitutes. This works aims to address these limitations by spatially controlling the commitment of primary dermal fibroblasts toward an osteoblastic (bone cell) lineage within three-dimensional polymeric matrices. The ***overall objective*** of this project was to investigate transcription factor-based gene therapy strategies for the differentiation of fibroblasts into a mineralizing cell source for orthopaedic tissue engineering applications. Our ***central hypothesis*** was that fibroblasts genetically engineered to express Runx2 via conventional and biomaterial-mediated *ex vivo* gene transfer approaches will differentiate into a mineralizing osteoblastic phenotype.

As a first step toward testing this hypothesis, we investigated retroviral gene delivery of the osteogenic transcription factor Runx2 as a mineralization induction strategy in primary dermal fibroblasts. We found that a combination of constitutive Runx2 overexpression and supplementation with the steroid hormone dexamethasone (DEX) synergistically induced osteogenic differentiation, including bone sialoprotein

gene expression, alkaline phosphatase activity, and biological mineral deposition in primary dermal fibroblast monolayer cultures. This unexpected result suggested that Runx2-engineered fibroblasts have the capacity to create mineralized templates for bone repair and may be a potential cell source for bone tissue engineering applications. Furthermore, the complete absence of native osteoblastic phenotype in hormone-only treated cultures suggested that these cells could be utilized as a robust experimental model to study the Runx2-dependent mechanisms of DEX-induced osteogenesis.

Further characterization of Runx2-engineered fibroblasts involved investigation of the cellular and molecular pathway(s) driving the induction of osteogenesis in this non-osteoblastic cellular phenotype. More specifically, we used these cells as a model system to study the effect of DEX on Runx2 serine phosphorylation and the functional role of this phosphorylation state during osteoblastic differentiation. We demonstrated that DEX decreased Runx2 phosphoserine levels, particularly on Serine^{125}, in parallel with the upregulation of MAPK phosphatase-1 (MKP-1). Mutation of Ser^{125} to glutamic acid, mimicking constitutive phosphorylation, inhibited Runx2-induced osteogenic differentiation, which was not rescued by DEX treatment. Conversely, mutation of Serine^{125} to glycine, mimicking constitutive dephosphorylation, markedly increased osteogenic differentiation, which was enhanced by but did not require additional DEX supplementation. The DEX-induced decrease in Runx2 phosphorylation correlated with upregulation of MKP-1 through a glucocorticoid-receptor-dependent mechanism. Furthermore, inhibition of MKP-1 abrogated the effect of DEX on Runx2 phosphoserine levels. Collectively, these results demonstrated that DEX induces osteogenesis, at least in part, by modulating the phosphorylation state of a negative regulatory serine residue

(Ser[125]) on Runx2 via MKP-1. This work identifies a previously unreported mechanism for glucocorticoid-induced osteogenic differentiation and provides insights into the role of Runx2 phosphorylation during skeletal development.

Runx2-expressing fibroblasts were then evaluated within the context of three-dimensional polymeric matrices for their potential as a mineralizing cell source for bone tissue engineering applications. Genetically modified fibroblasts were cultured *in vitro* on three commercially available scaffolds with highly divergent properties, including: fused deposition-modeled polycaprolactone (PCL), gas-foamed polylactide-co-glycolide (PLGA), and fibrous collagen disks. We demonstrated that the mineralization capacity of Runx2-engineered fibroblasts is scaffold-dependent, with collagen foams exhibiting ten-fold higher mineral volume compared to PCL and PLGA scaffolds. Constructs were differentially colonized by genetically modified fibroblasts, but the scaffold-directed changes in DNA content did not correlate with trends in mineral deposition. Sustained expression of Runx2 upregulated osteoblastic gene expression relative to unmodified control cells and the magnitude of this expression was modulated by scaffold properties. Histological analyses revealed that matrix mineralization co-localized with cellular distribution, which was confined to the periphery of fibrous collagen and PLGA sponges and around the circumference of PCL microfilaments. Fourier transform infrared analysis verified that mineral deposits within Runx2-engineered scaffolds displayed the chemical signature characteristic of carbonate-containing, poorly crystalline hydroxyapatite, whereas control constructs did not contain biologically-equivalent mineral. Importantly, Runx2-transduced fibroblasts formed mineralized templates *in vivo* after implantation in a subcutaneous, heterotopic site, whereas minimal mineralization

was evident in control constructs. Immunohistochemical analysis revealed that Runx2-expressing cells co-localized with mineral deposits *in vivo*, suggesting that mineral was primarily produced by transplanted donor cells. Taken together, these results establish Runx2-genetic engineering as a strategy for the conversion of a non-osteogenic cellular phenotype into a mineralizing osteoblastic cell source for bone repair.

Finally, we explored the feasibility of spatially regulating Runx2 expression in fibroblasts to engineer heterogeneous bone-soft tissue interfaces. Toward this end, we first demonstrated that biomaterial-mediated retroviral gene transfer is a feasible strategy for the genetic modification and differentiation of fibroblasts into a mineralizing osteoblastic phenotype. Viral uptake from these constructs was found to be highly dependent on the non-covalent adsorption of retroviral vectors to positively-charged poly-L-lysine prior to cell seeding. This observation was leveraged to create a graded distribution of Runx2 retrovirus within tissue engineered constructs. These 3-D retroviral gradients resulted in spatially regulated genetic modification of fibroblasts and, consequently, zonal organization of osteoblastic and fibroblastic cellular phenotypes in vitro. Moreover, implantation of heterogeneous constructs into a subcutaneous, ectopic site resulted in Runx2-induced spatial patterning of mineral deposition and non-mineralized fibroblastic extracellular matrix in vivo. Notably, discrete mineralized nodules co-localizing with transduced cell colonies were distributed throughout the interior of virus-coated constructs, suggesting that a biomaterial-mediated gene transfer approach may circumvent mass transport issues caused by the localization of a dense mineralized shell around the scaffold periphery. Collectively, these results indicate that heterogeneous bone-ligament-mimetic tissue interfaces can be developed by a simple,

one step seeding of autologous fibroblasts into polymeric scaffolds containing a graded distribution of the Runx2 retroviral vector. The concept of controlling expression of tissue-specific transcription factors to create spatial gradients of differential cell function within 3-D matrices may be applicable to the development of interfacial zones for a large number of tissue engineering applications.

In summary, this research has established transcription factor-based gene therapy strategies for the conversion of a non-osteoblastic cellular phenotype into a mineralizing cell source for orthopaedic tissue engineering applications. This work is significant because it leverages these genetically engineered fibroblasts to simultaneously (1) elucidate previously unreported molecular pathways involved in bone formation and (2) develop mineralized templates for orthopaedic (bone, ligament) tissue repair. This work is innovative because it utilizes novel biomaterial-mediated gene transfer technologies to engineer bone-soft tissue interfacial zones. Overall, these results are significant toward our ultimate goal of regenerating complex, higher order tissue structures which mimic the cellular and microstructural characteristics of native tissue. Cellular therapies based on primary dermal fibroblasts would be particularly beneficial for patients with a compromised ability to recruit progenitors to the sight of injury as result of traumatic injury, radiation treatment, or osteodegenerative disease.

CHAPTER 1

INTRODUCTION

Six million bone fractures are reported each year in the Unites States and roughly 10% of these require some form of orthopaedic graft [1, 2]. As a result, approximately 500,000 grafting procedures are performed annually in victims of non-healing defects caused by age-related bone deterioration, traumatic injury, tumor resection, or osteolytic disease [3]. Conventional skeletal grafting therapies typically involve the implantation of autogenic bone harvested from the patient's iliac crest or allogenic bone from cadaver tissue banks. Although successful in many cases, these grafts remain limited by inadequate osseointegration, donor site morbidity, poor mechanical properties, and/or the risk of disease transmission. More recently, formulations based on recombinant human bone morphogenetic proteins (BMP-2 and BMP-7) have been approved by the FDA for the treatment of severe orthopaedic conditions such as spinal fusion and skeletal nonunion [4-6]. However, the doses of recombinant protein required to accelerate healing in humans are significantly higher than the levels expressed during normal bone repair, likely due to suboptimal delivery vehicles and rapid *in vivo* protein degradation. These supraphysiologic concentrations are cost-prohibitive to widespread clinical usage and may be problematic if the non-selective targeting of neighboring non-osseous tissues leads to ectopic bone formation [7, 8].

Tissue engineering has emerged as a promising alternative to conventional skeletal repair strategies [9-12]. The general paradigm for this approach, in which phenotype-specific cells and/or bioactive growth factors are integrated into polymeric

1

matrices, has been successfully applied in recent years toward the development of skeletal tissues *in vitro* and *in vivo*. Cell-based strategies have shown particular efficacy in bone repair applications, as several groups have demonstrated healing of critical-sized defects by combining marrow-derived mesenchymal stem cells with three-dimensional scaffolds [13-18]. Although results in animal studies are promising, it is still unknown if MSC transplantation will induce an osteogenic response robust enough to heal critical-sized bone defects in humans. Moreover, these autologous osteogenic precursors remain intrinsically limited by their complex and painful cell procurement process and age- and passage-dependent decreases in mineralization capacity [16, 19]. These limitations leave a pressing need for alternative cell source options for bone repair.

Non-osteogenic cells, such as skin fibroblasts, are a particularly attractive cell source alternative because they are easy to harvest from autologous donors and display a high capacity for *in vitro* expansion. Ex vivo gene therapy strategies based on soluble, osteoinductive factors have been developed for the induction of osteogenesis in fibroblastic cell types [20-23]. Notably, dermal fibroblasts genetically engineered to express BMP-2 form significant amounts of bone in both ectopic implantation sites and critical sized calvarial defects [24, 25]. Despite these advances, complex release kinetics and uncontrolled paracrine signaling to neighboring non-osseous tissues may limit the clinical success of this approach [26-28]. The present research is fundamentally different from growth factor-based gene therapy strategies because it focuses on gene delivery of the transcription factor Runx2, a downstream intracellular effector, to primary dermal fibroblasts in order to avoid detrimental effects associated with unregulated protein secretion.

In addition to cell sourcing issues, the regeneration of complex tissue structures with graded interfacial tissue zones remains another significant challenge in current tissue engineering strategies. In particular, the lack of robust, functional interfaces between bone and soft tissues severely limits the integration and biological performance of engineered orthopaedic substitutes. One such complex structure is found at the insertion site between native anterior cruciate ligament (ACL) and bone, where there is a heterogeneous interface consisting of four distinct regions, including: ligament, non-mineralized fibrocartilage, mineralized fibrocartilage, and bone. ACL graft failure is typically localized to this insertion site, suggesting that regeneration of a heterogeneous tissue interface would promote graft osseointegration into the surrounding bone tissue and, consequently, enhance the long-term mechanical function of tissue engineered ACL replacements.

This work aims to address cell sourcing and osseointegration limitations associated with skeletal tissue engineering by spatially controlling the differentiation of fibroblasts into an osteoblastic phenotype within three-dimensional polymeric matrices. The **overall objective** of this project was to investigate transcription-factor based gene therapy strategies for the differentiation of fibroblasts into a mineralizing cell source for orthopaedic tissue engineering applications. Our **central hypothesis** was that fibroblasts genetically engineered to express Runx2 via conventional and biomaterial-mediated *ex vivo* gene transfer approaches will differentiate into a mineralizing osteoblastic phenotype. The overall objective was accomplished by testing our central hypothesis according to the following specific aims:

Aim1: **Elucidate the molecular mechanism(s) by which Runx2-expressing fibroblasts differentiate into a mineralizing osteoblastic phenotype.**

Our *working hypothesis* was that glucocorticoid hormones induce osteoblastic differentiation in fibroblasts by modulating the phosphorylation state of Runx2. We *tested this hypothesis* using Runx2-expressing fibroblasts as a model system. Site-directed mutagenesis was used to mutate a specific serine residue (Ser125) within Runx2 into glycine (mimicking constitutive dephosphosphorylation) or glutamic acid (mimicking constitutive phosphorylation). Primary fibroblasts were transduced with wild type Runx2 (Runx2-WT), Runx2-125Gly, or Runx2-125Glu retroviral vectors and cultured in osteogenic media supplemented with or without the synthetic glucocorticoid hormone dexamethasone. These experimental conditions were used to investigate the effect of dexamethasone on Runx2 serine phosphorylation, the functional role of this phosphorylation state during osteoblastic differentiation, and to identify upstream signaling molecules which modulate the phosphorylation state of Runx2.

Aim2: **Investigate Runx2-genetically engineered dermal fibroblasts as a mineralizing cell source for bone tissue engineering applications.**

Our *working hypothesis* was that primary fibroblasts genetically modified to constitutively express the osteoblastic transcriptional activator Runx2 will create mineralized templates *in vitro* and *in vivo*. We *tested this hypothesis* by integrating Runx2-transduced fibroblasts into three commercially available scaffolds with divergent properties: fused deposition-modeled polycaprolactone (PCL), gas-foamed polylactide-co-glycolide (PLGA), and fibrous collagen disks. Tissue-engineered constructs which

4

displayed the highest degree of osteogenic potential *in vitro* were implanted *in vivo* into an ectopic, subcutaneous site in order to assess the mineralization capacity of these cells in the absence of osteoinductive cues and cell-types typically present in orthotopic defects.

Aim3: Engineer a heterogeneous bone-ligament tissue interface by spatially regulating Runx2 expression in fibroblasts

Our *working hypothesis* was that zonal organization of bone and ligament tissue can be engineered by seeding primary fibroblasts onto three-dimensional scaffolds containing a spatial distribution of the Runx2 retroviral vector. We *tested this hypothesis* by transducing fibroblasts with a novel biomaterial-mediated gene transfer approach in which Runx2 retrovirus was non-covalently adsorbed to polymeric biomaterials. Retroviral gradients were created by partially coating the proximal portion of these scaffolds with poly-L-lysine prior to incubation in retroviral supernatant and cell seeding. The spatial distribution of bone and ligament markers, mineralization, and mechanical properties was characterized after both in vitro culture and in vivo implantation in a subcutaneous, ectopic site.

This work is *significant* because it develops hybrid *ex vivo* gene therapy/tissue engineering strategies to address the cell sourcing and osseointegration issues associated with cell-based orthopaedic therapies. First, it establishes the use of transcription factor-based genetic engineering strategies for the conversion of a non-osteogenic cell-type into a mineralizing cell source for bone tissue engineering applications. Second, it contributes

to the field of orthopaedic biology by elucidating a previously unreported mechanism for glucocorticoid-induced osteogenic differentiation. Third, it validates the feasibility of a biomaterial-mediated retroviral gene transfer approach to create heterogenous bone-soft tissue interfacial zones. The proposed research is ***innovative*** because it utilizes biomaterial-mediated retroviral gene transfer as a novel strategy for spatially-controlled genetic modification and transdifferentiation of fibroblasts within 3-D matrices. Overall, cellular therapies based on primary dermal fibroblasts would be particularly beneficial for patients with a compromised ability to recruit progenitors to the sight of injury as result of traumatic injury, radiation treatment, or osteodegenerative disease.

CHAPTER 2

LITERATURE REVIEW*

Bone Anatomy and Physiology

Bone is a specialized connective tissue which provides mechanical support and protection for the body's internal organs. Beyond this structural role, bone tissue also serves as a major reservoir for calcium and phosphate ions and contains a population of hematopoietic and stromal cell precursors within its marrow cavity. Thus, despite its inert appearance, bone is a metabolically active organ that undergoes continuous remodeling throughout life in order to maintain serum homeostasis and the structural integrity of the skeleton [29]. This remodeling process involves a complex series of highly regulated steps that primarily depend on the interplay of two cell types, the osteoblast and the osteoclast. Osteoblasts promote bone formation by regulating deposition of osteoid and mineral nucleation. Osteoclasts are primarily responsible for bone resorption through the secretion of hydrogen ions and acid proteases. Mature osteoblasts (termed osteocytes) are embedded within the dense extracellular matrix in lacunae and extend microfilament-rich canaliculi processes. These processes contact canaliculi originating from other cells through gap junctions, enabling the propagation of signals to the interior of the highly dense bone matrix.

Bone contains both cortical (compact) and trabecular (spongy) tissue types.

Although these tissues are structurally and functionally different, they contain the same fundamental constituents, including a highly organized extracellular matrix, bone resorbing cells (osteoclasts), and bone forming cells at various stages of maturation (e.g. osteoprogenitors, osteoblasts, osteocytes, and periosteal lining cells). The matrix is comprised of an inorganic, poorly crystalline hydroxyapatite mineral phase and a mixture of collagenous and noncollagenous (e.g. osteocalcin, bone sialoprotein, osteopontin, fibronectin) proteins. Trabecular bone is found within the marrow cavity and throughout the ends of long bones and consists of a latticework of reticulated spicules lined with osteoblasts and osteoclasts. Compact bone is located around the circumference of all bones and comprises the outer tubular shell surrounding the intramedullary marrow cavity in long bones. It consists of parallel cylindrical units (osteons), which contain a Haversian canal surrounded by concentric lamellar rings of osteocytes embedded within the calcified matrix. Blood vessels and nerves run through this canal system to allow for transport of nutrients and waste and to innervate osseous tissue. Finally, eriostemon, a thin layer of connective tissue, covers the outer surface of bone and contains progenitor cells capable of bone formation.

Bone Development

Normal skeletal development originates from two main processes: intramembranous ossification and endochondral ossification[30]. Intramembranous ossification primarily occurs during embryonic development of flat bones such as the calvarium and mandible. In this process, mesenchymal precursors within vascularized embryonic connective tissue differentiate directly into an osteoblastic phenotype.

8

Endochondral ossification is the primary mode of long bone development during embryogenesis, pre-pubescent limb growth, and fracture healing. This process differs from intramembranous bone formation in that it includes a highly complex, intermediate cartilaginous phase prior to mineralized matrix deposition. Briefly, pre-chondrocytes within the growth plate proliferate and differentiate into mature hypertrophic chondrocytes, which secrete matrix and undergo apoptosis. This avascular, cartilaginous matrix is then infiltrated with blood vessels, calcified, and eventually remodeled by osteoblasts and osteoclasts to form lamellar trabecular bone. Details of this complex process and the regulatory factors involved are beyond the scope of the current research and are discussed elsewhere[30, 31].

Bone Regulatory Factors

Recent advances in bone cell biology have identified a central role for numerous signaling molecules during bone development and regeneration. Differentiation of mesenchymal progenitor cells into an osteoblastic phenotype is tightly regulated by a complex spatiotemporal cascade of growth and differentiation factors, hormones, transcription factors, and extracellular matrix proteins. Among these, several soluble and extracellular matrix proteins bind to transmembrane receptors to initiate signaling pathways which converge to activate osteogenic transcription factors. These factors primarily have an intracellular mode of action to coordinate the expression of osteoblastic genes regulating the deposition of a mineralized matrix. A mechanistic understanding of these signaling pathways will enable researchers to more effectively develop strategies for skeletal gene therapy applications.

9

Osteoinductive growth and differentiation factors

Osteoinductive factors are typically embedded within the extracellular matrix and released during remodeling or injury. These proteins bind to specific transmembrane receptors to initiate signaling cascades which induce osteogenesis through autocrine and paracrine signaling. Among these, bone morphogenetic proteins (BMPs) have been identified as potent inducers of osteoblastic differentiation and ectopic and orthotopic bone formation[8, 32, 33]. Complex expression patterns of multiple BMP isoforms have been observed during bone growth, as BMP-2, -4, and -7 are expressed in overlapping patterns during bone development[34, 35] and BMP-2,-3,-4,-7, and -8 are expressed during fracture healing[36]. Furthermore, a comparative study of 14 different human isoforms revealed that BMP-2, -6, and -9 potently induce osteoblastic differentiation in mesenchymal stem cells[37]. The canonical mechanism of BMP signaling involves binding of this factor to a transmembrane receptor to initiate Smad-dependent and -independent signaling pathways that activate a cascade of osteogenic transcription factors, most notably Runx2/Cbfa1 and Osterix[38-41].

Insulin-like growth factors (IGF-I and IGF-II) serve as local regulators of bone matrix and remodeling. These factors enhance collagen synthesis, inhibit collagen degradation, and stimulate proliferation of cells within the osteoblastic lineage[42, 43]. Systemic injection of IGF-I has a net anabolic effect on bone mass and enhances bone healing *in vivo*[44]. However, discrepancies exist in the literature, as some studies report negligible effects of IGF on the skeleton[45].

Transforming growth factor-β (TGF-β) is present in high quantities within bone matrix and has pleiotropic regulatory effects during skeletal development and fracture

10

healing. TGF-β stimulates osteoid formation and osteoblast proliferation, but has been shown to inhibit mineral deposition and osteocalcin gene expression[46, 47]. Indeed, Opperman et al. reported that systemic TGF-β injection induces ectopic mineralization *in vivo* only after growth factor administration is discontinued[48]. Alternatively, i*n vivo* studies in fracture healing animal models have revealed that TGF-β enhances callus formation and mechanical strength compared to untreated fracture controls[49, 50]. Despite these promising results, the use of this factor as an osteoinductive therapeutic agent may be significantly limited because the exceptionally large doses required to enhance bone repair are often toxic to the host[51].

Fibroblast growth factors (aFGF/FGF-1 and bFGF/FGF-2) function mainly as angiogenic agents during limb development, craniofacial bone formation, and the process of fracture healing. Disruption of endogenous FGF signaling via blocking antibodies inhibits osteogenesis[52], while mutations rendering the FGF transmembrane receptor constitutively active lead to enhanced osteoblast activity and premature fusion of craniofacial sutures[53, 54]. Consistent with these results, administration of exogenous FGF enhances migration, proliferation, and differentiation of osteoprogenitors and ultimately accelerates fracture healing in long bones[55-57].

Osteogenic transcription factors

Osteoinductive factors, such as BMPs, bind to the extracellular domain of transmembrane receptors to initiate signaling cascades which converge to activate a program of downstream transcriptional regulators. Many transcription factors are expressed during bone development and fracture healing, including Runx2/Cbfa1, DLX-

11

3, DLX-5, MSX-2, AP-1, Osterix [58]. Among these, Runx2/Cbfa1 and Osterix have been extensively characterized for their role in regulating the commitment of multipotent mesenchymal stem cells into the osteoblastic lineage.

Runx2 is an essential transcriptional regulator of chondrocyte hypertrophy, osteoblast differentiation, and bone formation [59, 60]. Runx2$^{-/-}$ transgenic mice display an entirely cartilaginous skeleton with complete arrest of osteoblast activity and endochondral ossification [61]. Moreover, Runx2 haploinsufficiency causes the pathogenic skeletal phenotype cleidocranial dysplasia in mice and humans, characterized by short stature, hypoplastic clavicles, and dental abnormalities [62, 63]. Runx2 functions as a transcriptional scaffolding protein which associates with additional co-regulatory proteins and binds to the promoter region of skeletal target genes to regulate their expression [64, 65]. We and others have demonstrated that forced expression of Runx2 upregulates osteoblast-specific gene expression and induces mineralization in a cell-type-dependent manner [23, 24, 59, 66, 67]. Intriguingly, both postnatal disruption of Runx2 by dominant negative expression and overexpression of Runx2 from the pro- (I) collagen promoter induces bone fragility and osteopenia in transgenic mice [68, 69]. These studies collectively demonstrate that cellular regulation of Runx2 is critical for normal skeletal development and bone formation.

Osterix (OSX) is a zinc-finger-containing transcription factor that acts downstream of Runx2 to induce the differentiation of osteoprogenitors into mature osteoblasts. Homozygous deletion of Osterix inhibits osteoblast differentiation and activity, while chondrocyte hypertrophy proceeds normally in these transgenic mice[70]. Several reports have suggested that Runx2 directly regulates Osterix, as its expression is

completely absent in Runx2-null mice[70] and Runx2 binding sites have been identified in the Osterix promoter[71]. Regulation of these two osteoblastic transcription factors and their temporal expression with respect to each other is an active area of research. Notably, both Runx2 and Osterix are downstream effectors of BMP-2-activated signaling[72-76].

Biological and Synthetic Bone Grafts

Conventional skeletal grafting therapies typically involve the implantation of autogenic bone harvested from the patient's iliac crest or allogenic bone from cadaver tissue banks. Autograft implantation is considered the gold standard in bone repair, but the widespread clinical success of this procedure has been hindered by variable results associated with the quality of the bone graft, inadequate tissue supply, and donor site morbidity [77]. Allografts offer advantages for off-the-shelf tissue availability, but display reduced biological activity and mechanical properties due to tissue processing and carry the risk of disease transmission [78, 79]. Synthetic materials such as metals, calcium phosphate ceramics, bioactive glasses, and polymers have also been explored for bone grafting applications, but generally display insufficient regenerative potential to warrant the inflammatory host reaction [80]. More recently, osteogenic devices containing recombinant bone morphogenetic protein-2 (BMP-2) or BMP-7 have shown efficacy in human clinical trials and have been approved by regulatory agencies for the treatment of non-healing fractures and spinal fusion [4-6, 8]. Nevertheless, the wide-spread clinical success of this growth-factor based approach continues to be hampered by suboptimal delivery vehicles, short biological half-life, and safety issues associated with aphysiologic dosage [7, 8]. Although several approaches to augment bone formation are presently

13

available, it is clear that their limitations leave a pressing need for alternative bone regeneration strategies.

Gene Therapy Approaches to Bone Grafting

Gene therapy aims to introduce exogenous nucleic acid sequences into cells in order to alter their endogenous protein synthesis or induce the expression of therapeutic proteins. Both *in vivo* and *ex vivo* gene therapy strategies have been investigated for bone regeneration [20, 81]. Table 2.1 lists examples of *in vivo* gene delivery of osteogenic factors for bone repair. *In vivo* strategies involve vector delivery via intravenous injection or direct local implantation to a selected anatomic site. This simple, one-step process would promote high surgeon compliance and may be necessary for disorders requiring immediate treatment, but involves significant challenges associated with low transduction efficiency, inflammatory/immune limitations, and difficulty targeting the cell population of interest. Moreover, this strategy is highly dependent on the presence and responsiveness of host cells and may not be effective in patients with compromised ability to recruit osteoprogenitors to the site of injury as a result of disease, trauma, radiation treatment, or age-related tissue deterioration. *Ex vivo* strategies involve the harvest of a specific population of cells from the patient, followed by genetic modification of these cells under *in vitro* conditions and their subsequent implantation into the site of injury. Tables 2.2 and 2.3 provide examples of *ex vivo* strategies using osteogenic and non-osteogenic cell sources, respectively. *Ex vivo* gene delivery approaches allow for expansion of the target cell population prior to genetic modification and selection for cells expressing the transgene. Furthermore, *ex vivo* gene transfer in a

14

Table 2.1. Selected examples of *in vivo* gene therapy approaches for bone repair

Viral Vector	Target Gene	Target Tissue	Animal Model	Reference
Adenovirus	BMP-2	Intramuscular injection	SCID and immunocompentent mice	Musgrave et al., 1999.
Adeno-associated virus	BMP-4	Intramuscular injection	Immunocompetent rats	Luk et al., 2003
Adeno-associated virus	BMP-2	Intramuscular injection	Immunocompetent rats	Chen et al., 2003.
Adenovirus	BMP-2	Dorsal osseous nasal defect	Athymic nude rats	Lindsey et al., 2001.
Adenovirus	BMP-2 BMP-4 BMP-6	Intramuscular injection	Athymic nude rats	Jane et al, 2002.
Adenovirus	BMP-2	Intramuscular injection	Immunocompetent and athymic nude rats	Alden et al, 1999.
Adenovirus	BMP-4 BMP-9	Intramuscular injection	Different immunocompetent rat strains	Li et al., 2003.
Retrovirus	BMP-2/4	Periosteal injection adjacent to fracture	Critical-sized femoral defect in immunocompetent rats	Rundle et al., 2003.
Adeno-associated virus Adenovirus	BMP-6	Ectopic injection	Immunocompetent and athymic nude rats	Li et al., 2006.
Adenovirus	BMP-2 BMP-6 BMP-7 BMP-9	Intramuscular injection	Athymic mice	Kang et al., 2004.
Adenovirus	BMP-2 TGF-β	Critical-sized femoral segmental defect	New Zealand white rabbits	Baltzer et al., 2000.
Adenovirus	BMP-2	Critical-sized iliac crest defect	White mountain sheep	Egermann et al., 2006.

15

cell-based delivery vehicle may be safer in a clinical setting than direct injection of viral particles *in vivo*. Although cells can be screened for tumorigenicity before implantation into the host, these initial steps are often labor intensive and would involve significant cost and complexity.

Both *in vivo* and *ex vivo* gene therapy strategies have been investigated for bone regeneration [20, 81]. *In vivo* approaches for bone repair have predominantly utilized transient adenoviral vectors to avoid risks associated with retroviral-mediated insertional mutagenesis. Direct injection of adenoviral vectors expressing BMP-2 led to increased bone formation in critical-sized rat mandibular defects [82] and rabbit femoral segmental defects [83]. Importantly, Baltzer et al. reported detection of transgene expression at high levels in muscle tissue surrounding femoral defects for at least 6 weeks, suggesting that muscle-derived osteoprogenitors contributed to bone formation [84]. In a separate study, intramuscular injection of BMP-2-expressing adenovirus induced ectopic bone formation in mice, but a more robust osteogenic response was observed in immunodeficient compared to immunocompetent animals [85]. This observation corroborated reports from several groups that the host immune response induced by first-generation adenoviral vectors is strong enough to attenuate the efficacy of adenovirus-based approaches [86-88]. In an attempt to overcome issues associated with viral immunogenicity, Rundle et al. pursued an *in vivo* strategy based on a retroviral vector encoding a BMP-2/4 fusion protein [89]. Although accelerated fracture healing was observed after retroviral injection in a rat femoral defect at early time points, both treatment and control fractures eventually remodeled to comparable dimensions and mineral levels. Nevertheless, evidence of vector integration into surrounding non-skeletal tissues was not observed,

16

suggesting that retroviral-based *in vivo* gene therapy strategies may be safe for specific local tissue repair applications [89].

Ex vivo approaches based on different cell-types, gene delivery vectors, and target genes have been extensively explored for bone repair applications. One strategy that has shown particular promise is the implantation of bone marrow stromal cells (BMSCs) genetically engineered to overexpress BMP-2 into critical-sized defects [90-96]. Lieberman et al. reported that autologous Ad-BMP-2-expressing BMSCs embedded within a demineralized bone matrix carrier significantly healed segmental femoral defects in syngeneic rats compared to carrier only and Ad-LacZ-expressing BMSC controls [92]. Importantly, these investigators directly compared this *ex vivo* approach to the delivery of a clinical dose of rhBMP-2 protein and showed that genetically engineered cells produce more robust trabecular architecture than recombinant protein injection. In an independent study, Tsuchida et al. investigated the bone healing capacity of allogenic BMSCs infected with a BMP-2 adenoviral vector in a rat femoral segmental defect [97]. BMP-2-expressing allogenic cells in combination with the immunosuppressant FK506 induced fracture repair *in vivo* to levels comparable to BMP-2-expressing autologous cells. Notably, investigation into the cellular origin of bone formation suggested that genetically engineered cells secrete BMP-2 for paracrine signaling and also directly participate in bone formation. In contrast to studies focused on transient adenoviral gene delivery, an *ex vivo* approach based on constitutive retroviral overexpression of BMP-4 in BMSCs was recently investigated by Gysin et al [96]. BMP-4-expressing BMSCs healed critical-sized calvarial defects in rats, while untransduced BMSCs showed limited bone formation. Collectively, these results suggest that *ex vivo* genetic manipulation of

17

mesenchymal stem cells may provide a more robust strategy for bone formation than the direct implantation of these cells alone.

Cell-based Tissue Engineering Approaches to Bone Grafting

Bone tissue engineering has emerged as a promising alternative to conventional grafting strategies.[98-100] The general paradigm for this approach involves the integration of osteogenic cells and/or bioactive growth factors into three-dimensional scaffolds to produce hybrid constructs for skeletal repair.[101] The success of bone tissue engineering to date has been limited in part by inadequate availability of a mineralizing cell source which can be easily obtained in sufficient quantities and maintain osteoblastic phenotype during *in vitro* culture and expansion.

Cell Source

Traditional cell-based approaches typically involve the use of terminally differentiated osteoblasts,[102, 103] osteogenic cell lines, [104, 105] unfractionated bone marrow stroma,[106, 107] or purified mesenchymal stem cells [108-110]. Primary osteoblasts are difficult to isolate in sufficient quantities from calvarial or trabecular bone and display a limited capacity for proliferation. Immortalized osteogenic cell-lines are clonally-derived and well-characterized, but exhibit abnormal regulatory mechanisms that may lead to tumorigenic growth *in vivo*. Because of these limitations, a large number of cell transplantation strategies are based on primary bone marrow stromal cells (BMSCs) [14, 108, 109, 111-113]. These cells contain a subpopulation of osteoprogenitors and mesenchymal stem cells (MSCs) which have shown significant mineralization capacity *in vitro* and *in*

18

Table 2.2. Selected examples of *ex vivo* gene therapy approaches for bone repair in osteogenic cells

Viral Vector	Target Gene	Target Cells	Animal Model	Reference
Adenovirus	BMP-9	Human mesenchymal stem cells	Ectopic intramuscular site in athymic nude rats	Dayoub et al., 2003.
Adenovirus	Runx2	Primary bone marrow stromal cells	Ectopic subcutaneous site in immunocompetent mice	Zhao et al., 2005.
Retrovirus	Runx2	Primary bone marrow stromal cells	Ectopic subcutaneous site and critical-sized calvarial defect in immunocompetent syngeneic rats	Byers et al., 2004. Byers et al., 2006.
Adenovirus Liposomes	BMP-2	Primary bone marrow stromal cells	Critical-sized mandibular defects in immunocompetent rats	Park et al., 2003.
Retrovirus	BMP-7	Primary periosteal cells	Critical-sized cranial effects in New Zealand white rabbits	Breitbart et al., 1999.
Retrovirus	BMP-4	Primary bone marrow stromal cells	Critical-sized calvarial defect in syngeneic rats	Gysin et al., 2002.
Lentivirus	BMP-2	Primary bone marrow stromal cells	Ectopic intramuscular site in SCID mice	Sugiyama et al., 2005.
Adenovirus Retrovirus Liposomes	BMP-2	Primary bone marrow stromal cells	Critical-sized calvarial defects in rats	Blum et al, 2003.
Adenovirus Recombinant protein	BMP-2	Primary bone marrow stromal cells	Critical-sized femoral segmental defect in syngeneic rats	Lieberman et al., 1999
Adenovirus	BMP-2	Bone marrow stromal cell line	Ectopic intramuscular site in SCID mice and critical-sized femoral segmental defect in athymic rats	Lieberman et al., 1998.
Adenovirus	BMP-2	Allogeneic bone marrow-derived mesenchymal stem cells	Critical-sized femoral segmental defect in immunocompetent rats treated with immunosuppresants	Tsuchida et al., 2003.

19

Table 2.3. Selected examples of *ex vivo* gene therapy approaches for bone repair in non-osteogenic cell-types

Viral Vector	Target Gene	Target Cells	Animal Model	Reference
Retrovirus Adenovirus	BMP-2	Muscle-derived stem cells	Critical-sized calvarial defect in SCID mice	Lee et al., 2002.
Adenovirus	LMP-1	Peripheral blood-derived buffy coat cells	Spine fusion in immunocompetent rabbits	Viggeswarapu et al., 2001.
Retrovirus	BMP-4 and VEGF	Muscle-derived stem cells	Ectopic intramuscular site and critical-sized calvarial defect in immunocompetent mice	Peng et al., 2002.
Adenovirus	BMP-4	Muscle-derived stem cells	Critical-sized calvarial defect in immunocompetent rats	Wright et al., 2002.
Adenovirus	BMP-4	Muscle-derived stem cells and primary bone marrow stromal cells	Critical-sized femoral defect in immunocompetent rats	Rose et al., 2003.
Adenovirus	BMP-7	Rat dermal fibroblasts	Ectopic subcutaneous site and critical-sized calvarial defect in immunocompromised mice	Krebsbach et al., 2000.
Adenovirus	BMP-2 and BMP-7 BMP-4 and BMP-7	Murine embryonic fibroblast cell line	Ectopic subcutaneous site in immunocompetent mice	Zhao et al., 2005.
Retrovirus	Runx2	Primary dermal fibroblasts	Ectopic subcutaneous site in immunocompetent syngeneic rats	Phillips et al., 2006.
Retrovirus	Runx2	Skeletal myoblasts	Ectopic intramuscular site in immunocompetent syngeneic mice	Gersbach et al., 2006.
Adenovirus	BMP-2 and Runx2 BMP-2 Runx2	C3H10T1/2 cell line	Ectopic subcutaneous site in immunodeficient mice	Yang et al., 2003.
Adenovirus	BMP-2 Runx2	Primary dermal fibroblasts	Ectopic subcutaneous site and critical-sized calvarial defect in immunocompetent mice	Hirata et al., 2003.
Adenovirus	BMP-2	Human diploid fetal lung cell-line and primary bone marrow stromal cells and primary dermal fibroblasts	Ectopic intramuscular site in SCID mice	Gugala et al., 2003.
Adenovirus	BMP-2	Adipose-derived stem cells	Ectopic intramuscular site in SCID mice	Dragoo et al., 2003.
Adenovirus	BMP-2	Adipose-derived stem cells	Critical-sized femoral defect in athymic rats	Peterson et al., 2005.

20

vivo [13, 14, 17, 18, 114]. Although results in animal studies are promising, it is still unknown if BMSC transplantation will induce an osteogenic response robust enough to heal critical-sized bone defects in humans.

Ex vivo gene therapy strategies, such as the ones discussed above, have further enhanced the bone healing capacity of bone marrow-derived osteogenic cells (see Table 2.2 for representative examples). Yet, the clinical use of these precursors is still hindered by their complex and painful cell procurement process [115], potential for dedifferentiation during *in vitro* expansion, low frequency in healthy marrow [111, 116], and reduced mineralization capacity associated with increased age and disease-state of the donor [16, 19]. These limitations leave a pressing need for alternative cell source options for bone regeneration.

Genetic engineering strategies have been employed for the differentiation of non-osteogenic cells, such as fibroblasts and skeletal myoblasts, into a mineralizing osteoblastic phenotype (see Table 2.3 for selected examples). Rat dermal fibroblasts transduced with adenoviral vectors encoding for either BMP-2 or BMP-7 form significant amounts of bone in both ectopic implantation sites and critical sized defects [21, 24, 25]. Furthermore, Ad-BMP-7-expressing human gingival fibroblasts induced osteogenic differentiation *in vivo* after subcutaneous implantation in immunocompromised animals [25]. Importantly, an assessment of fibroblast fate after implantation revealed that genetically engineered fibroblasts directly differentiate into osteoblast-like cells and secrete osteoinductive factors which stimulate mineral deposition by host cells. In a separate study, skeletal myoblasts engineered to overexpress BMP-2 with a retroviral vector deposited significant amounts of ectopic mineralization after intramuscular

implantation into the hind limbs of immunocompetent syngeneic mice [117]. Finally, an *ex vivo* strategy based on buffy coat cells derived from peripheral blood has successfully induced spinal fusion in animal studies [118]. This particular approach is attractive for therapeutic use because cells are harvested, transected, and re-implanted during the same operation. Overall, non-osteogenic cell sources have promising clinical relevance because they are easily obtained in large quantities by minimally invasive biopsy from autologous donors.

More recently, osteocompetent stem cell populations have been isolated from muscle tissue and human liposuction aspirates [119-123]. Huard and colleagues showed that muscle-derived stem cells (MDSCs) transduced with a BMP-4 retroviral vector induce orthotopic bone formation in rat critical-sized calvarial and femoral defects [124, 125]. Importantly, robust mineral production by these allogenic MDSCs was observed in immunocompetent animal models despite the presence of CD4+ and CD8+ lymphocytes. Moreover, an analysis of cell fate suggested that genetically engineered MDSCs differentiate down the osteogenic lineage to directly contribute to bone repair and secrete osteoinductive factors which promote mineral deposition by host cells. In a separate approach, adipose-derived mesenchymal progenitors transduced with a BMP-2 adenovirus formed bone *in vivo* after implantation into the hind limb of SCID mice [126]. Moreover, these BMP-2-expressing cells also healed critical sized defects in immunodeficient rats, while unmodified liposuction aspirate control cells did not mineralize [127]. Adipose-derived stem cells are particularly advantageous because a large amount of autologous tissue can be harvested from various anatomic locations with minimal donor site morbidity and negligible loss of some critical function to the host.

The optimal cell source for gene therapy-based bone repair strategies has not been determined. A comparative study conducted by Gugala et al. suggested that bone healing efficacy is independent of cell type [128]. In this report, no significant difference in ectopic *in vivo* mineralization capacity was observed between BMSCs, primary dermal fibroblasts, and a human diploid fetal lung cell line transduced with a BMP-2-expressing adenoviral vector. However, these investigators did observe a marked difference in bone formation due to the type of viral delivery vector and the subsequent amount of the osteoinductive factor produced [128]. In contrast, Rose et al. reported that BMP-4-expressing muscle-derived stem cells form significantly more bone in critical-sized femoral defects compared to BMP-4-expressing BMSCs [129]. It is clear from these conflicting results that additional comparative studies will be necessary to determine the relative potency of these osteoblastic and nonosteoblastic cell-types for bone regeneration. Nevertheless, beyond requirements for osteoinductive potency, the ideal cell source for *ex vivo* gene therapy strategies would be easily harvested with minimal donor site morbidity, available in large quantities, and susceptible to genetic manipulation by gene transfer vectors. In general, autologous cells would be preferred in order to minimize potential host immune response. Studies characterizing cell fate after implantation and the cellular origin of bone formation will become increasingly important in the clinical application of these strategies to human bone defects.

Target Genes

As evidenced by the above discussion, gene therapy strategies based on soluble growth factors, such as BMP-2, BMP-4, and BMP-7, have been successfully applied to

augment bone formation in preclinical animal models. Despite promising results, the clinical feasibility of these growth factor-based gene therapy approaches may be hampered by complex release kinetics and unregulated, ectopic bone formation caused by paracrine signaling to neighboring non-osseous tissues. The delivery of downstream transcriptional activators has been extensively explored to address these limitations. In particular, overexpression of genes encoding LIM mineralization protein-1 (LMP-1), Runx2/Cbfa1, and Osterix have been explored in various cell-types for their bone regenerative potential [67, 118, 130, 131, 131, 132].

In contrast to growth factor-based therapies, which have been administered as recombinant proteins or genetic sequences, most attempts to utilize transcription factors with an intracellular mode of action have involved the use of a genetic engineering approach. LMP-1 is an intracellular protein which has been shown to induce secretion of soluble factors such as BMP-2, BMP-4, BMP-6, and BMP-7 [133]. Adenoviral overexpression of LMP-1 in buffy coat cells successfully induced spinal fusion in rodents and rabbits [118, 134]. In a different approach, we and others have demonstrated that Runx2 overexpression directs the differentiation of a wide range of osteogenic and non-osteogenic cell-types toward an osteoblastic lineage *in vitro* [59, 66, 67, 135, 136]. Both transient and long-term expression of Runx2 in primary BMSCs enhances *in vivo* mineral deposition compared to unmodified BMSCs [137-139]. More recently, we have demonstrated that primary dermal fibroblasts transduced with a Runx2 retroviral vector create mineralized templates *in vivo* after implantation in a subcutaneous, heterotopic site [131]. In this report, Runx2-expressing fibroblasts co-localized with mineral deposits *in vivo*, suggesting that bone formation primarily originated from transplanted donor cells.

Finally, Tu et al. recently observed that retroviral gene delivery of Osterix enhances the mineralization capacity of primary bone marrow stromal cells *in vitro*, suggesting that this strategy may lead to stimulation of bone formation *in vivo* [140].

In order to more closely mimic the signaling pathways involved in natural bone formation, several investigators have pursued strategies based on simultaneous delivery of multiple regenerative molecules. Franceschi and colleagues investigated a combinatorial gene therapy approach based on the overexpression of multiple genes encoding osteoinductive growth factors. Co-infection of murine embryonic fibroblasts with BMP-2/BMP-7 adenoviral vectors synergistically enhanced *in vivo* bone formation compared to overexpression of individual molecules alone [22]. Peng et al. investigated the ability of an angiogenic factor to promote blood vessel infiltration and cartilage formation during BMP-induced endochondral ossification [141]. Genetic modification of muscle-derived stem cells with a combination of BMP-4 and vascular endothelial growth factor (VEGF) synergistically enhanced ectopic and orthotopic bone formation compared to BMP-4-expressing or VEGF-expressing cells alone. Finally, the osteogenic potential of a combinatorial strategy based on co-expression of a soluble factor with a transcription factor has been recently evaluated. Yang *et al.* reported that the C3H10T1/2 fibroblastic cell-line expressing Ad-BMP-2 and Ad-Runx2 synergistically induced subcutaneous bone formation compared to BMP-2-expressing or Runx2-expressing cells alone [23]. Taken together, these results highlight the potential of combinatorial factor delivery as a strategy to enhance *in vivo* bone formation.

Preliminary evidence suggests that BMP-2-based genetic engineering strategies may have a more potent osteoinductive effect *in vivo* than those based on Runx2 [23, 24].

25

This heightened osteogenic response is likely due to paracrine signaling by BMP-2 cells, which may be absent or attenuated in Runx2-expressing cells. As these strategies move forward, further characterization of the protein release profile and the threshold of factor delivery necessary to achieve efficacy in each scenario will be necessary. In general, it is unlikely that one single target gene will be universally appropriate for the treatment of the numerous orthopaedic conditions requiring bone grafting.

Rationale for Genetic and Tissue Engineering Strategies

It is evident from the preceding discussion that the natural processes of skeletal development and fracture healing involve a complex spatiotemporal cascade of local and systemic factors. These highly regulated signaling pathways result in an intricately designed osseous tissue containing multiple cell-types and extracellular matrix proteins woven together into a precise three-dimensional structure. It is not currently well understood whether the optimal bone regenerative strategy must perfectly mimic the precise architecture and biochemical properties of native bone. Indeed, it is likely that the degree of native tissue recapitulation will be dependent on the anatomic location of the defect and the level of damage to vasculature and progenitor cell populations within the host tissue bed surrounding the repair site. For example, one could postulate that healing could be induced in certain applications by transplants which serve only as bridging scaffolds to support mechanical function temporarily, to initiate the endogenous healing response, and then be eventually remodeled and replaced by endogenous bone. Nevertheless, it is likely that the complex biomolecular organization of endogenous skeletal tissue cannot be achieved by the delivery of a single dose of recombinant protein to the repair site in a poorly-controlled manner. Even after the development of an

26

optimal protein delivery vehicle has been realized, recombinant growth factor-based approaches may still be insufficient to induce an adequate osteogenic response in patients with compromised tissue beds because they require the presence of an endogenous cell population capable of osteogenic differentiation. Gene transfer technologies may enable the design of therapies which result in bone tissue that more closely mimics the complex spatial and temporal cascade of proteins involved in bone formation. In theory, the temporally-regulated delivery of genetic sequences encoding a combinatorial group of osteoinductive factors would be capable of an enhanced osteogenic response compared to a single bioactive factor or cell-based approach alone. Furthermore, combinatorial gene therapy strategies would have advantages over combinatorial protein delivery strategies because they may avoid issues such as high cost, toxic protein doses, short factor half-life, and suboptimal delivery vehicles. Finally, it is important to note that the biomaterial delivery vehicle or matrix supporting cell delivery/activity plays an important role in modulating the efficacy of these genetic engineering approaches and providing a structural role in the healing response. A thorough discussion of these biomaterial-related considerations is beyond the scope of the present literature review.

Biological and Synthetic Ligament Grafts

Ligaments are densely organized, fibrous connective tissues that are primarily responsible for the attachment of two or more bones across a joint. The ligaments which connect the femur to the tibia stabilize the knee against abnormal translational and rotational motion and are particularly susceptible to sports-related traumatic injury [142]. Partial tears or full rupture of the anterior cruciate ligament (ACL) and/or the medial

27

collateral (MCL) ligament account for over 90% of all knee ligament injuries [143]. The MCL has a propensity for spontaneous repair due to its high vascularity [144, 145]. However, the biochemical composition and extracellular matrix organization of this healing tissue is significantly different than native MCL, resulting in suboptimal mechanical properties for up to 2 years after injury [146, 147]. In contrast, surgical intervention is typically required to restore ACL function, which has limited healing capacity because it is poorly vascularized and surrounded by synovial fluid [148].

Over 100,000 ACL reconstructions are performed each year in the United States with an estimated cost totaling over $5 billion dollars [149, 150]. Autologous hamstring tendon or patellar tendon grafts with bony attachments on the proximal and distal ends represent the most common reconstruction materials. Procedures based on these autografts are considered the gold standard in ligament repair, but are associated with side effects such as donor site morbidity, pain, tendonitis, arthritis, and the formation of restrictive scar tissue [151]. Allogenic tissue derived from the achilles tendon has shown a comparable clinical outcome to autogenic tendon in some cases, but has disadvantages for the risk of disease transmission, limited tissue supply, and inadequate mechanical properties [152]. Finally, approaches based on engineered synthetic grafts (e.g. Leeds-Keio polyethylene terephthalate, polypropylene-based Kennedy ligament augmentation device (LAD), polyester (Dacron), polytetrafluoroethylene (Gore-Tex), and multifilament or braided collagen fibers have also been explored [149, 153]. Many of these synthetic grafts have shown a high rate of mechanical failure when used for primary ACL repair. This tissue failure has been attributed to multiple factors, including suboptimal tissue anchorage to bone, inability to support tissue ingrowth and remodeling, and generation of

28

particulate matter due to prostheses abrasion and wear [144]. Beyond the selection of a grafting template, even reconstructions which fully restore tissue function involve an extensive rehabilitation process that can take from 4 months up to 3 years [142, 154].

Ligament Anatomy and Biochemistry

Human ligaments display complex time- and history-dependent viscoelastic behavior that is highly dependent on the biochemical composition and microstructure of the extracellular matrix. Most ligament tissues consist of 65-80% water and 20-35% solids such as collagen, decorin, elastin, and fibronectin [148]. The majority of collagen within this matrix is the type I isoform, but types II, III, V, IX, X, XI, and XII have also been detected depending on the species, age, and disease state of the animal model [155]. Collagen fibrils are densely packed into a crimped pattern within fasicular subunits, which are arranged in parallel to the long axis of the ligament into a higher order structure of functional bands. Heterogeneous zones of ligament, fibrocartilage, mineralized fibrocartilage, and bone are found at the transitionary region between bone and soft tissue. The collagen structure shifts toward a more helical and/or non-parallel orientation in this bone-ligament interface in order to avoid the formation of stress concentrations that may lead to failure during loading. Populations of fibroblasts are interspersed throughout the matrix and function in tissue remodeling, adaptation, and healing. Ultimately, the structural arrangement of these biochemical constituents gives the human ACL an average tensile strength of 1730 N, an average linear stiffness of 182 N/mm, and an average energy absorbed at failure of 12.8 N-m. It is the inability of most

29

grafting templates to mimic the complex geometry and stress-strain behavior of native ligament tissue that eventually leads to mechanical failure [149].

Growth and Differentiation Factors in Ligament Repair

Specific growth factors, including platelet derived growth factor (PDGF), epidermal growth factor (EGF), basic fibroblast growth factor (bFGF), transforming growth factor beta (TGF-β), and insulin-like growth factor (IGF-I), have altered expression levels following ligament injury [156-158]. Furthermore, *in vitro* studies have demonstrated that many of these proteins specifically modulate migration, proliferation, and/or matrix deposition by ligament fibroblasts [159]. In particular, fibroblast proliferation is stimulated by EGF, IGF-I, bFGF, or PDGF-BB, while TGF-β regulates collagen deposition by these cells [160-162]. Additionally, both PDGF-BB and TGF-β are chemoattractants which stimulate fibroblast migration through ligament tissue [163]. Direct administration of recombinant PDGF has been reported to significantly improve the mechanical properties of healing ligament tissue [164]. In contrast, conflicting reports exist regarding local delivery of TGF-β, which has shown isoform- and concentration-dependent enhancement in the healing of rabbit MCL tissue [165-167]. More recently, combinatorial delivery of both TGF-β1 and EGF has been shown to improve MCL healing in canines [168]. Despite promising results in preclinical animal models, these recombinant protein-based therapies are limited by suboptimal delivery vehicles, rapid *in vivo* protein degradation, and cost-prohibitive supraphysiologic concentrations. Because of these complications, gene therapy and tissue engineering strategies have been pursued

as an alternative strategy for the sustained delivery of therapeutic proteins to the compromised tissue site [155, 169].

Gene Therapy Approaches to Ligament Repair

Reporter Gene Delivery to Ligament and Tendon

The feasibility of both *in vivo* and *ex vivo* gene transfer to ligament and/or tendon tissue has been investigated in a variety of animal models [170]. Because the signaling pathways involved in ligament healing are poorly understood, the majority of these approaches have focused on proof-of-principle studies involving delivery of a reporter gene. Gerich et al. isolated fibroblasts from ACL, PCL, MCL, patellar tendon and semitendinosus tendon tissue harvested from New Zealand white rabbits [171, 172]. All five cell types were reported to be susceptible to transduction *in vitro* with both a first generation adenoviral vector and a retroviral vector encoding for the β-galactosidase (LacZ) gene. *In vivo* gene delivery of this LacZ adenovirus via direct injection into the patellar tendon of New Zealand white rabbits resulted in a limited level of LacZ expression adjacent to the site of delivery [171, 173]. In a separate approach, Huard and colleagues genetically engineered an autologous semitendinosus tendon graft with adenovirus-LacZ or adenovirus-luciferase *in vitro* [174]. Reporter genes were detected around the periphery of this tissue for 6 weeks *in vitro*, suggesting that fibroblasts could be genetically modified in situ within the native three-dimensional environment [175]. Finally, Lou et al. found that *in vivo* transduction efficiency after injection into chicken tendon and tendon sheath was highly dependent on the titer of LacZ adenovirus [176]. Positive staining was observed for up to 75 days *in vivo*, suggesting that the host immune

31

response against adenoviral vectors may not be as robust in certain connective tissues compared to most highly vascularized tissues. Moreover, the observed confinement of the virus to the tissue periphery suggested that the collagenous composition and structure may serve as a barrier against plasmid penetration into the center of certain connective tissues [177].

An *ex vivo* approach was explored by Gerich et al. in which allogenic primary tendon fibroblasts were genetically engineered with a LacZ retroviral vector and implanted directly into the patellar tendon of healthy New Zealand White rabbits[171]. Notably, a significantly higher number of LacZ-expressing fibroblasts were detected after 6 weeks *in vivo* with this cell-based approach compared to direct injection of virus [171]. These results were corroborated by a study by Menetrey et al. where myoblasts and ACL-derived fibroblasts were infected with an adenoviral vector encoding LacZ and transplanted into healthy ACLs of adult rabbits. Transgene expression was detected for up to 21 days with this *ex vivo* approach, while direct injection of adenoviral particles resulted in marker gene expression through 42 days [178]. In order to determine if this strategy would be technically feasible for the healing of injured ligaments, Woo and colleagues implanted allogenic LacZ-expressing fibroblasts into a ruptured MCL in skeletally mature rabbits, while the contralateral controls received saline injections [179]. Importantly, LacZ expression was upregulated at comparable levels in both ruptured and unruptured MCL tissue compared to control tissue, suggesting that transduction is independent of the injury state of the ligament. Results from this study indicate that natural ligament healing process may not disrupt expression of an exogenously delivered transgene.

In Vivo Gene Therapy for Ligament and Tendon Repair

The studies discussed above demonstrated that *in vivo* and *ex vivo* techniques can be used to maintain expression of an exogenous transgene for up to 8 weeks in preclinical animal models. Techniques optimized in these proof-of-concept studies have been utilized by some investigators to study the effects of therapeutic molecules gene delivery on ligament and/or tendon healing [180]. Lou et al. used an *in vivo* gene transfer strategy based on direct injection of adenoviral vectors encoding for sense and antisense focal adhesion kinase (FAK) into the tendon and tendon sheath of White Leghorn chickens. Tendons overexpressing FAK showed an increase in adhesion formation compared to unmodified and antisense FAK-expressing controls, suggesting that this molecule may have a critical role in regulating the formation of restrictive tendon adhesions during tissue healing [181]. More recently, Manske and colleagues reported that adenovirus-mediated gene delivery of BMP-12 into primary chicken tendon cells increased type I collagen synthesis *in vitro* [182]. Ad-BMP-12 was directly injected into a completely lacerated toe tendon in White Leghorn chickens. Tendons expressing BMP-12 displayed a two-fold increase in tensile strength and stiffness compared to controls expressing a reporter gene, suggesting that BMP-12 enhances mechanical properties of healing tendons *in vivo* [183]. Finally, Nakamura et al. investigated the direct injection of hemagglutinating virus of Japan (HVJ)-conjugated liposomes containing PDGF-BB cDNA into injured patellar ligament in Wistar rats [184]. PDGF expression was detected around the wound for up to 4 weeks after injection. Overexpression of this protein enhanced angiogenesis at early time points (7 days) and stimulated collagen I matrix deposition and organization at late time points (28 days) compared to control ligaments

expressing HVJ-liposomes without DNA [185]. Taken together, these studies suggest that *in vivo* gene transfer of a therapeutic molecule may be a promising strategy for the functional repair of injured ligament tissue.

Ex Vivo Gene Therapy for Tendon Repair

The use of *ex vivo* genetic engineering techniques for the delivery of therapeutic transgenes to ligament tissue has not been reported to the best of the authors' knowledge. However, advances have been made in the application of *ex vivo* gene therapy strategies toward tendon repair. Gazit and colleagues have recently reported a novel approach based on transient transfection of the mesenchymal progenitor C3H10T1/2 cell line *in vitro* with cDNA encoding the Smad8 transcription factor [186]. Notably, co-expression of Smad8 and BMP-2 inhibited osteogenesis and promoted differentiation toward a tenocyte-like phenotype *in vitro* compared to BMP-2- or Smad8-engineered cells alone. Importantly, *in vivo* implantation of these Smad8/BMP-2-expressing C3H10T1/2 progenitor cells resulted in the formation of ectopic tendon tissue in mice and the induction of tissue repair in an Achilles tendon partial defect in rats [187]. This landmark study highlights the potential of *ex vivo* gene therapy for repair of tendon/ligament connective tissue. Future advances in the understanding of the signaling pathways involved in this healing process will likely drive the identification of novel therapeutic targets for ligament regeneration.

Antisense Gene Therapy for Connective Tissue Repair

34

Previous research has demonstrated that healing ligaments often develop scar tissue with different biochemical constituents and inferior mechanical properties to native tissue. More specifically, scar tissue has been reported to have elevated content of the proteoglycan decorin, enhanced fibronectin and type III collagen expression, decreased type I collagen levels, decreased collagen fibril diameter, and abnormal collagen organization and cross-linking compared to native tissue [188-192]. The presence of this scar tissue increases the probability of ligament re-injury and/or the development of arthritis within the knee joint. Notably, reports have shown that the diameter of collagen fibrils is directly proportional to ligament tissue mechanical properties and may be negatively regulated by decorin and type V collagen [193, 194]. Nakamura et al. developed an *in vivo* gene therapy method based on HVJ-liposome-mediated delivery of inhibitory antisense oligodeoxynucleotides (ODNs) against decorin to specifically block mRNA and protein expression of this proteoglycan in a rabbit MCL gap injury model [195-197]. Overexpression of decorin antisense increased the mechanical properties and collagen fibril diameter of MCL scar tissue compared to sense and empty HVJ-liposome treated ligaments. In addition, Woo and colleagues investigated a similar approach for reducing scar tissue formation based on antisense ODNs against type III collagen and the type V procollagen alpha1 chain [198, 199]. These investigators identified sequences which would efficiently suppress types III or V collagen in human patellar tendon fibroblasts *in vitro* and have proposed experiments to test these sequences *in vivo* [200]. Taken together, these preliminary studies indicate that antisense gene therapy may improve the biochemical and mechanical properties of healing ligament tissue.

Tissue Engineering Approaches for Ligament Repair

Tissue engineering has recently emerged as a promising alternative strategy to address the limitations associated with conventional ACL reconstruction procedures. In this approach, cells and/or bioactive growth factors are combined with polymeric scaffolds to produce ligament grafting templates. Because the ligament serves as a structural tissue, research efforts to date have focused heavily on the development and optimization of scaffolds based on collagen, silk, synthetic polymers, and/or a composite blend [149, 201-204]. More recently, investigators have discovered that the cellular phenotype and extracellular matrix organization also play an essential role in mimicking the complex structure-function relationship of native tissue. For this reason, cellular therapies based on bone marrow-derived mesenchymal stem cells (MSCs) have also been investigated for their ligament healing capacity in preclinical animal models [15, 149, 159, 205-210]. Mechanical loading regimes and tissue bioreactors have also been developed for the manipulation of matrix organization *in vitro* [211-214].

Genetic and Tissue Engineering for Enhanced Soft Tissue Graft Osseointegration

Investigators have also pursued gene therapy and tissue engineering strategies to improve the integration of autologous tendon grafts into the surrounding bone at the bone-tendon interface. Huard and colleagues reported an *ex vivo* approach based replacement of the ACL in New Zealand white rabbits with an autologous double-bundle semitendinosus tendon graft [215]. These grafts were explanted and genetically engineered *in vitro* with adenoviral vectors encoding BMP-2, luciferase, or LacZ before *in vivo* implantation. Histological analysis of Ad-BMP-2-transduced grafts revealed evidence of

mineral, mineralized cartilage, and nonmineralized fibrocartilage tissue at the tendon-bone interface, while control grafts (unmodified, LacZ-expressing, luciferase-expressing) deposited a dense matrix resembling Sharpey fibers. BMP-2-expressing grafts also displayed enhanced mechanical properties compared to control tendons [216]. This study demonstrated that gene delivery of BMP-2 can enhance osseointegration of tendon grafts used for ACL reconstruction. More recently, alternative strategies based on the design of multi-phase scaffolds or the integration of multiple cell types (i.e. osteoblasts, fibroblasts, chondrocytes) into a single scaffold have been explored for the generation of interfacial bone-soft tissue zones [217-219].   Overall, the tissue engineered ligament grafts which are currently available continue to be limited by failure at the bone-tendon insertion site and inadequate mechanical properties, suggesting that genetic engineering techniques could add significant value to the currently available cell-based tissue engineering strategies.

CHAPTER 3

RUNX2-GENE THERAPY IN COMBINATION WITH DEXAMETHASONE TREATMENT SYNERGISTICALLY INDUCES OSTEOGENESIS IN PRIMARY DERMAL FIBROBLAST MONOLAYER CULTURES*

Introduction

It is well documented that adenoviral and retroviral gene delivery of Runx2 upregulates osteogenic gene expression in osteoblastic and non-osteoblastic cell types [59, 66, 67, 137]. However, we and others have reported that forced Runx2 expression induces matrix mineralization in a cell type-dependent manner and is insufficient to direct significant *in vitro* nodule formation in NIH3T3 and IMR-90 fibroblasts, primary murine fibroblasts, and the C3H10T1/2 pluripotent fibroblastic cell line [23, 24, 66]. These results suggested that Runx2-mediated mineralization requires additional cofactors, which may not be endogenously expressed in certain nonosteoblastic cells. In this study, primary dermal fibroblasts were genetically engineered to constitutively express the Runx2 type II isoform and cultured in differentiation media supplemented with and without 10 nM DEX. We hypothesized that the putative signaling pathways necessary for mineralization in this non-osteogenic cell source can be activated by DEX.

Materials and Methods

Cell Culture and Reagents

Primary fibroblasts were harvested from 8- to 16-week-old male Wistar rats by enzymatic digestion of the dermal skin layer [220]. Cells were expanded in growth media consisting of DMEM, 10% fetal bovine serum, and 1% penicillin-streptomycin. Antibiotics and cell culture media were obtained from Invitrogen (Carlsbad, CA), fetal bovine serum was purchased from Hyclone (Logan, UT), and all other cell culture supplements and reagents were acquired from Sigma Chemical Company (St. Louis, MO).

Retroviral Transduction

The Runx2 retroviral vector utilizes the promoter activity of a 5' long terminal repeat to express a single, bicistronic mRNA encoding the murine cDNA for the type II MASNSLF Runx2 isoform, followed by an internal ribosomal entry site and a Zeocin resistance-enhanced green fluorescent fusion protein. Plasmid DNA was purified from transformed E. coli using Megaprep kits from Qiagen (Valencia, CA). Retroviruses were packaged by transient transfection of helper-virus free ΦNX amphotropic producer cells with plasmid DNA as described elsewhere [66]. ΦNX cells were cultured in growth media (DMEM, 10% fetal bovine serum, 100 U/ml penicillin G sodium, 100 μg/ml streptomycin sulfate) in a humidified 5% CO_2 atmosphere at 37 °C and plated 9 x 104 cells/cm2 24 h prior to transfection. Cells were transfected with 0.5 μg/cm2 of plasmid DNA, either Runx2 or empty vector (no Runx2 insert), using calcium phosphate coprecipitation and 25 μM chloroquine for 8-12 h prior to refeeding with fresh growth media. Twenty-four hours after the start of the transfection, media was replaced with

39

fresh growth media and dishes were transferred to a humidified 5% CO_2 atmosphere at 32 °C for enhanced stability of retroviral particles. Retroviral supernatants were collected at 48, 60, and 72 h post-transfection, filtered through a 0.45 μm cellulose acetate filter, aliquoted, snap frozen, and stored at -80 °C until use.

Passage four primary fibroblasts were plated on 6-well tissue culture polystyrene plates coated with 0.1% type I collagen (Vitrogen, Palo Alto, CA). Cells at 50-70% confluence were transduced with retroviral stocks and maintained in differentiation media consisting of DMEM, 10% fetal bovine serum, 100 U/ml penicillin G sodium, 100 μg/ml streptomycin sulfate, 50 μg/ml L-ascorbic acid, 2.1 mM sodium β-glycerophosphate, and with or without 10 nM DEX [66]. Tissue culture media was changed every 2 days until end-point assay. No differences were observed between empty vector retrovirus (negative control) and unmodified cells in all experiments. Runx2-transduced cells were analyzed for transduction efficiency by quantification of eGFP expression via flow cytometry. High levels of eGFP were detected in $\geq$ 65% of primary dermal fibroblasts at 72 hours post-transduction.

Real Time RT-PCR

Total RNA was isolated at 1, 3, and 7 days post transduction using the RNeasy RNA isolation kit (Qiagen). cDNA synthesis was performed on DNaseI-treated (27 Kunitz units/sample) total RNA (1 μg) by oligo(dT) priming using the Superscript™ First Strand Synthesis System for RT-PCR (Invitrogen). Real-time PCR using SYBR Green intercalating dye was performed with the ABI Prism 7700 Sequence Detection System (Applied Biosystems, Foster City, CA, 40 cycles, melting: 15 sec at 95ºC, annealing and

extension: 60 sec at 60ºC)24. Real-time PCR oligonucleotide primers (Table 3.1) were designed using ABI Primer Express software and purchased from IDTDNA (Coralville, IA). Primer specificity was confirmed by agarose gel electrophoresis and ABI Prism 7700 Dissociation Curve Software. Standards for each gene were amplified from cDNA using real-time oligonucleotides (Table 3.1), purified using a Qiagen PCR Purification kit, and diluted over a functional range of concentrations. Transcript concentration in template cDNA solutions was quantified from a linear standard curve, normalized to 1 μg of total RNA, and expressed as femtomoles of transcripts per μg of total RNA. Detection limits for each gene were determined by reactions without cDNA and were at least an order of magnitude below the most dilute sample.

Western Blotting

Cells were washed with PBS and lysed in cold radioimmunoprecipitation assay (RIPA) buffer (1% Triton X-100, 1% sodium deoxycholate, 0.1% SDS, 150 mM NaCl, 150 mM Tris-HCl pH 7.2, 350 μg/ml phenylmethylsulfonyl fluoride, 10 μg/ml leupeptin, 10 μg/ml aprotinin, and 1 mM sodium orthovanadate) for 20 min. Lysates were pipetted up and down ~25 times to shear the DNA and then clarified by centrifugation at 10,000g for 10 min. Protein concentration was then determined using a Micro BCA protein assay kit (Pierce, Rockford, IL). Equal amounts of protein (25 μg) were boiled in Laemmli sample buffer (2% SDS, 10% glycerol, 100 mM DTT, 60 mM Tris-HCl pH 6.8, and 0.001% bromophenol blue) for 10 min and separated by SDS-PAGE. Proteins were transferred by electrophoresis onto nitrocellulose membranes and blocked with Blotto (5% non-fat dry milk, 0.02% sodium azide, 0.2% Tween 20 in PBS w/o Ca2+/Mg2+)

41

overnight at 4ºC. Membranes were then incubated with 1 µg/ml anti-AML3 (Oncogene, San Diego, CA) or 9 µg/ml anti-GAPDH (Chemicon, Temecula, CA) in Blotto for 1 h at room temperature under gentle rocking. Membranes were washed in TBS-Tween (20 mM Tris HCl pH 7.6, 137 mM NaCl, 0.1% Tween 20) for 30 min and incubated in secondary antibody (biotin-conjugated anti-rabbit/mouse IgG, 1:20,000 dilution in Blotto, Jackson ImmunoResearch, West Grove, PA) for 1 h at room temperature. Membranes were washed again in TBS-Tween for 30 min and incubated in tertiary antibody (alkaline phosphatase-conjugated anti-biotin IgG, 1:10,000 dilution in Blotto, Sigma) for 1 h at room temperature. After antibody incubation, membranes were washed in TBS-Tween for 30 min and immunoreactivity was detected using ECF fluorescent substrate (Amersham Bioscience, Piscataway, NJ) and a Fuji Image Analyzer.

Alkaline Phosphatase Biochemical Activity

As a marker of osteoblastic enzyme activity, alkaline phosphatase (ALP) activity was quantified at 7 days post-transduction as previously described[24]. Cells were rinsed and scraped into ice-cold 50 mM Tris·HCl, pH 7.4. Following sonication and centrifugation, total soluble protein concentration was quantified using the MicroBCA Protein Assay Kit. Equal amounts of protein (2.5 µg) were added to 60 µg/mL 4-methylumbelliferyl-phosphate fluorescent substrate in diethanolamine buffer (pH 9.5). Following incubation for 60 min at room temperature, the fluorescence was read at 360 nm excitation/465 nm emission on an HTS 7000 Plus BioAssay Reader (Perkin Elmer, Norwalk, CT). Enzymatic activity was standardized using purified calf intestinal alkaline phosphatase (Sigma) and normalized to total protein concentration.

von Kossa Histochemical Analysis

Cultures were fixed in 70% ethanol at 14 and 21 days and examined histochemically for mineralized matrix by von Kossa staining for phosphate deposits. Plates were stained with 5% AgNO3 under uniform light exposure for 30 min, fixed in 5% Na2SO3 for 2 min, and air-dried. Mineralized surface area was quantified by automated capturing and averaging of twenty-four representative 2X images using Image Pro analysis software.

FTIR Spectroscopy

Cell culture samples at 21 days post-transduction were fixed in 100% ethanol, craped from the culture dish, and dried at 50ºC overnight. Bone samples were scraped from a lyophilized rat cranium. Bulk samples were mixed with KBr (Sigma) and pressed into pellets. Samples were analyzed with a Nicolet Nexus 470 FTIR spectrometer ThermoNicolet, Madison, WI) equipped with a DTGS detector. 64 scans were acquired at 4 cm-1 resolution under N2 purge.

Data Analysis

Unless otherwise stated, experiments were performed at least three times in triplicate, each with unique Runx2 retroviral supernatant preparations, and two independent fibroblast isolates. No differences were observed between unmodified and empty vector transduced cells in all assays. Data are reported as mean ± standard error of the mean (SEM), and statistical comparisons using SYSTAT 8.0 were based on an

43

analysis of variance (ANOVA) and Tukey's test for pairwise comparisons within timepoints, with a p-value < 0.05 considered significant. In order to make the variance independent of the mean, statistical analysis of real-time PCR data was performed following logarithmic transformation of the raw data [66].

Results

Dex enhances Runx2-induced osteoblastic gene expression

In order to assess the effects of DEX on Runx2-mediated osteogenesis in the absence of native osteoblastic signals, primary dermal fibroblasts were genetically engineered to constitutively express the Runx2 type II isoform and cultured in differentiation media supplemented with and without 10 nM DEX. We hypothesized that a combination of forced Runx2-expression and DEX supplementation would induce osteoblastic differentiation in primary dermal fibroblasts. Skeletal gene expression was investigated at 1, 3, and 7 days post-transduction by quantitative RT-PCR (Fig. 3.1). Runx2 mRNA levels were upregulated by 2 orders-of-magnitude in transduced cultures compared to control cells at day 3, and this relative difference decreased to one order-of-magnitude as cells reached confluence at day 7. eGFP transgene expression was detectable by flow cytometry through 21 days, demonstrating integrated and sustained expression of the Runx2 transgene. Runx2 primers utilized in this study [137] were designed to detect both type I and type II Runx2 isoforms [221, 222]. Thus, the absence of Runx2 mRNA transcripts in untransduced cultures indicates that the Runx2 type II isoform is the predominant isoform expressed in transduced cultures. Osteocalcin (OCN) is the most abundant non-collagenous extracellular matrix protein in bone and a marker
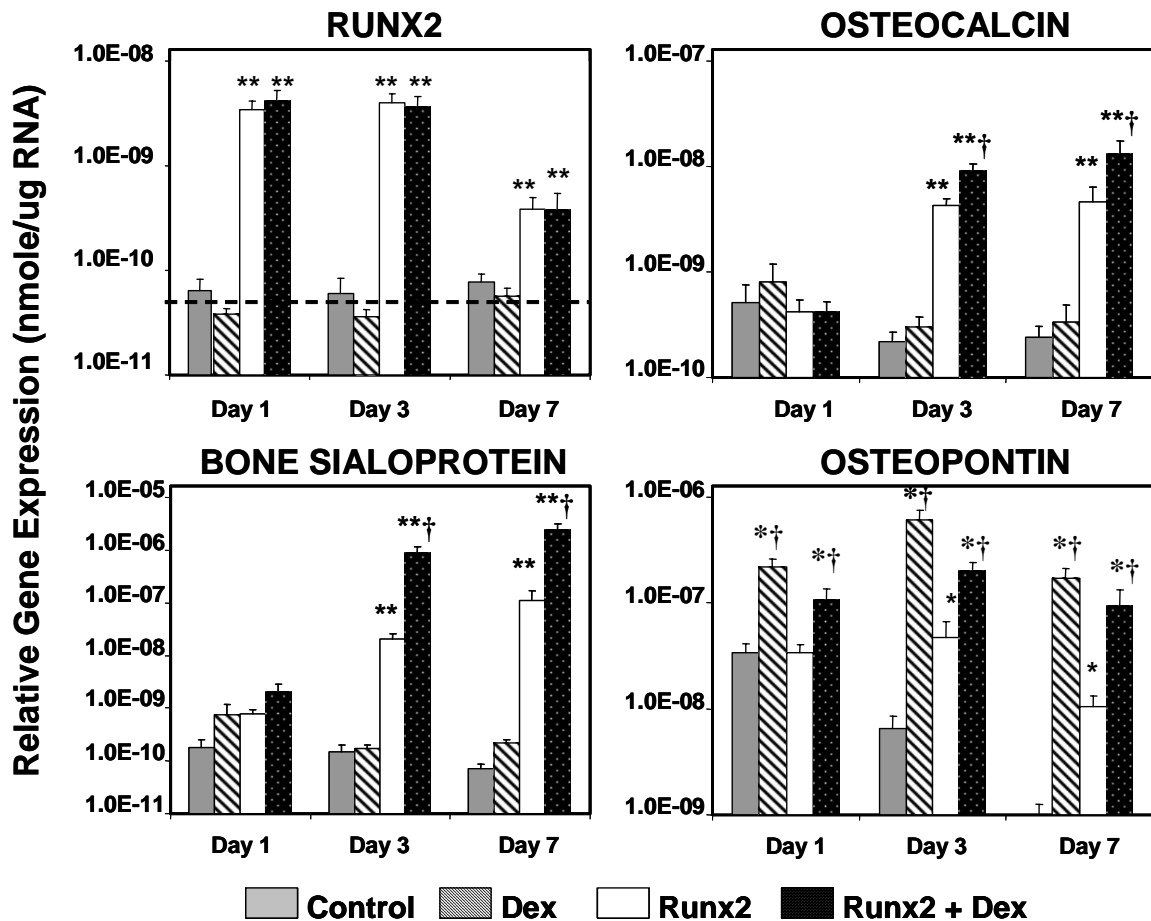
Figure 3.1. DEX enhances Runx2-induced osteoblastic gene expression. Primary dermal fibroblasts were transduced with Runx2 or empty vector retrovirus and cultured in osteogenic media with and without 10 nM DEX. mRNA expression was investigated by quantitative RT-PCR at 1, 3, and 7 days post-transduction (Mean + SEM, n=16; ANOVA: p<1E-11; * different from empty vector control, ** different from empty vector and DEX controls, and †different from Runx2 (p< 0.05)). Relative gene expression is expressed on a logarithmic scale. Detection limits for each gene were determined by reactions without cDNA and are shown as dotted lines.

of mature osteoblasts [223]. Bone sialoprotein (BSP) and osteopontin (OPN) are extracellular matrix glycoproteins implicated in the regulation of mineralized nodule nucleation [224]. BSP mRNA levels were upregulated by 3 orders-of-magnitude in Runx2-transduced cells, while OCN and OPN demonstrated a 10-fold increase at 7 days post-transduction compared to control cultures. Notably, addition of DEX to Runx2-expressing cultures resulted in significant enhancements in OCN, BSP, and OPN mRNA levels at days 3 and 7 compared to untreated Runx2-expressing cultures. DEX supplementation alone significantly increased OPN mRNA compared to untreated controls, but had no effect on Runx2, OCN and BSP mRNA levels. These results demonstrate that sustained expression of Runx2 upregulates osteoblastic gene expression and treatment with DEX enhances this effect.

Runx2 and DEX synergistically induce osteoblastic differentiation

Alkaline phosphatase (ALP) is a membrane-bound enzyme that hydrolyzes phosphate esters, thereby making inorganic phosphate available for incorporation into mineral deposits [224]. The activity of this enzyme was examined at 7 days post-transduction (Fig. 3.2A). Runx2-overexpression stimulated a 15-fold increase in ALP activity compared to control cultures. Moreover, addition of DEX to Runx2-transduced cultures resulted in a synergistic increase in ALP activity. Matrix mineralization was assessed at 14 and 21 days post-transduction by von Kossa staining and image analysis (Fig. 3.2B,C). Notably, co-treatment with Runx2 and DEX synergistically induced matrix mineralization in primary dermal fibroblasts, while Runx2-expressing cultures alone displayed minimal staining and sparse nodule formation. No mineral was detected

in empty vector or DEX-treated control cultures. FTIR spectroscopy was utilized to analyze the chemical composition of the mineral phase because osteogenic culture conditions can lead to non-biological calcium phosphate precipitation [225, 226]. (Fig. 3.2D). Runx2 and cranial bone samples displayed amide I and II peaks indicative of extracellular matrix proteins, an enhanced phosphate peak at 1100 cm^{-1}, a doublet split phosphate peak at 560 and 605 cm^{-1}, and a carbonate peak at 870 cm^{-1}, which represent the characteristic bands of a carbonate-containing, poorly crystalline hydroxyapatite [227]. These bands were absent in empty vector and DEX-only control cultures. Collectively, these results demonstrate that a combination of constitutive Runx2 overexpression and DEX supplementation synergistically induces osteoblastic differentiation in primary dermal fibroblasts.

Discussion

Forced expression of Runx2 upregulates osteogenic gene expression in a variety of osteoblastic and non-osteoblastic cell types [59, 66, 67]. However, we and others have demonstrated that Runx2 overexpression induces matrix mineralization in a cell type-dependent manner and is insufficient to produce significant levels of nodule formation in primary murine fibroblasts and fibroblastic cell-lines [66]. This suggests that Runx2-mediated mineralization requires additional cofactors, which may not be endogenously expressed in non-osteoblastic cells. In this study, dermal fibroblasts were analyzed for their osteogenic potential following retroviral gene delivery of Runx2. We hypothesized that the putative signaling pathways necessary for mineralization in this non-osteogenic cell source can be activated by DEX. We demonstrate that sustained expression of

Runx2 was necessary but not sufficient to promote terminal osteogenic differentiation in primary dermal fibroblasts and that DEX is required for robust matrix mineralization in this model system. DEX synergistically enhanced BSP gene expression, ALP activity, and mineralization in Runx2-expressing cells, while hormone-only treated cultures exhibited minimal expression of these markers. The absence of osteogenic phenotype expression in DEX-only treated cultures makes it unlikely that distinct subpopulations of DEX-responsive and Runx2-responsive cells cause the synergistic effect of DEX supplementation and Runx2-overexpression. Overall, this data suggests that DEX induces osteogenesis by a Runx2-dependent molecular mechanism, but does not rule out the possibility of a Runx2-independent mode of action in this model system.

Overall, these results demonstrate that a combination of constitutive retroviral Runx2-expression and treatment with the steroid hormone dexamethasone synergistically induces osteogenic differentiation in primary dermal fibroblasts cultured in monolayer. This surprising result suggests that Runx2-engineered primary dermal fibroblasts have the capacity to create mineralized templates for bone repair and may still have potential as a cell source for bone tissue engineering applications if exposed to the appropriate osteogenic cues. Furthermore, the absence of osteoblastic phenotype in hormone-only treated cultures suggests that Runx2-transduced fibroblasts may represent a robust experimental model system for the investigation of Runx2-dependent molecular pathway(s) involved in glucocorticoid-induced osteogenesis.
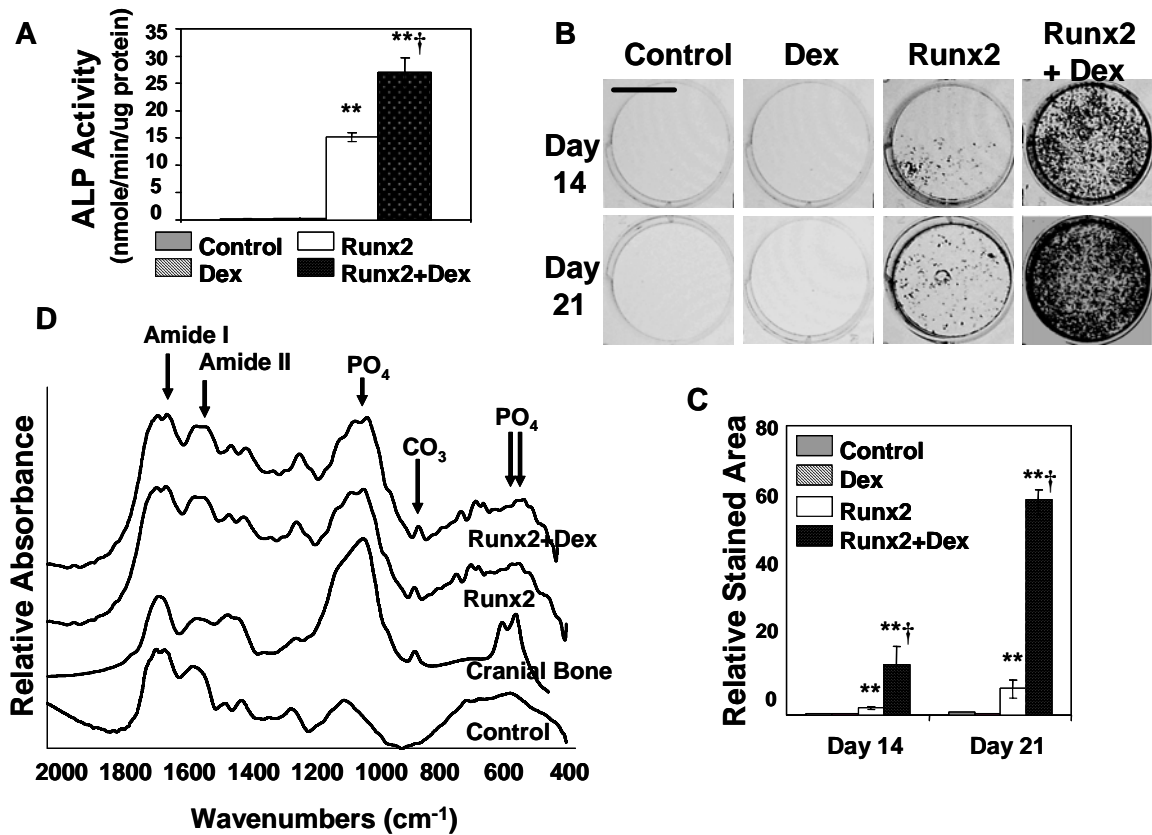
Figure 3.2. DEX and Runx2 synergistically induce osteoblastic differentiation.
Primary dermal fibroblasts were transduced with Runx2 or empty vector retrovirus and cultured in osteogenic media with and without 10 nM DEX.   (A) ALP activity was examined by a biochemical assay at 7 days post-transduction (Mean ± SEM, n=12; ANOVA: p<1E-8; ** different from empty vector and DEX controls, and †different from Runx2 (p< 0.05)).   (B) Mineralized matrix deposition was assessed via von Kossa staining for phosphate-positive regions and (C) quantified by image analysis at 14 and 21 days post-transduction (Mean ± SEM, n=12; ANOVA: p<1E-9, ** different from empty vector and DEX controls, and †different from Runx2 (p< 0.05)).   Scale bar 2 cm. (D) Chemical composition of the mineral phase was analyzed by Fourier transform infrared spectroscopy. Bone samples scraped from a lyophilized rat cranium served as a positive control.

49

CHAPTER 4

GLUCOCORTICOID-INDUCED OSTEOGENESIS IS NEGATIVELY REGULATED BY RUNX2/CBFA1 SERINE PHOSPHORYLATION*

Introduction

Glucocorticoids (GCs) are steroid hormones secreted by the adrenal cortex that play a pivotal role in the regulation of a variety of developmental, metabolic, and immune functions. The classic mechanism of GC action is primarily at the level of transcription, where the hormone forms a transcriptionally active complex with its cognate intracellular receptor. This complex can either enhance or attenuate gene expression by binding to GC response elements in the promoter region of target genes or by non-covalently associating with additional co-regulatory proteins [228].

Synthetic GC derivatives, such as dexamethasone (DEX), have complex stimulatory and inhibitory effects on skeletal metabolism and bone formation [229]. DEX is widely utilized at pharmacological doses for the treatment of inflammatory and autoimmune diseases. However, long-term administration of this hormone has adverse side effects on the skeleton, inducing osteoporosis by impairing osteoblast activity [230]. The mechanism(s) by which pharmacological doses of DEX induce bone loss include: (a) attenuated osteoblast proliferation [231, 232], (b) impaired collagen synthesis [233], (c) increased osteoblast apoptosis [234], (d) inhibition of osteogenic growth factors [230, 235, 236],

and (e) downregulation of osteogenic gene expression [237]. In contrast to these catabolic effects, physiologic levels (10 nM) of DEX promote osteoblastic differentiation *in vitro* [238, 239]. Furthermore, it has been recently demonstrated that GC signaling is required for normal bone volume and architecture in transgenic models, suggesting that endogenously expressed GCs may have an anabolic effect on skeletal metabolism and bone formation *in vivo* [240]. The mechanism(s) by which DEX promotes osteogenesis remain poorly understood, largely due to conflicting results associated with the various species and differentiation states of the model systems used to study this hormone *in vitro* [228, 241-246].

Runx2/Cbfa1 (Osf2/AML3/PEBP2αA) is an essential transcriptional regulator of osteoblast differentiation and bone formation. Homozygous deletion of Runx2 arrests osteoblast maturation, resulting in the absence of endochondral and intramembranous ossification [247]. Moreover, Runx2 haploinsufficiency causes the pathogenic skeletal phenotype cleidocranial dysplasia in mice and humans, characterized by short stature, hypoplastic clavicles, and dental abnormalities [62, 63]. Runx2 directs osteogenic differentiation by binding to OSE2 cis-acting elements in the promoter region of skeletal target genes and regulating their expression [59]. We and others have demonstrated that forced expression of Runx2 upregulates osteoblast-specific genes expression and induces mineralization in a cell type-dependent manner [24, 59, 66, 248]. Intriguingly, both postnatal disruption of Runx2 by dominant negative expression and overexpression of Runx2 from the pro-α (I) collagen promoter induces bone fragility and osteopenia in transgenic mice [68, 69]. These studies collectively demonstrate that cellular regulation of Runx2 is critical for normal skeletal development and bone formation.

51

Runx2 is regulated at multiple levels by a complex spatiotemporal cascade of growth factors, hormones, transcription factors, and cell-matrix interactions [65, 221, 249, 250]. In particular, DEX has differential effects on Runx2 mRNA transcript expression, protein levels, and DNA-binding activity depending on the species, osteogenic cell type, and culture conditions used to study this hormone *in vitro* [237, 243, 244]. These conflicting results suggest that DEX may regulate Runx2 by modulating its post-translational modification. The mitogen activated protein kinase (MAPK) pathway has been shown to phosphorylate Runx2 on residues within the C-terminal proline-serine-threonine-rich (PST) domain [64, 251]. This increase in phosphorylation strongly correlates with enhanced Runx2 transactivation and is stimulated by signaling via extracellular matrix, fibroblast growth factor-2, and mechanical loading [252-254]. In contrast, Wee and colleagues have reported that the activity of the human Runx2 type I isoform is negatively regulated by phosphorylation of two serine residues, Ser^{104} and Ser^{451} (corresponding to Ser^{125} and Ser^{472} in the murine type II Runx2 isoform) [255]. The putative signaling cascades or effector molecules that regulate these inhibitory phosphorylation events, as well as the functional significance of these residues, remain poorly understood.

In the present study, we investigated the effect of DEX on Runx2 serine phosphorylation and the functional role of this phosphorylation state during osteoblastic differentiation. Runx2-transduced primary dermal fibroblasts were utilized as the experimental model in order to investigate the Runx2-dependent molecular pathway(s) involved in DEX-mediated osteogenesis. This reconstituted model system allowed for the direct examination of DEX and Runx2 interactions in the absence of native osteoblastic components, such as endogenous Runx2 isoforms or Runx2-independent signaling

pathways, which may confound the analysis. We show that DEX induces osteogenesis, at least in part, by modulating the phosphorylation state of a negative regulatory serine residue (Ser[125]) on the Runx2 type II isoform. We demonstrate that the phosphorylation state of this specific serine residue plays a critical role in both early osteoblastic differentiation and late stage mineralization induction. Interestingly, the mutation of Ser[125] to arginine, which possibly mimics the steric hindrance caused by phosphorylation of this residue, has been identified in a human patient with cleidocranial dysplasia [256]. Thus, this work assists in elucidating a mechanism of GC-mediated osteogenesis and provides insights into the functional importance of Runx2 phosphorylation during skeletal pathogenesis.

Materials and Methods

Cell Culture and Reagents

Primary fibroblasts were harvested from 8- to 16-week-old male Wistar rats by enzymatic digestion of the dermal skin layer [220]. Primary bone marrow stromal cells (BMSC) were harvested from the femora of 8- to 16-week-old Wistar rats as described previously [137]. Cells were expanded in growth media consisting of DMEM (fibroblasts) or α-MEM (BMSC), 10% fetal bovine serum, and 1% penicillin-streptomycin. Antibiotics and cell culture media were obtained from Invitrogen (Carlsbad, CA), fetal bovine serum was purchased from Hyclone (Logan, UT), and all other cell culture supplements and reagents were acquired from Sigma (St. Louis, MO).

Retroviral Transduction

The Runx2 retroviral vector utilizes the promoter activity of a 5' long terminal repeat to express a single, bicistronic mRNA encoding the murine cDNA for the type II MASNSLF Runx2 isoform, followed by an internal ribosomal entry site and a Zeocin resistance-enhanced green fluorescent fusion protein [66]. Plasmid DNA was purified from transformed *E. coli* using Megaprep kits from Qiagen (Valencia, CA). Retroviruses were packaged by transient transfection of helper-virus free ΦNX amphotropic producer cells with plasmid DNA as described elsewhere [66].

Passage four primary fibroblasts and passage two BMSC were plated on 6-well tissue culture polystyrene plates coated with 0.1% type I collagen (Vitrogen, Palo Alto, CA). Cells at 50-70% confluence were transduced with retroviral stocks and maintained in differentiation media consisting of DMEM (fibroblasts) or α-MEM (BMSC), 10% fetal bovine serum, 100 U/ml penicillin G sodium, 100 μg/ml streptomycin sulfate, 50 μg/ml L-ascorbic acid, 2.1 mM sodium β-glycerophosphate, and with or without 10 nM DEX. Culture media was changed every 2 days until end-point assay. No differences were observed between empty vector retrovirus (negative control) and unmodified cells in all experiments. Runx2-transduced cells were analyzed for transduction efficiency by quantification of eGFP expression via flow cytometry. High levels of eGFP were detected in ≥ 65% of primary dermal fibroblasts and ≥ 45% BMSC at 72 hours post-transduction.

Site-Directed Mutagenesis

Single amino acid mutations were performed on the Runx2 plasmid with the QuikChange site-directed mutagenesis kit (Stratagene, La Jolla, CA). The codon, AGT,

encoding Ser[125] of the Runx2 Type II isoform was mutated to glycine and glutamic acid. The codon, TCT, encoding Ser[472] of the Runx2 Type II isoform was mutated to alanine and a glutamic acid. The forward primer 5'-CCGCACCGAC<u>GGT</u>CCCAACTTCCTG-3' (mutation underlined) and reverse primer 5'-CAGGAAGTTGGG<u>ACC</u>GTCGGTGCGG-3' were used to mutate Ser[125] to Gly[125], while the forward primer 5'-TGGTCCGCACCGAC<u>GAG</u>CCCAACTTCCTGTGCT-3' and reverse primer 5'-AGCACAGGAAGTTGGG<u>CTC</u>GTCGGTGCGGACCA-3' were used to mutate Ser[125] to Glu[125]. The forward primer 5'-GGGGGAGACCGGG<u>GCA</u>CCTTCCAGGATGGT-3' and reverse primer 5'-ACCATCCTGGAAGG<u>TGC</u>CCGGTCTCCCCC-3' were used to mutate Ser[472] to Ala[472], while the forward primer 5'-CGGGGGAGACCGG<u>GAG</u>CCTTCCAGGATGGTC-3' and reverse primer 5'-GACCATCCTGGAAGG<u>CTC</u>CCGGTCTCCCCCG-3' were used to mutate Ser[472] to Glu[472]. The Runx2 gene was sequenced to verify the presence of the desired mutation (Seqwright, Houston, TX).

Osteoblastic Differentiation Assays

Osteoblastic differentiation assays were performed as described previously [66, 67]. Gene expression was investigated at 1, 3, and/or 7 days post-transduction by quantitative RT-PCR using rat-specific primers [137]. Primers used for the analysis of MKP-1 (NM_053769) were 5'-AGTTTCACGTGCCACCGG-3' (forward) and 5'-GTTATTGCATTGCTCCTCCCA -3' (reverse). Alkaline phosphatase (ALP) activity was quantified at 7 days post-transduction using 4-methyl-umbelliferyl-phosphate substrate and normalized to total protein. Matrix mineralization was assessed at 14 and

55

21 days post-transduction by von Kossa histochemical staining for phosphate deposits. Mineralized surface area was quantified by automated image analysis of twenty-four representative 2X images. FTIR spectroscopy was performed on ethanol-fixed cultures pressed into KBr pellets using a Nexus 470 FTIR spectrometer (ThermoNicolet, Madison, WI).

Immunoprecipitation and Western Blot Analysis

Cells were lysed in 50 mM Tris-HCl, pH 7.5, 150 mM NaCl, 0.5% (v/v) NP-40, 350 μg/ml PMSF, 10 μg/ml leupeptin, 10 μg/ml aprotinin, 1 mM Na_3VO_4, and 50 mM NaF after 7 days in culture. Whole cell extracts (150 μg protein) were immunoprecipitated with 5 μl of anti-Runx2 antibody (Santa Cruz Biotechnology, Santa Cruz, CA) and 20 μl protein A agarose beads. Immune complexes were resolved on 12% SDS-PAGE gels, transferred to nitrocellulose, and blotted with anti-AML3 (Oncogene, San Diego, CA) and anti-phosphoserine (ab9335, Abcam, Cambridge, MA or 7F12, Biomol, Plymouth Meeting, PA), followed by sequential incubation in biotin-conjugated anti-IgG and alkaline phosphatase-conjugated anti-biotin antibodies. Immunoreactivity was detected using ECF substrate (Amersham Bioscience, Piscataway, NJ) and a Fuji Image Analyzer. Similar trends were observed for both phosphoserine antibodies. Western blot analysis of whole cell lysates was performed with anti-AML3, anti-ERK (Santa Cruz Biotechnology, Santa Cruz, CA), anti-phosphoERK (Cell Signaling Technology, Beverly, MA), anti-MKP-3 (C-20: Santa Cruz Biotechnology), anti-MKP-1 (M-18 or C-19: Santa Cruz Biotechnology), and anti-GAPDH (Chemicon, Temecula,

CA) antibodies. Adobe Photoshop image analysis software was used to quantify the intensity of the Western blot bands.

Data Analysis

Experiments were performed at least three times in triplicate, each with unique Runx2 retroviral supernatant preparations, and two independent fibroblast isolates. No differences were observed between unmodified and empty vector-transduced cells in all assays. Data are reported as mean ± standard error of the mean, and statistical comparisons using SYSTAT 8.0 were based on an analysis of variance and Tukey's test for pairwise comparisons within timepoints, with a p-value < 0.05 considered significant. In order to make the variance independent of the mean, statistical analysis of real-time PCR data was performed following logarithmic transformation of the raw data [66].

Results

DEX decreases Runx2 serine phosphorylation

Because DEX treatment did not alter Runx2 gene expression, we examined the effects of this hormone on Runx2 total protein and phosphoserine levels by immunoprecipitation and Western blot analysis. Significant amounts of Runx2 protein were detected in Runx2-transduced samples compared to unmodified control cells (Fig. 4.1A,B). Surprisingly, addition of DEX to Runx2-transduced cells significantly decreased Runx2 serine phosphorylation, while total Runx2 protein levels remained unchanged (Fig. 4.1C,D). Omission of immunoprecipitation antibody or cell lysates in negative controls demonstrated the stringency and specificity of the immunoprecipitation

57

procedure. These findings indicate that DEX regulates Runx2 phosphorylation, with no net effect on Runx2 mRNA or protein levels. This DEX-mediated decrease in Runx2 serine phosphorylation correlates with and may be functionally linked to DEX-mediated synergistic induction of osteoblastic differentiation.

Mutation of Ser^{125} decreases Runx2 serine phosphorylation

Several serine phosphorylation sites have been identified on the Runx2/Cbfa1 type I isoform; however, Ser^{104} (corresponding to Ser^{125} on Runx2 type II) was the only residue that exhibited changes in phosphorylation during BMP-2 induced osteogenesis in C2C12 cells [255]. Furthermore, phosphorylation of this serine negatively regulated the transcriptional activity of Runx2. In order to assess whether Ser^{125} is involved in the observed net decrease in Runx2 serine phosphorylation following DEX-treatment, site-directed mutagenesis was performed on this residue in the full-length Runx2 construct (Fig. 4.2A). Mutation of Ser^{125} to glutamic acid (125Glu) mimics constitutive phosphorylation of this residue by placing a bulky, negatively charged group at the site in the same manner as the presence of phosphoserine [257]. Mutation of Ser^{125} to glycine (125Gly) leads to constitutive dephosphosphorylation by preventing post-translational modification of this residue. Primary dermal fibroblasts were transduced with wild-type Runx2 (Runx2-WT), Runx2-125Gly, or Runx2-125Glu retrovirus and cultured in osteogenic media with or without DEX. Retroviral transduction efficiency was approximately 65% for all retroviral stocks (Fig. 4.2B). Runx2 mRNA expression was upregulated by 2 orders-of-magnitude at 3 days post-transduction with Runx2-WT, Runx2-125Gly, and Runx2-125Glu retroviral vectors compared to control cells (Fig.

58
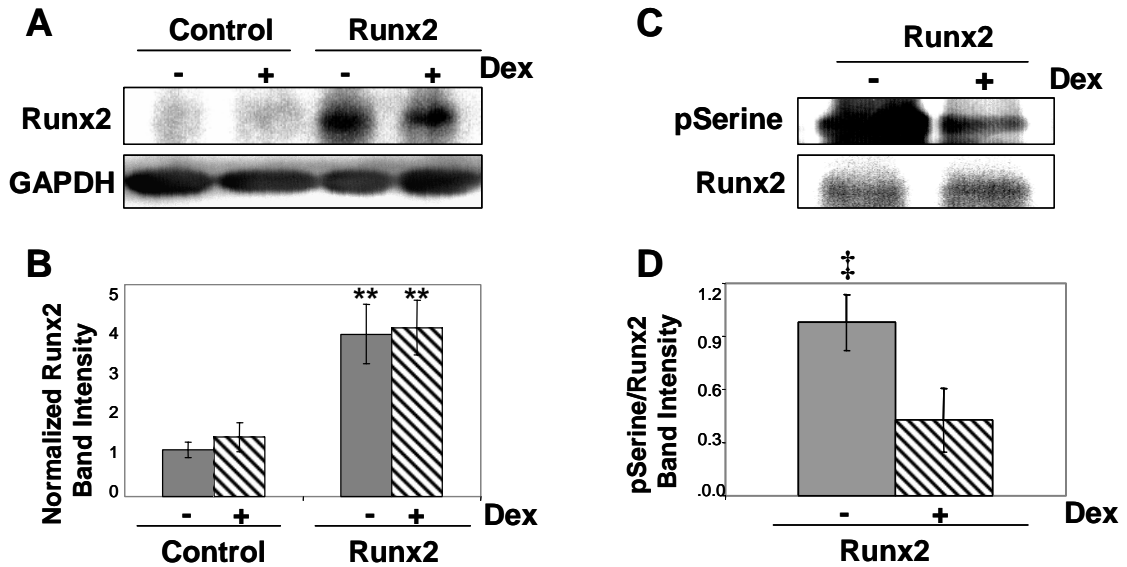
Figure 4.1. DEX decreases Runx2 serine phosphorylation. Primary dermal fibroblasts were transduced with Runx2 or left unmodified for controls and cultured in osteogenic media with and without 10 nM DEX. (A) Runx2 protein levels were examined at 7 days post-transduction by Western blotting of whole cell lysates with a polyclonal antibody against Runx2. GAPDH was used as a loading control. (B) Quantification of Runx2 band intensities (Mean + SEM, n=9; ANOVA: p<0.05; ** different from unmodified and DEX only controls (p< 0.05)). (C) Runx2 phosphoserine levels were assessed by immunoprecipitation of whole cell lysates with an antibody against Runx2 and Western blotting with antibodies against Runx2 and phosphoserine. (D) Quantification of Runx2 phosphoserine band intensities (Mean ± SEM, n=9; ANOVA: p<0.05; ‡ different from Runx2+DEX (p< 0.05)).
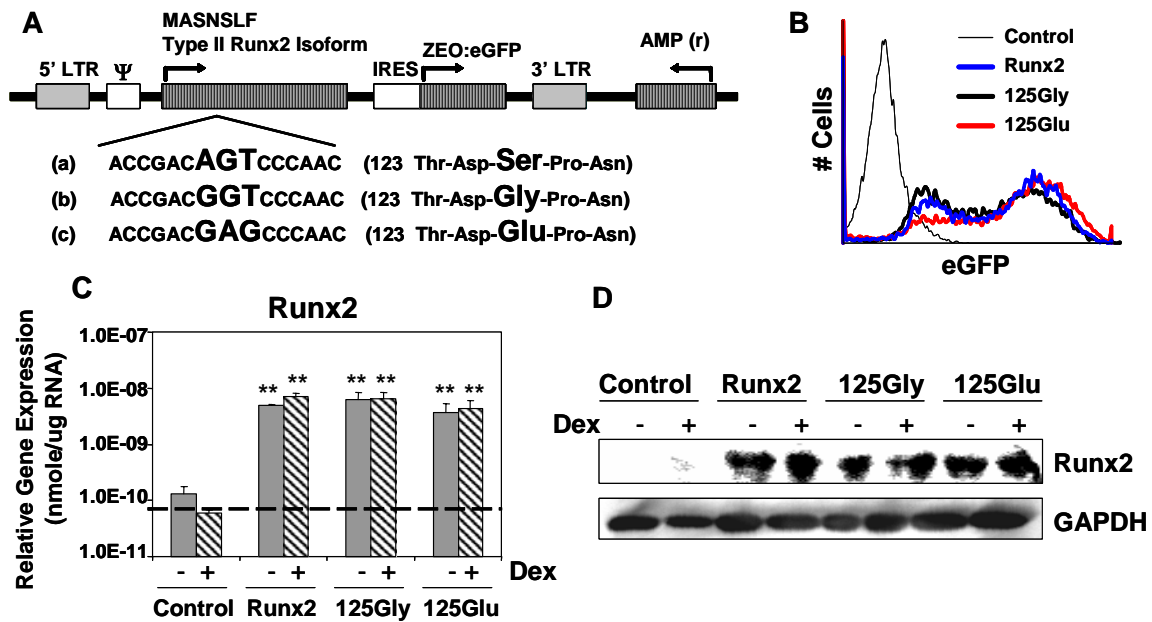
Figure 4.2. Site directed mutagenesis of the Runx2 retroviral vector. (A) Schematic diagram of the Runx2 retroviral expression vector and its mutated derivatives, including (a) Runx2-WT control, (b) Runx2-125Gly (mimicking constitutively dephosphorylation), and (c) Runx2-125Glu (mimicking constitutively phosphorylation). Primary dermal fibroblasts were transduced with Runx2-WT, Runx2-125Gly, or Runx2-125Glu retrovirus and cultured in osteogenic media with (+) and without (-) 10 nM DEX. (B) Retroviral transduction efficiency was determined at 3 days post-transduction by flow cytometry detection of eGFP expression. Unmodified cells were used to detect autoflourescence. (C) Runx2 mRNA expression was assessed by quantitative RT-PCR at 3 days post-transduction and expressed on a logarithmic scale (Mean + SEM, n=12; ANOVA: $p < 1E-11$; ** different from unmodified and DEX only controls ($p < 0.05$)). Detection limit was determined by reactions without cDNA is shown as a dotted line. (D) Runx2 protein levels were examined at 7 days post-transduction by Western blotting of whole cell lysates with a polyclonal antibody against Runx2. GAPDH was used as a loading control. Blot is representative of data from two separate experiments in triplicate.

60

4.2C). Moreover, equivalent levels of Runx2-WT, Runx2-125Gly, and Runx2-125Glu protein were detected at 7 days post-transduction (Fig. 4.2D). Overall, there were no differences in Runx2 mRNA or protein levels between transduced samples, excluding the possibility that experimental results obtained with these retroviral vectors were skewed by differences in Runx2 protein levels and/or transduction efficiencies.

The effect of Ser^{125} on Runx2 phosphoserine levels was investigated at 7 days post-transduction by immunoprecipitation and Western blotting (Fig. 4.3). Mutation of Ser^{125} to glycine significantly reduced total Runx2 serine phosphorylation in the absence of DEX, suggesting that this serine residue is a major phosphorylation site on exogenously-expressed Runx2 in primary dermal fibroblasts. Furthermore, no apparent net change in Runx2-125Gly serine phosphorylation was observed upon addition of DEX, while the hormone significantly reduced phosphoserine levels in Runx2-WT. Mutation of Ser^{125} to glutamic acid had similar effects on Runx2 phosphoserine levels as those observed upon mutation of this residue to glycine (unpublished data). These results indicate that Runx2 is phosphorylated at a basal level in untreated cultures, particularly on Ser^{125}, and suggest that DEX modulates the phosphorylation state of Runx2 Ser^{125} in parallel with the stimulation of osteogenesis.

Runx2-Ser^{125} phosphorylation regulates DEX-induced osteoblastic differentiation

Phosphorylation of Ser^{125} has been reported to negatively regulate Runx2 transactivation in NIH3T3 cells transfected with an OCN promoter-driven reporter gene [255]. However, the direct effects of wild-type Runx2 and its mutated derivatives on osteoblastic differentiation have not been examined. We hypothesized that the

61

A

| | Runx2 | | | | | | 125Gly | | | | | | Dex |

pSerine

Runx2

B

‡ ¥ ##

pSerine/Runx2 Band Intensity

(y-axis: 0, 0.2, 0.4, 0.6, 0.8, 1.0, 1.2, 1.4)

Dex: - + (Runx2), - + (125Gly)

Figure 4.3. Mutation of Ser[125] decreases Runx2 serine phosphorylation. Primary dermal fibroblasts were transduced with Runx2-WT or Runx2-125Gly retrovirus and cultured in osteogenic media with (+) and without (-) 10 nM DEX.   (A) Runx2 phosphoserine levels were assessed by immunoprecipitation of whole cell lysates with an antibody against Runx2 and Western blotting with antibodies against Runx2 and phosphoserine. (B) Quantification of normalized Runx2 phosphoserine band intensities (Mean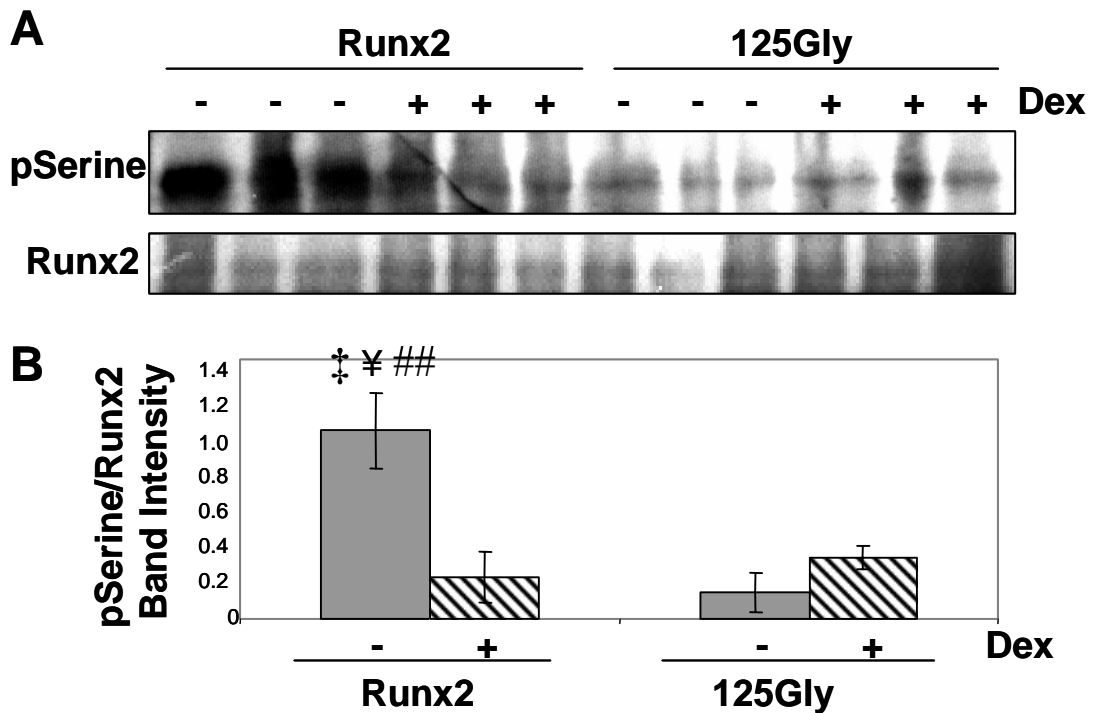 ± SEM, n=3; ANOVA: $p < 0.05$; ‡ different from Runx2 + DEX, ¥ different from 125Gly - DEX, and ## different from 125Gly + DEX ($p < 0.05$); representative data from three separate experiments in triplicate).

phosphorylation state of Runx2-Ser[125] plays a critical role in DEX-induced osteogenesis. Primary dermal fibroblasts were transduced with Runx2-WT, Runx2-125Gly, or Runx2-125Glu retrovirus and cultured in osteogenic media supplemented with or without 10 nM DEX. Mutation of Ser[125] to glycine, mimicking constitutive dephosphorylation, significantly upregulated OCN, BSP, and OPN mRNA transcript expression compared to Runx2-WT in the absence of DEX (Fig. 4.4). Treatment of Runx2-125Gly-expressing cultures with DEX had no significant effect on OCN gene expression, but enhanced BSP and OPN gene expression. In contrast, mutation of Serine[125] to glutamic acid, mimicking constitutive phosphorylation, inhibited Runx2 transactivation of all three osteoblastic genes, while DEX partially recovered the effect of Runx2-125Glu on OCN and BSP gene expression only. These results corroborate the observations of Wee et al. that Ser[125] phosphorylation inhibits Runx2 transactivation of an OCN-driven reporter gene.

Consistent with alterations in osteoblastic gene expression, mutation of Ser[125] to glycine stimulated ALP activity to levels significantly higher than Runx2-WT cultures and comparable to Runx2-WT + DEX treated cultures (Fig. 4.5A). DEX had no additional effect on ALP activity in Runx2-125Gly-expressing cultures. Mutation of Ser[125] to glutamic acid diminished ALP activity to levels comparable to unmodified control cultures and DEX treatment partially recovered this activity. Furthermore, mutation of Ser[125] to glycine also significantly enhanced matrix mineralization compared to Runx2-WT-expressing cultures in the absence of DEX (Fig. 4.5B,C). DEX treatment synergistically enhanced mineralization in both Runx2-WT and Runx2-125Gly expressing cells. Conversely, mutation of Ser[125] to glutamic acid completely blocked mineralization of these cultures in the absence and presence of DEX. The mineral phase
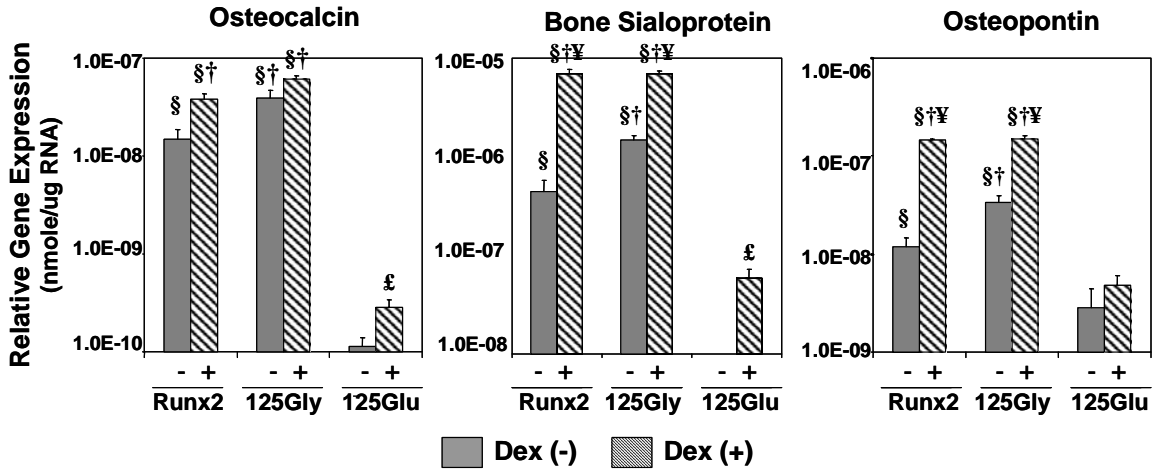
Figure 4.4. Constitutive Ser^{125} phosphorylation negatively regulates Runx2-mediated expression of osteoblastic genes. Primary dermal fibroblasts were transduced with Runx2-WT, Runx2-125Gly, or Runx2-125Glu retrovirus and cultured in osteogenic media with (+) and without (-) 10 nM DEX. mRNA levels were investigated by quantitative RT-PCR at 7 days post-transduction (Mean + SEM, n=6; ANOVA: $p<1E-6$; † different from Runx2 - DEX, ¥ different from 125Gly - DEX, § different from 125Glu - DEX and 125Glu + DEX, and £ different from 125Glu - DEX ($p< 0.05$)). Relative gene expression is expressed on a logarithmic scale.

in Runx2-WT and Runx2-125Gly cultures displayed FTIR spectrograms similar to those shown in Fig. 3.2D with the characteristic bands of a carbonate-containing, poorly crystalline hydroxyapatite (data not shown).

Finally, these experiments were repeated in primary bone marrow stromal cells (BMSCs) in order to ensure that results were not an artifact of the non-osteogenic cell source used in this study (Fig. 4.6A,B). DEX treatment alone stimulated osteoblastic differentiation in BMSCs, including ALP activity and matrix mineralization, compared to untransduced controls. Moreover, co-treatment with Runx2-WT and DEX enhanced osteogenic differentiation in BMSCs compared to Runx2-WT overexpression or DEX treatment alone. Mutation of Ser^{125} to glycine stimulated ALP activity and mineralized nodule formation to levels significantly higher than Runx2-WT cultures and equivalent to Runx2-WT + DEX treated cultures. DEX treatment showed no additional effect on osteogenesis in Runx2-125Gly-expressing cultures. Mutation of Ser^{125} to glutamic acid antagonized ALP activity and mineralization to similar levels as untransduced BMSC controls with or without DEX. Overall, these results demonstrate equivalent functional effects of Runx2-Ser^{125} during DEX-induced osteogenesis in primary BMSCs and Runx2-engineered primary dermal fibroblasts. We speculate that the low levels of ALP activity and mineralization observed in untransduced and Runx2-125Glu-expressing BMSCs may be due to interactions between DEX and endogenously-expressed Runx2 or additional Runx2-independent pathways.
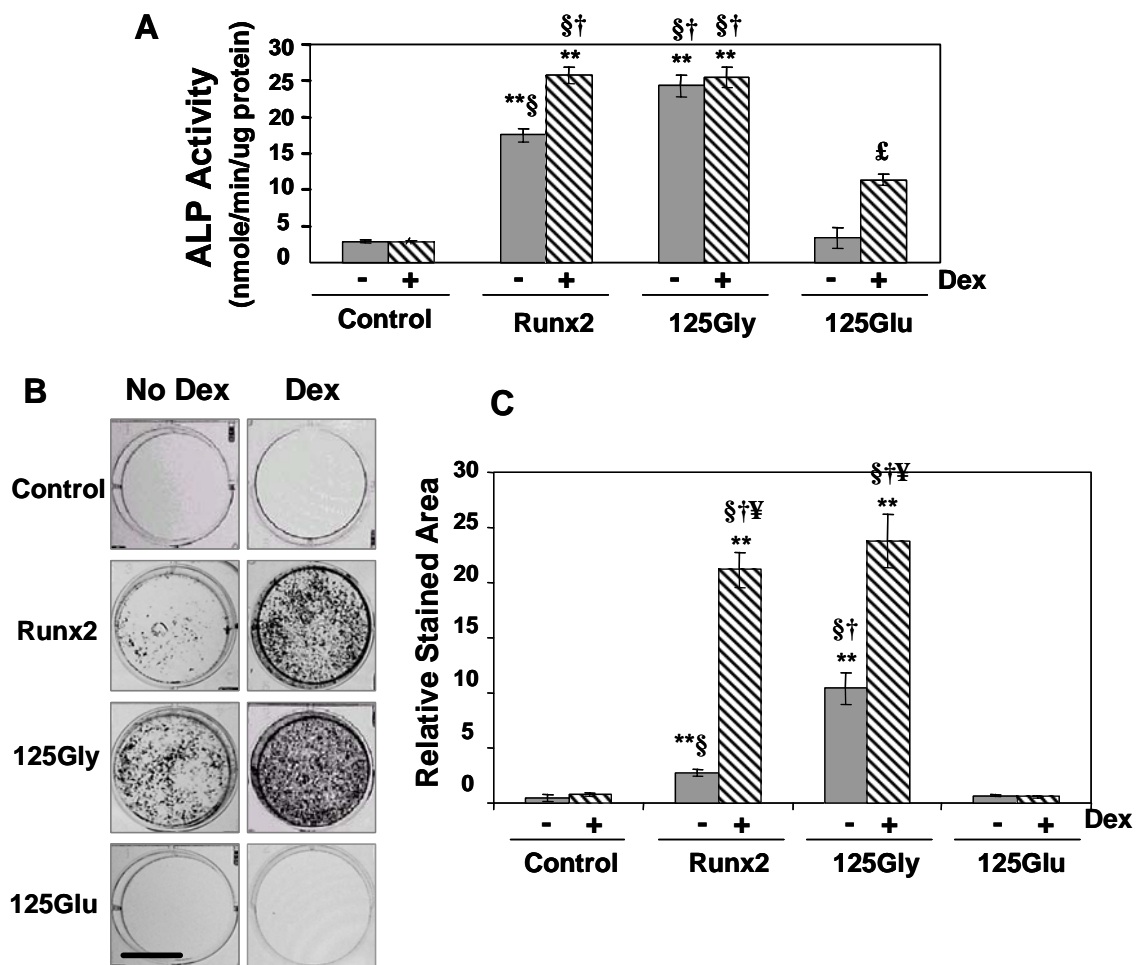
Figure 4.5. **Constitutive phosphorylation of Runx2 Ser[125] inhibits osteoblastic differentiation.** Cells were transduced with Runx2-WT, Runx2-125Gly, or Runx2-125Glu retrovirus and cultured in osteogenic media with (+) and without (-) 10 nM DEX. (A) ALP activity was examined by a biochemical assay at 7 days post-transduction (Mean ± SEM, n=6; ANOVA: $p<1E-11$; ** different from unmodified and DEX only controls, † different from Runx2 - DEX, Φ different from 125Gly - DEX, § different from 125Glu - DEX and 125Glu + DEX, and Ω different from 125Glu ($p< 0.05$)). (B) Mineralized matrix deposition was assessed by von Kossa staining for phosphate-positive regions and (C) quantified by image analysis at 14 days post-transduction (Mean ± SEM, n=6; ANOVA: $p<1E-11$, ** different from unmodified and DEX only controls, † different from Runx2 - DEX, ¥ different from 125Gly - DEX, § different from 125Glu - DEX and 125Glu + Dex, and £ different from 125Glu - DEX ($p< 0.05$)). Scale bar 2 cm.
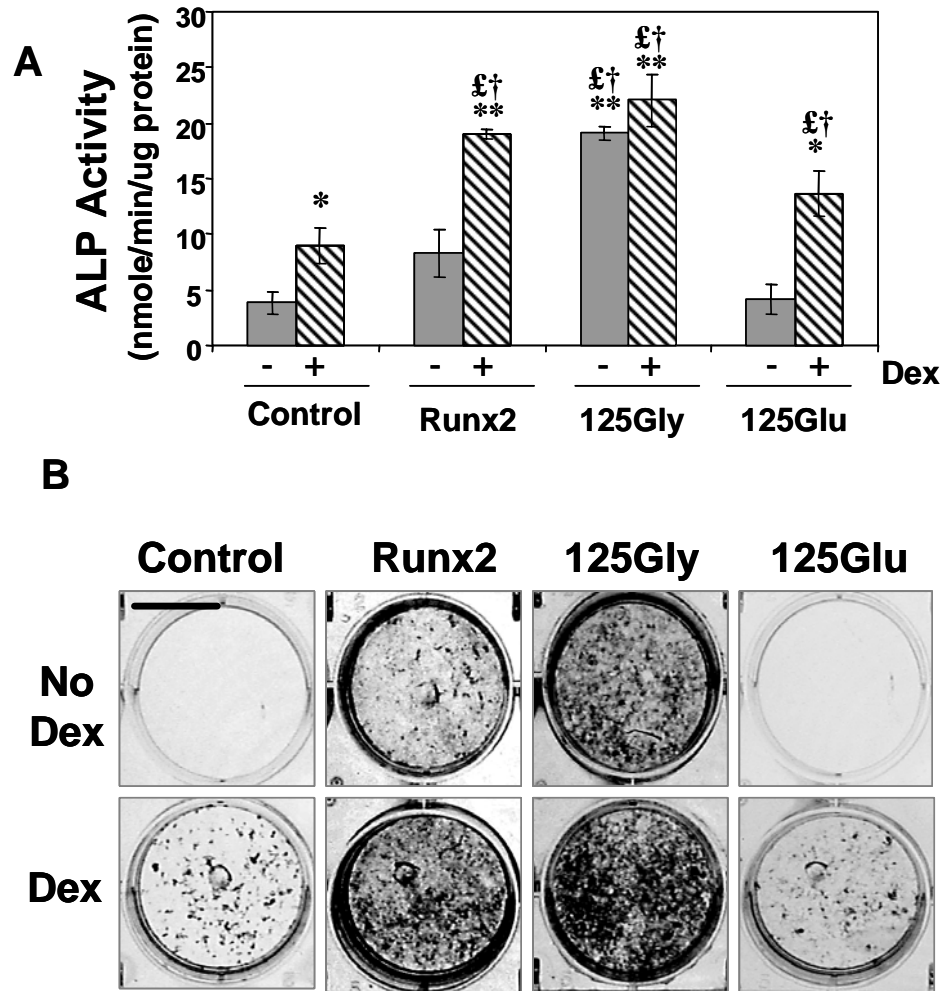
Figure 4.6. Runx2 phosphorylation regulates osteoblastic differentiation in primary bone marrow stromal cells. BMSC were transduced with Runx2-WT, Runx2-125Gly, or Runx2-125Glu retrovirus and cultured in osteogenic media with (+) and without (-) 10 nM DEX. (A) ALP activity was examined by a biochemical assay at 7 days post-transduction (Mean ± SEM, n=3; ANOVA: $p<1E-4$; * different from unmodified cell control, ** different from unmodified and DEX only controls, † different from Runx2 - DEX, and £ different from 125Glu - DEX ($p< 0.05$)). (B) Mineralized matrix deposition was assessed by von Kossa staining for phosphate-positive regions and image analysis at 14 days post-transduction. Image represents data from two separate experiments in triplicate. Scale bar indicates 2 cm.

67

DEX upregulates MKP-1 through a GC receptor-mediated transcriptional mechanism

As a first step toward elucidating the DEX-mediated mechanism(s) involved in the regulation of Runx2 phosphorylation, we examined the ability of DEX to activate components of the mitogen-activated protein kinase (MAPK) signaling pathway. In particular, MAPK phosphatase-1 (MKP-1) is a dual specificity phosphatase that dephosphorylates and inactivates MAPKs such as extracellular signal-regulated kinase (ERK1/2), c-Jun N-terminal kinase (JNK), and p38 protein kinase [258-261]. Pharmacological doses of DEX ($\geq$ 100 nM) have been shown to upregulate MKP-1 in a variety of cell types [261-264]. We postulated that MKP-1 may be stimulated by physiologic concentrations of DEX during osteoblastic differentiation in our experimental model. Primary fibroblasts transduced with Runx2 retrovirus or left unmodified as controls were cultured in osteogenic media supplemented with or without DEX. MKP-1 mRNA and protein levels were evaluated at 1, 3, and 7 days post-transduction by quantitative RT-PCR and Western blot analysis, respectively. DEX treatment stimulated MKP-1 gene (Fig. 4.7A) and protein (Fig. 4.7B) expression in unmodified and Runx2-expressing cultures relative to untreated controls. MKP-1 was upregulated after 3 days and remained elevated through 7 days in culture, which correlates with the decrease in Runx2 serine phosphorylation observed after treatment with DEX for 7 days. Overexpression of Runx2 significantly inhibited MKP-1 mRNA and protein levels at 3 and 7 days post-transduction compared to unmodified controls and addition of DEX to Runx2-transduced cultures restored MKP-1 to basal expression levels. Moreover, the induction of MKP-1 mRNA by DEX was abrogated by treatment with the partial GC receptor-agonist/antagonist RU486 (100 nM) for 72 hours (Fig. 4.7C). 18S gene expression
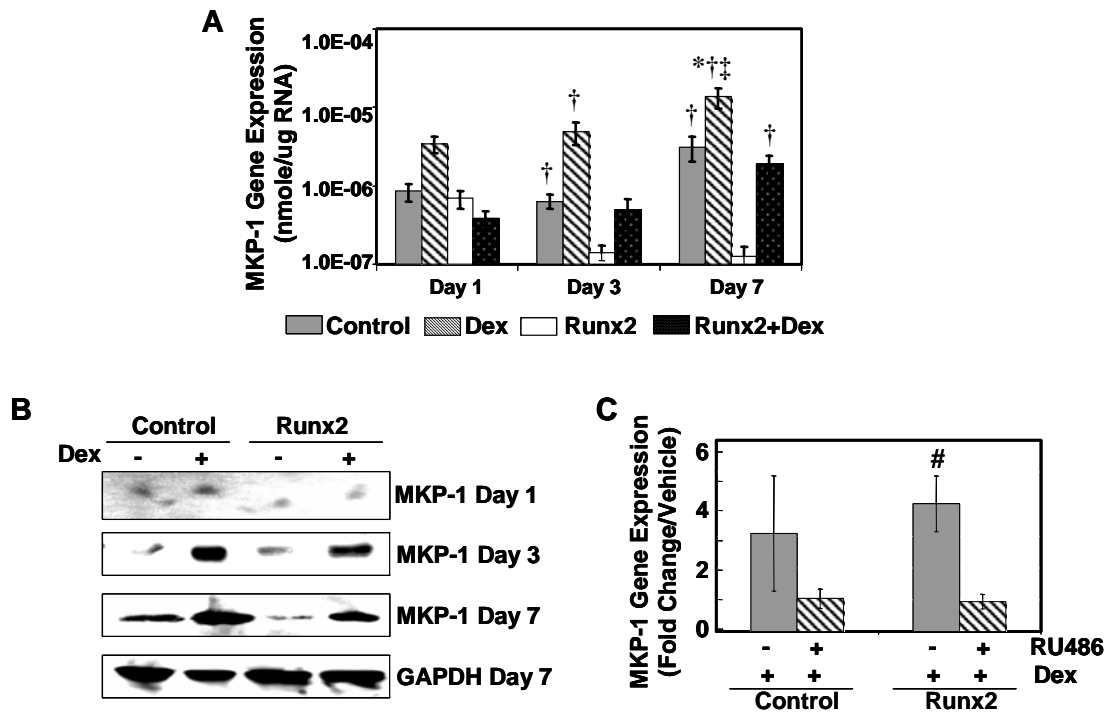
Figure 4.7. **DEX upregulates MKP-1 through a GC receptor-mediated transcriptional mechanism.** Primary dermal fibroblasts were transduced with Runx2 retrovirus or left unmodified for controls and cultured in osteogenic media with (+) and without (-) 10 nM DEX. (A) MKP-1 mRNA expression was investigated by quantitative RT-PCR at 1, 3, and 7 days post-transduction and expressed on a logarithmic scale (Mean + SEM, n=12; ANOVA: $p<1E-11$; * different from unmodified cell control, † different from Runx2, and ‡ different from Runx2+DEX ($p< 0.05$)). (B) MKP-1 protein levels were examined at 1, 3, and 7 days post-transduction by Western blot analysis. GAPDH was used as a loading control. Blots are representative of data from three separate experiments in triplicate. (C) MKP-1 mRNA expression was investigated by quantitative RT-PCR at 3 days post-Runx2 transduction after treatment with vehicle (ethanol), DEX (10 nM) or concomitant DEX/RU486 (100 nM) for 72 hours. Fold induction is shown relative to control samples without (-) DEX treatment (Mean + SEM, n=3; ANOVA: $p<0.05$; # different from Runx2+DEX+RU486 ($p< 0.05$)).

69

remained unchanged for all treatment groups in this experiment. Finally, no differences in p38 MAPK, protein phosphatase 5, and protein tyrosine phosphatase type D expression were observed among experimental groups, suggesting that the observed shifts in expression were specific for MKP-1. Taken together, this data demonstrates that DEX induces MKP-1 in Runx2-expressing fibroblasts through a GC receptor-mediated mechanism.

Inhibition of MKP-1 attenuates the DEX-mediated decrease in Runx2 serine phosphorylation

Sanguinarine has recently been identified as a potent and selective inhibitor of MKP-1 activity, exhibiting at least a 3-fold selectivity for MKP-1 over dual specificity phosphatases such as MKP-3, VH-1-related phosphatase, Cdc25B, and protein-tyrosine phosphatase 1B [265]. We utilized this inhibitor to assess the role of MKP-1 during the DEX-mediated modulation of Runx2 serine phosphorylation. Primary dermal fibroblasts were transduced with Runx2 retrovirus or left unmodified for controls and cultured in osteogenic media with (+) and without (-) 10 nM DEX. After 7 days in culture, cells were treated with vehicle (ethanol), vehicle+DEX (10 nM), sanguinarine (50 μM), or sanguinarine (50 μM) + DEX (10 nM) for 30 minutes. Protein expression for MKP-1, MKP-3, phospho-ERK, ERK, and GAPDH was assessed by Western blotting (Fig. 4.8A). MKP-1 protein levels were markedly decreased by sanguinarine in unmodified and Runx2-expressing fibroblasts. Consequently, the decrease in ERK phosphorylation caused by DEX-induction of MKP-1 was reversed upon treatment with sanguinarine. ERK and GAPDH total protein levels remained unchanged for all experimental

70

conditions. Notably, MKP-3 protein levels were not significantly altered by sanguinarine, suggesting that the inhibitor was selective for MKP-1 over this closely related dual specificity phosphatase. Runx2 phosphoserine levels were then examined by immunoprecipitation and Western blot analysis (Fig. 4.8B). Sanguinarine treatment blocked the DEX-mediated decrease in Runx2 serine phosphorylation, suggesting that DEX modulates the inhibitory phosphorylation of Runx2 via MKP-1.

Discussion

We demonstrate that a combination of DEX supplementation and constitutive Runx2 overexpression synergistically induced osteoblastic differentiation in primary dermal fibroblasts, as characterized by enhanced OCN and BSP gene expression, alkaline phosphatase activity, and biological mineral deposition. DEX treatment decreased Runx2 phosphoserine levels, particularly on Serine[125]. Mutation of Ser[125] to glutamic acid, mimicking constitutive phosphorylation, inhibited Runx2-induced osteogenic differentiation, which was not rescued by DEX treatment. Conversely, mutation of Ser[125] to glycine, mimicking constitutive dephosphorylation, markedly increased osteogenic differentiation, which was enhanced by but did not require additional DEX supplementation. The DEX-induced decrease in Runx2 phosphorylation correlated with upregulation of MKP-1 through a GC-receptor-dependent mechanism. Furthermore, inhibition of MKP-1 abrogated the effect of DEX on Runx2 phosphoserine levels. To our knowledge, this is the first time that DEX-activated MKP-1 expression has been implicated in the regulation of Runx2 phosphorylation. Collectively, these results suggest that DEX induces osteogenesis by modulating the phosphorylation state of a

71

A

	Vehicle				Sanguinarine			
	control		Runx2		control		Runx2	
Dex	-	+	-	+	-	+	-	+

MKP-1

MKP-3

phospho-p44 ERK
phospho-p42 ERK

p44 ERK
p42 ERK

GAPDH

B

	Runx2			
	Vehicle		Sanguinarine	
Dex	-	+	-	+
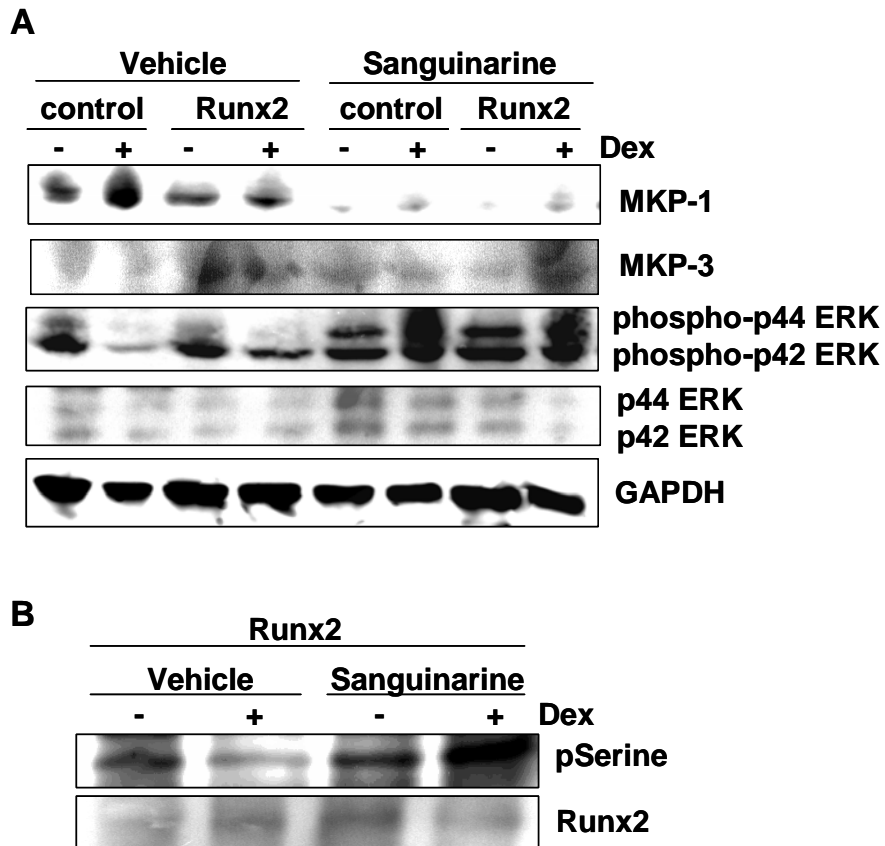
pSerine

Runx2

Figure 4.8. Inhibition of MKP-1 attenuates the DEX-mediated decrease in Runx2 serine phosphorylation. Primary dermal fibroblasts were transduced with Runx2 retrovirus or left unmodified for controls and cultured in osteogenic media with (+) and without (-) 10 nM DEX. After 7 days in culture, cells were treated with vehicle (ethanol), vehicle+DEX (10 nM), sanguinarine (50 μM), and sanguinarine (50 μM) + DEX (10 nM) for 30 minutes. (A) Western blot analysis of whole cell lysates after 7 days in culture was conducted with antibodies against MKP-1, MKP-3, pERK, and ERK. GAPDH was used as a loading control. Blot is representative of data from three separate experiments in triplicate. (B) Runx2 phosphoserine levels were assessed by immunoprecipitation of whole cell lysates with an antibody against Runx2 and Western blotting with antibodies against Runx2 and phosphoserine. Blot is representative of data from two separate experiments in triplicate.

negative regulatory serine residue (Ser[125]) on Runx2/Cbfa1 via MKP-1. This work offers important insights into the role of Runx2 during hormone-regulated skeletal development and maintenance.

Primary dermal fibroblasts engineered to express elevated and sustained levels of Runx2 were utilized for the investigation of the effects of DEX on osteoblastic differentiation. A major advantage of this model system is that it allows for direct analysis of the Runx2 type II isoform and its mutants during GC-induced osteogenesis in the absence of endogenous Runx2 and DEX-responsive, osteoblast-specific pathways. Notably, DEX stimulation of Runx2-expressing fibroblasts induced several important components of the osteoblastic differentiation program, including osteocalcin and bone sialoprotein gene expression, ALP activity, and matrix mineralization, whereas DEX treatment alone did not significantly influence any of these osteoblastic markers. This enhancement in osteogenesis is consistent with the effects of DEX on several osteoblastic systems, including rat calvarial cells, rat and human bone marrow stromal cells, and chick periosteal cells [137, 238, 239, 241, 242, 266]. While these model systems have been instrumental in the elucidation of numerous DEX-responsive signaling pathways, they are limited because they prevent the isolation of Runx2-dependent from Runx2-independent pathways. Finally, in order to ensure that these results were not an artifact of the non-osteogenic cell source, we analyzed the effects of Runx2-WT and Runx2-Ser[125] mutants during DEX-induced osteoblastic differentiation in primary bone marrow stromal cells. This osteoblastic model exhibited equivalent functional responses during DEX-induced osteoblastic differentiation compared to Runx2-engineered fibroblasts. Based on these

results, we hypothesized that the anabolic effects of GCs *in vitro* occur through a Runx2-dependent mechanism involving the post-translational modification of Runx2.

We demonstrate that DEX decreases Runx2 phosphoserine levels, particularly on Serine[125], in parallel with osteoblastic differentiation. In contrast, Shui et al. reported that phosphorylation of Runx2 on tyrosine, threonine, and serine residues increases during DEX-induced osteoblastic differentiation in human bone marrow stromal cells [246]. However, this report did not include a "No DEX" condition to isolate the effects of DEX from alternative pathways activated during the onset of osteogenesis. Thus, beyond this correlative evidence, a direct link between DEX and Runx2 phosphorylation has not been established prior to this work. Previous analyses have also shown that collagen, fibroblast growth factor-2, and mechanical loading enhance Runx2 transcriptional activity via the MAPK pathway [252-254]. Moreover, protein kinase A (PKA) also phosphorylates Runx2, and parathyroid hormone enhances Runx2 transactivation of the collagenase-3 promoter through a PKA-dependent pathway [267, 268]. These pathways stimulate Runx2 phosphorylation on putative residues within the C-terminal PST domain [251, 268], but the specific residues targeted have not been identified. Interestingly, while these stimulatory phosphorylation sites were found in the PST domain, Ser[125] is located within the N-terminal runt domain, suggesting that phosphorylation at different regions within the Runx2 protein may play different functional roles in osteoblastic differentiation. Finally, it is important to note that our results do not rule out the possibility that additional Runx2 phosphorylation sites are altered during DEX-induced osteogenesis.

The mutagenesis analysis conducted in this study demonstrates that the phosphorylation state of Runx2-Ser[125] plays a critical role during DEX-induced osteoblastic differentiation. These results offer important insights into skeletal pathogenesis, as mutation of this residue to arginine has been documented in one patient with cleidocranial dysplasia [256]. Ito and colleagues recently identified Ser[14], Ser[104], Ser[451], Ser[485], and Ser[489] as potential phosphorylation sites on the human Runx2/Cbfa1 type I isoform. Of these residues, Ser[104] and Ser[451] were implicated in the negative regulation of Runx2 transcriptional activity. Mutation of Ser[104], corresponding to Ser[125] on the murine Runx2 type II isoform, to both glycine and glutamic acid inhibited Runx2 transactivation of an OCN promoter-driven reporter gene [255]. These results are consistent with our observations for Runx2-mediated differentiation, but contradict reports that mutation of Runx1/AML1c Ser[94], analogous to RUNX2 Ser[125], had no effect on transcriptional activity [269]. Wee and colleagues also reported that the phosphorylation state of Ser[451], corresponding to Ser[472] on the murine Runx2 type II isoform, has a critical role in the transcriptional activity of Runx2 [255]. However, the phosphorylation state of Ser[472] had no apparent effect on Runx2-induced osteogenic gene expression, alkaline phosphatase activity, or mineralization in the present study (unpublished data). Similarly, mutation of Runx1/AML1c Ser[424], corresponding to Runx2 type II Ser[472], did not alter transcriptional activity of this runt domain protein family member [269]. Overall, it is evident that disparities exist in the phosphorylation pattern of Runx protein family members, suggesting that the phosphorylation state of Ser[125] and Ser[472] may be isoform-specific, cell type-specific, or regulated by independent signaling pathways.

The present analysis supports a mechanism by which DEX induces osteoblastic differentiation by modulating the phosphorylation state of a negative regulatory serine on Runx2. The ability of DEX to partially recover osteogenic gene expression and ALP activity in cultures expressing Runx2-125Glu suggests that the hormone may also have auxiliary modes of regulating Runx2 beyond the mechanism detailed in this study. Indeed, GCs may also mediate osteogenesis by a Runx2-dependent mechanism involving the physical association of the transcription factor with co-regulatory proteins. Recent evidence suggests that Runx2 serves as a molecular scaffold, which facilitates the assembly of co-regulatory proteins and accessory transcription factors into a macromolecular transcriptional regulatory complex [65]. Runx2 contains specific functional regions that physically interact with a number of accessory factors [270]. In particular, the runt domain is a 128 amino acid conserved region, which is essential for DNA binding and heterodimerization with transcription factors such as Cbfβ/PEBP2β [271, 272], LEF-1 [273], and c-Fos/c-Jun [267, 274, 275]. The C-terminal PST domain contains a nuclear localization signal, a transcriptional activation region, and a repressor region, and has been shown to co-localize with SMADs [276, 277], CCAAT/Enhancer-binding proteins (C/EBPβ and δ) [278], HES-1, and Groucho/TLE proteins [279]. Osteogenic agents, such as PTH and BMP, regulate the association of Runx2 with several of these factors, but the role of DEX in these protein-protein interactions is poorly understood. Interestingly, Wee et al. found that the mutation of Ser[104] to glutamic acid, which decreased Runx2 transcriptional activity, also appeared to destabilize the protein and inhibit the heterodimerization of Runx2 with CBF-β. Thus, it is possible that the DEX-mediated

regulation of Runx2 phosphorylation alters the interaction of this transcription factor with accessory proteins, which may have downstream effects on Runx2 transcriptional activity. Finally, these results do not rule out the possibility GCs may mediate osteogenesis by Runx2-independent signaling pathway(s), which may cooperatively act with Runx2-stimulated gene products to synergistically induce matrix mineralization.

In summary, we have demonstrated that DEX induces osteogenesis, at least in part, by modulating the phosphorylation state of a negative regulatory serine residue (Ser^{125}) on Runx2 through an MKP-1 dependent mechanism. While this particular mechanism is likely not the sole signaling pathway activated by DEX during osteogenic differentiation, it provides significant insights toward the role of Runx2 phosphorylation during GC-regulated skeletal development.

77

CHAPTER 5

DERMAL FIBROBLASTS GENETICALLY MODIFIED TO EXPRESS RUNX2 AS A MINERALIZING CELL SOURCE FOR BONE TISSUE ENGINEERING*

Introduction

Over 600,000 bone grafting procedures are performed annually in the United States to treat non-healing skeletal defects caused by traumatic injury, osteodegenerative diseases, and cancer.[3, 80] Autograft implantation is considered the gold standard in bone repair, but is limited by donor site morbidity, pain, and inadequate supply of tissue.[77] Because of these complications, allogenic bone and synthetic materials have been increasingly utilized as bone graft substitutes.[80] However, allografts suffer from reduced bioactivity and poor mechanical properties due to tissue processing, while synthetic materials typically incite an inflammatory response in the host.[78, 79] Synthetic materials such as metals, calcium phosphate ceramics, bioactive glasses, and polymers have also been explored for bone grafting applications, but generally display insufficient regenerative potential to warrant the inflammatory host reaction [80]. More recently, osteogenic devices containing recombinant bone morphogenetic protein-2 (BMP-2) or BMP-7 have shown efficacy in human clinical trials and have been approved by regulatory agencies for the treatment of non-healing fractures and spinal fusion.[4, 6]

Nevertheless, the clinical success of this growth-factor based approach continues to be hampered by suboptimal delivery vehicles, short biological half-life, and safety issues associated with aphysiologic dosage.[7, 8]

Bone tissue engineering has emerged as a promising alternative to conventional grafting strategies.[99, 280, 281] In this approach, osteogenic cells and/or bioactive growth factors are integrated into three-dimensional scaffolds to produce hybrid constructs for skeletal repair.[101] The success of bone tissue engineering to date has been limited in part by inadequate availability of a mineralizing cell source which can be easily obtained in sufficient quantities and maintain osteoblastic phenotype during *in vitro* culture and expansion. Traditional cell-based approaches typically involve the use of terminally differentiated osteoblasts,[102, 103] osteogenic cell lines,[105, 282] unfractionated bone marrow stroma,[106, 107] or purified mesenchymal stem cells.[108, 109, 283] Marrow-derived progenitors, in particular, have been successfully utilized to repair orthotopic bone defects in animal models.[13, 14, 17, 18, 114] However, the widespread use of these precursors remains limited by their low frequency in healthy marrow,[116] complex and painful cell procurement process,[284] and reduced mineralization capacity associated with the age and disease-state of the donor.[16, 19] Overall, the identification of a sustained, autologous mineralizing cell source would be significant toward development of mechanically robust bone grafts which genetically match the patient and are capable of healing large, critical sized defects.

Non-osteogenic cells, such as skin fibroblasts, are a particularly attractive cell source alternative because they are easy to harvest from autologous donors and display a high capacity for *in vitro* expansion. Genetic engineering strategies focusing on soluble

79

osteoinductive factors have been effectively applied to promote osteoblastic differentiation in fibroblastic cell types.[20-23] Notably, dermal fibroblasts transduced with adenoviral vectors encoding for either BMP-2 or BMP-7 form significant amounts of bone in both ectopic implantation sites and critical-sized calvarial defects.[24, 25] Despite these advances, complex release kinetics and uncontrolled paracrine signaling to neighboring non-osseous tissues may limit the clinical success of this approach.[285]

The present work is fundamentally different from BMP-based gene therapy strategies because it focuses on retroviral gene delivery of the osteogenic transcription factor Runx2/Cbfa1 and may avoid detrimental side effects associated with unregulated growth factor secretion. Runx2 is an essential transcriptional regulator of osteoblast differentiation and bone formation.[59, 60] It functions as a transcriptional scaffolding protein which binds to the promoter region of skeletal target genes and regulates their expression.[64, 65] Homozygous deletion of this transcription factor arrests osteoblast maturation, resulting in total absence of endochondral and intramembranous ossification.[61] We and others have established that viral overexpression of Runx2 upregulates osteogenic gene expression in a wide range of cell types, including the MC3T3-E1 osteoblastic cell line,[66] primary BMSCs,[137, 286, 287] and primary skeletal myoblasts.[117, 135] In contrast, mineral deposition is induced by Runx2 gene delivery in a cell type-dependent manner and has been reported by several groups as insufficient to induce significant nodule formation in primary dermal fibroblasts and fibroblastic cell lines both *in vitro* and *in vivo*.[23, 24, 66] However, we have recently demonstrated that a combination of constitutive retroviral Runx2-expression and treatment with the steroid hormone dexamethasone synergistically induces matrix mineralization in primary dermal

80

fibroblasts cultured in monolayer.[136] This surprising result suggested that Runx2-engineered primary dermal fibroblasts have the capacity to create mineralized templates for bone repair and may still have potential as a cell source for bone tissue engineering applications if exposed to the appropriate osteogenic cues.

In the present study, we describe a hybrid *ex vivo* gene therapy/tissue engineering strategy based on retroviral gene delivery of the osteogenic transcription factor Runx2 to non-osteoblastic primary dermal fibroblasts. We demonstrate that sustained expression of Runx2 induces osteoblastic differentiation and biological mineral deposition in primary dermal fibroblasts cultured on fibrous collagen scaffolds *in vitro* and *in vivo*. These results establish Runx2-genetic engineering as a strategy for the conversion of a non-osteogenic cellular phenotype into a mineralizing cell source for bone tissue engineering applications.

Materials and Methods

Cell Culture and Reagents

Primary fibroblasts were harvested from 8- to 16-week-old male Wistar rats by enzymatic digestion of the dermal skin layer.[220] Cells were expanded in growth media consisting of DMEM, 10% fetal bovine serum, and 1% penicillin-streptomycin. Antibiotics and cell culture media were obtained from Invitrogen (Carlsbad, CA), fetal bovine serum was purchased from Hyclone (Logan, UT), and all other cell culture supplements and reagents were acquired from Sigma (St. Louis, MO).

Retroviral Transduction

81

The Runx2 retroviral vector utilizes the promoter activity of a 5' long terminal repeat to express a single, bicistronic mRNA encoding the murine cDNA for the type II MASNSLF Runx2 isoform,[221, 222] followed by an internal ribosomal entry site and a Zeocin resistance-enhanced green fluorescent fusion protein (eGFP).[66] Empty vector control vector lacked the Runx2 insert. Plasmid DNA was purified from transformed *E. coli* using Megaprep kits from Qiagen (Valencia, CA). Retroviruses were packaged by transient transfection of helper-virus free ΦNX amphotropic producer cells with plasmid DNA as described elsewhere.[66]

Passage four primary fibroblasts were plated on tissue culture-grade polystyrene coated with 1 mg/ml type I collagen (Cohesion, Palo Alto, CA). Cells at 40-60% confluence were transduced with Runx2 or empty vector retroviral stocks and maintained in osteogenic growth media consisting of DMEM, 10% fetal bovine serum, 100 U/ml penicillin G sodium, and 100 μg/ml streptomycin sulfate. Runx2-transduced cells were analyzed for transduction efficiency by quantification of eGFP expression via flow cytometry with a Vantage SE cell sorter (Becton-Dickinson, San Jose, CA). High levels of eGFP were detected in ≥ 65% of primary dermal fibroblasts at 72 hours post-transduction. Transgene expression was still detectable at 21 days post-transduction (data not shown), demonstrating sustained and integrated expression of the target gene by the retroviral vector. Selection of Runx2/eGFP-positive cells was not performed.

Scaffold Seeding

Fibrous collagen disks (8 mm diameter x 2 mm thick, average pore size 61.7 μm, 93.7% pore volume, Kensey Nash, Exton, PA) were coated with 20 μg/ml fibronectin in

order to promote initial cell adhesion. At sixty hours post-infection, Runx2-transduced, empty vector-infected, and unmodified cells were trypsinized and seeded at $5x10^5$ cells/scaffold in osteogenic growth media. Constructs were transferred twenty-four hours post-seeding to osteogenic differentiation media consisting of DMEM, 10% fetal bovine serum, 100 U/ml penicillin G sodium, 100 µg/ml streptomycin sulfate, 50 µg/ml L-ascorbic acid, 2.1 mM sodium β-glycerophosphate, and 10 nM dexamethasone. Culture media was changed every 2 days until end-point assay. No differences were observed between empty vector retrovirus (negative control) and unmodified cells in all experiments.

Cell Viability

Scaffolds were harvested at 1, 21, and 42 days post-seeding, rinsed in complete Dulbecco's phosphate buffered saline (PBS), and incubated in 4 µM calcein-AM and 4 µM ethidium homodimer-1 (Molecular Probes, Eugene, OR) in PBS for 30 minutes under gentle agitation. Constructs were then rinsed (3 x 10 minutes) in PBS and analyzed with a Zeiss LSM 510 Confocal Microscope using Ar and HeNe lasers and a 5x objective lens.

Cell Seeding Efficiency

Samples were harvested 24-hours post-seeding, rinsed with PBS, and frozen at -80°C. Scaffolds and serially diluted cell standards were thawed, lyophilized, and digested at 55°C in 500 µl of 0.25 mg/ml proteinase K (Fisher Scientific, Pittsburgh, PA) in 100 mM ammonium acetate (pH 7.0) for 24 hours. Digested samples were assessed for DNA content via the PicoGreen dsDNA Quantitation Kit (Molecular Probes, Eugene,

OR). Raw DNA data was converted to cell numbers using a linear standard curve and normalized by original seeding density (500,000 cells/scaffold) to determine cell seeding efficiency.

Real time RT-PCR

Total RNA was isolated at 7 and 21 days post-seeding using the RNeasy RNA isolation kit with RNAlater stabilization reagent (Qiagen). cDNA synthesis was performed on DNaseI-treated (27 Kunitz units/sample) total RNA (0.25 μg) by oligo(dT) priming using the Superscript™ First Strand Synthesis System for RT-PCR (Invitrogen, Carlsbad, CA). Gene expression was assessed by quantitative RT-PCR using SYBR Green intercalating dye (Molecular Probes) and rat-specific primers as previously described.[66, 137] Primer specificity was confirmed by ABI Prism 7700 Dissociation Curve Software. Standards for each gene were amplified from cDNA using real-time oligonucleotides, purified using a Qiagen PCR Purification kit, and diluted over a functional range of concentrations. Transcript concentration in template cDNA solutions was quantified from a linear standard curve, normalized to 0.25 μg of total RNA, and expressed as nanomoles of transcripts per μg of total RNA. Detection limits for each gene were determined by reactions without cDNA and fall below the y-axis minimum.

Microcomputed Tomography

High resolution X-ray microcomputed tomography (micro-CT) with a Scanco μCT Medical CT 40 imaging system (Bassersdorf, Switzerland) was used to quantify *in vitro* and *in vivo* mineralization of 3-D scaffolds. Formalin-fixed specimens were

scanned in 70% ethanol at 16 μm voxel resolution and evaluated at a threshold corresponding to a linear attenuation of 0.96 cm^{-1}, filter width of 1.2, and filter support of 2.0. Reconstructed and thresholded images were evaluated using direct distance transformation methods to calculate mineralized matrix volume within each construct.[288]

FTIR Spectroscopy

Scaffolds at 42 days post-seeding were fixed in 100% ethanol and dried at 50ºC overnight. Bone samples were scraped from a lyophilized rat cranium and used as a positive control. Bulk samples were mixed with KBr (Sigma) and pressed into pellets with a custom built apparatus. Samples were analyzed with a Nicolet Nexus 470 FTIR spectrometer (ThermoNicolet, Madison, WI) equipped with a DTGS detector. Sixty-four scans were acquired at 4 cm^{-1} resolution under N_2 purge.

Subcutaneous Implantation

Cell-seeded constructs were subcutaneously implanted into the backs of 7-week-old syngeneic rats after 24 hours pre-culture in non-osteogenic growth media. Two implants were placed in each animal, one on each side of a midline incision into subcutaneous pockets made by blunt dissection. Four groups (n = 6 samples for each group) of constructs were implanted: (i) Runx2-engineered cells, (ii) empty vector-infected control cells, (iii) unmodified control cells, and (iv) empty (cell-free) scaffolds. Constructs were explanted after 4 weeks of implantation following euthanasia by CO_2 inhalation. All procedures were carried out according to an IACUC-approved protocol as previously described.[138]

Histology and Immunohistochemistry

Formalin-fixed constructs were paraffin embedded and sectioned at 5 μm thickness. Sections were stained with hematoxylin-eosin and von Kossa to observe cellular distribution and matrix mineralization within 3-D constructs, respectively. eGFP and Runx2 protein expression was observed by immunostaining using a colorimetric avidin-biotin kit (Vector Labs, Burlingame, CA). Sections were deparaffinized, rehydrated, and then pretreated using heat-induced antigen retrieval in 10 mM citrate buffer (pH 6.0). After pretreatment, slides were incubated in rabbit polyclonal primary antibodies against eGFP (Molecular Probes) or Runx2/AML3 (Oncogene, San Diego, CA), followed by sequential incubation in biotinylated anti-rabbit secondary antibody and avidin-biotin linked alkaline phosphatase. Slides were then incubated in Vector Red substrate and counterstained with hematoxylin.

Data Analysis

All *in vitro* experiments were performed three times in triplicate, each with unique Runx2 retroviral supernatant preparations, and two independent isolates of primary dermal fibroblasts. Data are reported as mean ± standard error of the mean (SEM), and statistical comparisons using SYSTAT 8.0 were based on an analysis of variance (ANOVA) and Tukey's test for pairwise comparisons, with a p-value < 0.05 considered significant. In order to make the variance independent of the mean, statistical analysis of real-time PCR data was performed following logarithmic transformation of the raw data.[66]

Results

Fibroblasts remain viable and colonize fibrous collagen disks in vitro

Runx2-expressing and unmodified fibroblasts were seeded on fibrous collagen disks at a density of 500,000 cells/scaffold and cultured statically *in vitro* in osteogenic differentiation media. Scaffold seeding efficiency was evaluated by quantification of DNA content at 1 day post-seeding (Fig. 5.1A). Approximately 200,000 cells were present on both Runx2-expressing and unmodified cell-seeded scaffolds, corresponding to cell seeding efficiencies of $43.9 \pm 6.5\%$ and $39.6 \pm 2.5\%$, respectively. Scaffold colonization and cellular viability were assessed at 1, 21, and 42 days post-seeding by confocal microscopy and Live (green)/Dead (red) fluorescence staining (Fig. 5.1B). No differences were observed in cell viability between Runx2-expressing and unmodified control cells at any time point. After 1 day in culture, cells were evenly distributed throughout collagen scaffolds, with spread morphology and minimal cell-cell contact. Cells remained viable for the entire 42 day culture period, with confluent cell populations localized to the construct periphery. Isolated necrotic regions were detected at all time points, but minimal cell death (<5%) was observed in the dense cellular layer at the construct surface.

Runx2 induces osteoblastic gene expression in fibroblasts cultured on collagen scaffolds in vitro

Gene expression of osteoblastic markers, including Runx2, alkaline phosphatase (ALP), osteocalcin (OCN), and bone sialoprotein (BSP), was investigated at 7 and 21 days post-seeding by quantitative RT-PCR (Fig. 5.2). ALP is a membrane-bound
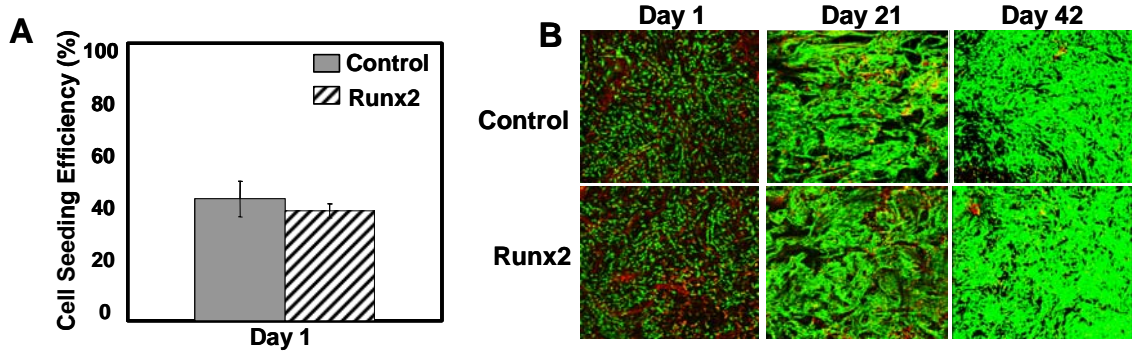
Figure 5.1. **Primary dermal fibroblasts remain viable and populate collagen scaffolds** *in vitro*. Fibroblasts were transduced with Runx2 retrovirus or left unmodified for controls, seeded on fibrous collagen disks, and cultured *in vitro* with osteogenic media. (A) Cell seeding efficiency was determined by quantification of DNA content and cell number present in scaffolds at 1 day post-seeding (Mean + SEM, n=6; ANOVA: $p < 0.05$). (B) Cellular viability was assessed at 1, 21, and 42 days post-seeding by confocal microscopy and Live (green)/Dead (red) fluorescence staining. Scale bar indicates 1 mm.
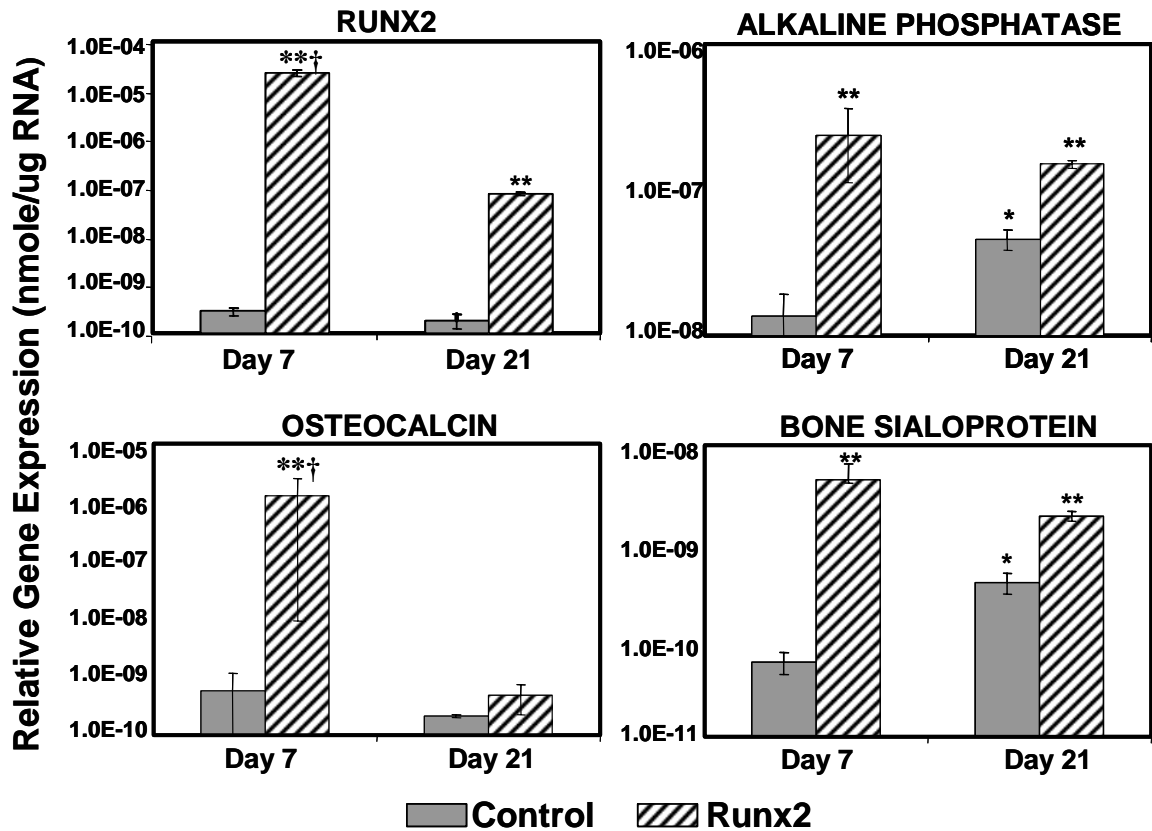
Figure 5.2. Runx2 upregulates osteoblastic gene expression in fibroblasts seeded on collagen scaffolds *in vitro*.   mRNA transcript levels were investigated by quantitative RT-PCR at 7 and 21 days post-seeding (Mean + SEM, n=3; ANOVA: p<0.05; * different from day 7 control, ** different from both day 7 and day 21 controls, and † different from day 21 Runx2 (p< 0.05)).

enzyme that hydrolyzes phosphate esters, thereby making inorganic phosphate available for incorporation into mineral deposits.[224]   OCN is the most abundant non-collagenous extracellular matrix protein in bone and a marker of mature osteoblasts,[223] while BSP is an extracellular matrix glycoprotein implicated in the regulation of mineralized nodule nucleation.[224]   Runx2 mRNA levels were upregulated by 5 orders-of-magnitude in Runx2-transduced cultures compared to control cells at day 7, and this relative difference decreased to 2.5 orders-of-magnitude at day 21.   The temporal decrease in Runx2 expression may be a result of the non-transduced fibroblastic population proliferating faster than Runx2-expressing cells or cell necrosis within the inner core of constructs due to mass transport limitations.   Sustained expression of Runx2 significantly upregulated ALP, OCN, and BSP mRNA expression compared to control fibroblasts at 7 days post-seeding.   After 21 days, OCN mRNA levels were reduced in Runx2-expressing cells to levels comparable to control cultures.   ALP and BSP gene expression remained elevated in Runx2-expressing cells through 21 days in culture.   Moreover, an unexpected increase in the expression of these two osteoblastic markers was also observed in unmodified cells at day 21 compared to day 7.

Runx2-transduced fibroblasts deposit biological matrix mineralization on collagen scaffolds in vitro

Mineral deposition on fibrous collagen disks was quantified at 28 and 42 days post-seeding by micro-CT imaging (Fig. 5.3A+B).   Runx2-expressing fibroblasts deposited significantly higher amounts of mineral on collagen scaffolds cultured *in vitro* compared to unmodified cells.   Mineralized regions were localized primarily to the lateral

90
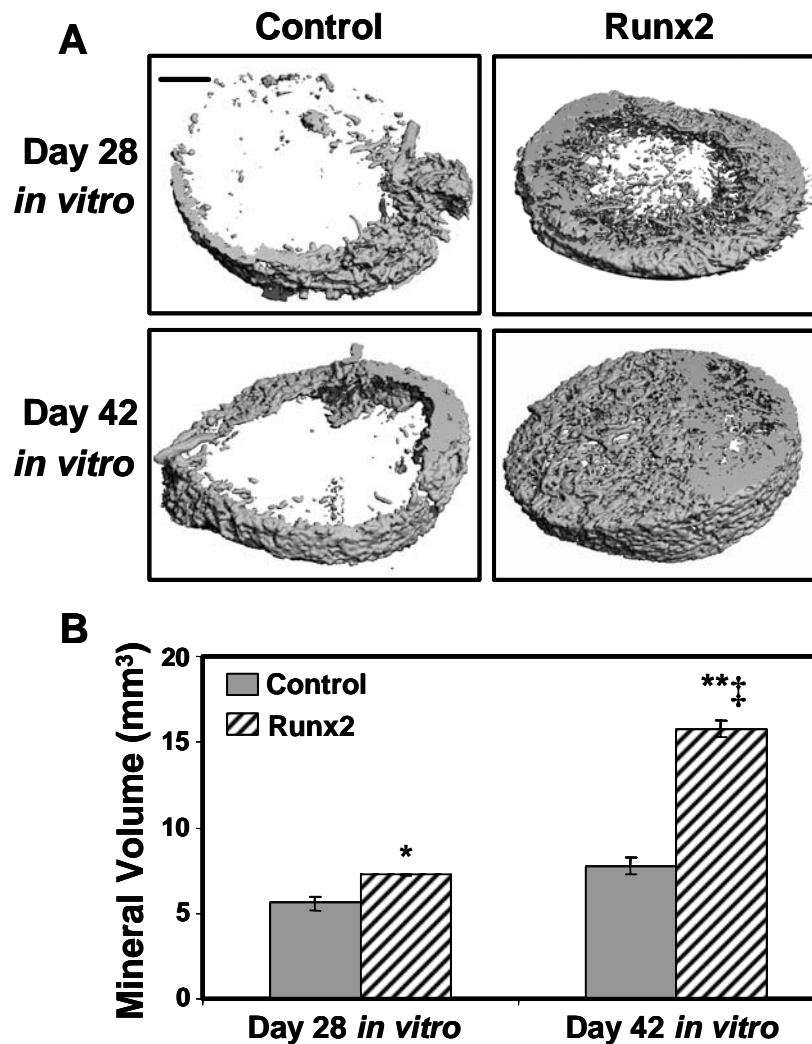
Figure 5.3. Runx2-transduced fibroblasts deposit mineral within collagen scaffolds *in vitro*.   (A) Representative micro-CT images of Runx2-expressing and unmodified fibroblasts seeded on collagen scaffolds and cultured in osteogenic media for 28 and 42 days. Scale bar indicates 1 mm. (B) Quantification of bone volume by micro-CT image analysis of constructs after 28 and 42 days *in vitro* culture in osteogenic media (Mean + SEM, n=6; ANOVA: p<0.00005; * different from day 28 control, ** different from both day 28 and day 42 controls, and ‡ different from day 28 Runx2 (p< 0.0005)).

91

edges of these Runx2-engineered constructs after 21 days in culture, but spread to the upper face of disks as the magnitude of mineral increased through 42 days. Notably, scaffolds seeded with unmodified cells showed a low level of radiopaque material at 28 and 42 days. These radiopaque regions remained confined to the construct periphery and appeared to have an arbitrary, disordered distribution which did not significantly increase with time in culture. Furthermore, the presence of these deposits was highly dependent on the lot of serum (data not shown), suggesting that the *in vitro* culture conditions utilized in this study lead to precipitation of non-biological mineral. These results are consistent with reports that high levels of sodium β-glycerophosphate or unidentified components from specific serum lots may lead to von Kossa-positive mineral deposits which do not resemble the chemical composition of bone mineral.[225, 289]

The chemical composition of the mineral phase deposited on Runx2-engineered and control constructs was analyzed by Fourier Transform Infrared spectroscopy (FTIR) (Fig. 5.4). Runx2-engineered mineral displayed amide I and II peaks indicative of proteins, an enhanced phosphate peak at 1100 cm^{-1}, a doublet split phosphate peak at 560 and 605 cm^{-1}, and a carbonate peak at 870 cm^{-1}. This chemical signature represents the characteristic bands of a carbonate-containing, poorly crystalline hydroxyapatite and is equivalent to that of the cranial bone positive control.[227] Notably, the carbonate and phosphate doublet peaks were absent in control samples, indicating that the radiopaque regions observed on these scaffolds corresponded to non-biological mineral deposits.[289]

Cellular distribution within collagen scaffolds after 42 days *in vitro* culture was visualized by hematoxylin-eosin (H&E) staining of histological sections (Fig. 5.5A). Runx2-expressing and unmodified fibroblasts displayed equivalent patterns of scaffold
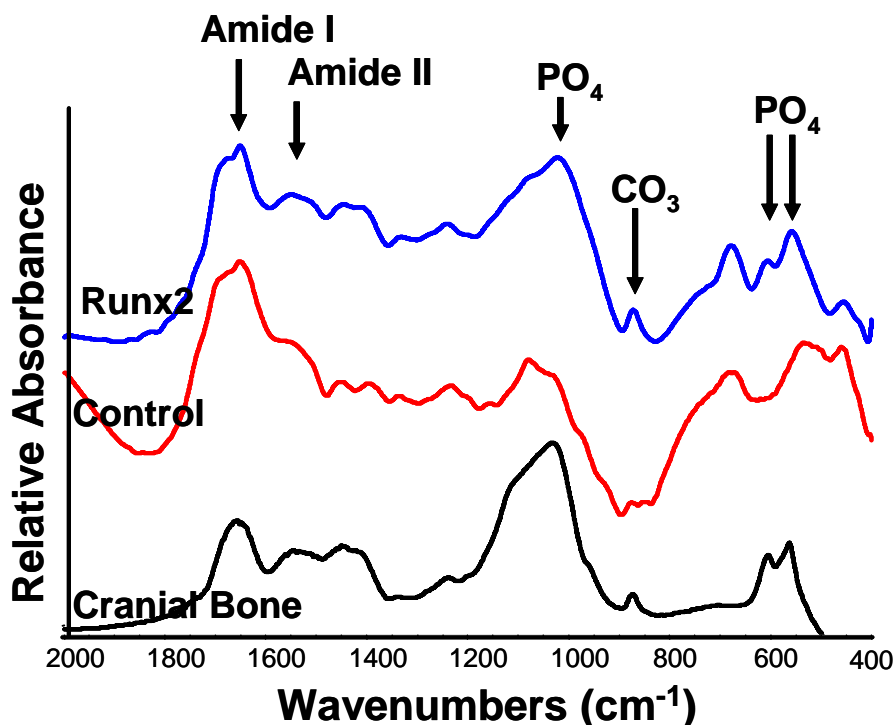
Figure 5.4. Runx2-engineered constructs display FTIR bands characteristic of carbonate-containing, poorly crystalline hydroxyapatite. Chemical composition of the mineral phase was analyzed by Fourier transform infrared spectroscopy (FTIR) at 42 days post-seeding. Runx2 and cranial bone samples displayed amide I and II peaks indicative of proteins, an enhanced phosphate peak at 1100 cm^{-1}, a doublet split phosphate peak at 560 and 605 cm^{-1}, and a carbonate peak at 870 cm^{-1}, which represent the characteristic bands of a carbonate-containing, poorly crystalline hydroxyapatite. Carbonate and phosphate doublet peaks were absent in control samples, indicating that the radiopaque regions observed on these scaffolds corresponded to non-biological mineral deposits.

colonization, with confluent cell populations localized to the outer 100-250 μm of the scaffold periphery. Minimal cell growth was observed within the construct interior, likely due to mass transport limitations associated with static culture.[290, 291] The presence of mineralized matrix within Runx2-engineered constructs was confirmed by von Kossa staining of histological sections (Fig. 5.5B). Phosphate-positive regions were detected adjacent to Runx2-expressing fibroblasts and were confined to the outer 400-600 μm of the scaffold periphery. von Kossa positive staining was also observed on the side borders of control scaffolds, likely due to detection of artifactual phosphate precipitates. Histological analyses were corroborated by cross-sectional micro-CT images (Fig. 5.5C). Mineral deposition by Runx2-transduced cells was observed on the sides and upper face of the scaffold circumference, co-localizing with cellular distribution. Conversely, radiopaque regions detected in control samples remained confined to the side borders of each construct despite the presence of dense cell populations throughout the construct periphery.

Runx2-transduced dermal fibroblasts form mineralized templates in vivo

Tissue-engineered constructs were implanted into an ectopic, subcutaneous site in order to assess the mineralization capacity of these cells in the absence of osteoinductive cues and cell-types typically present in orthotopic defects. Importantly, collagen scaffolds seeded with Runx2-expressing cells displayed a significant increase in mineral volume after 28 days *in vivo*, while controls (unmodified cells, empty vector cells, empty scaffold) showed minimal radiodense regions (Fig. 5.6A+B).

94
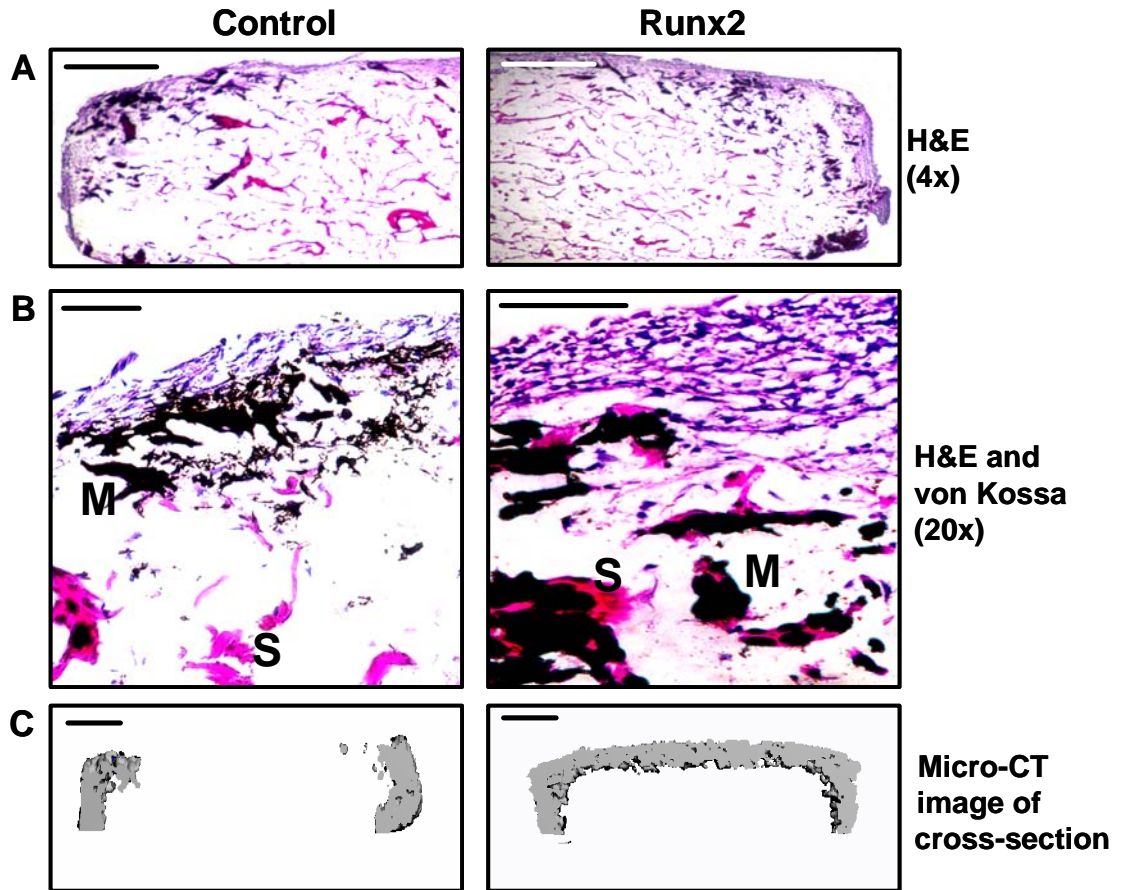
Figure 5.5. Fibroblasts and mineral deposits co-localize to construct periphery *in vitro*. Histological and micro-CT analyses were conducted on cell-seeded scaffolds after 42 days *in vitro* culture. (A) Cellular distribution within collagen disks was visualized by hematoxylin-eosin (H&E) staining of histological sections. Scale bar indicates 1 mm. (B) Matrix mineralization within collagen disks was assessed by von Kossa staining of histological sections for phosphate deposits typically present within mineralized nodules (M = mineral and S = scaffold). Scale bar indicates 250 μm. (C) Cross-sectional micro-CT images depicting the distribution of mineralized matrix on collagen scaffolds seeded with Runx2-expressing and unmodified control cells. Scale bar indicates 1 mm.

95
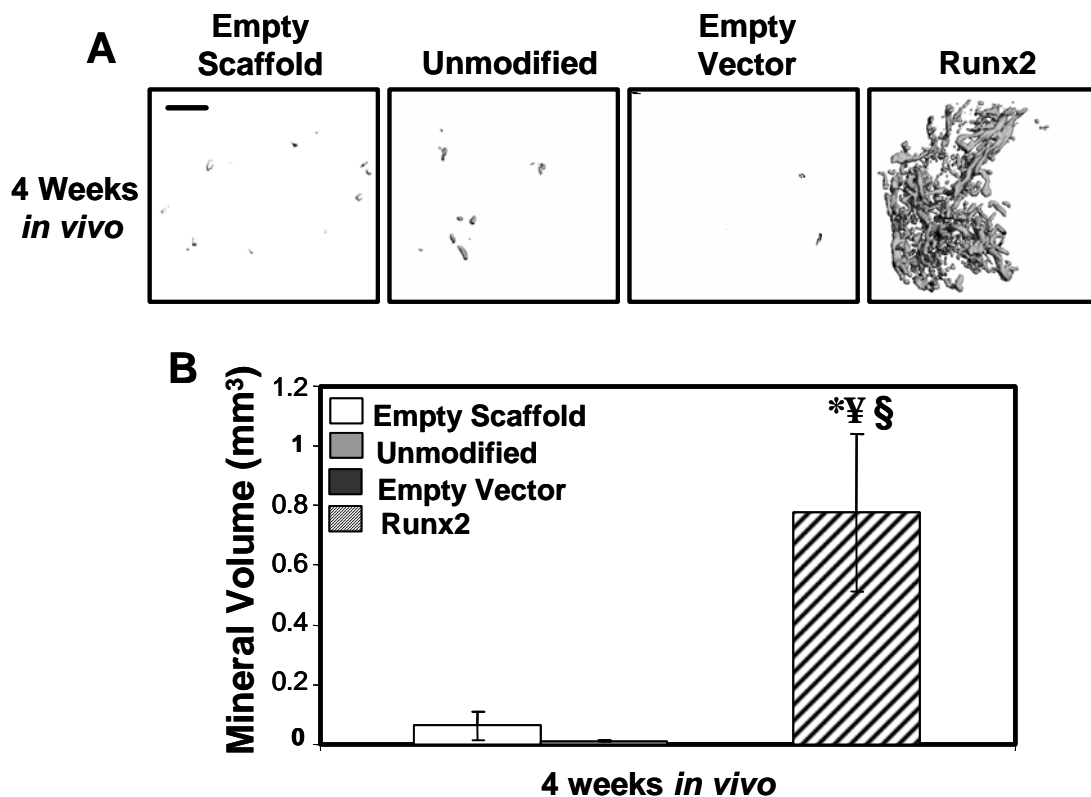
Figure 5.6. Runx2-transduced primary dermal fibroblasts mineralize collagen scaffolds *in vivo*. Primary dermal fibroblasts were transduced with Runx2 retrovirus, empty vector retrovirus, or left unmodified for controls, seeded on fibrous collagen disks, and transplanted into a subcutaneous, heterotopic site for 28 days. (A) Representative micro-CT images of explanted constructs after 28 days subcutaneous implantation. Scale bar indicates 1 mm. (B) Quantification of bone volume by micro-CT image analysis of constructs. (Mean + SEM, n=6; ANOVA: $p < 0.01$; * different from unmodified fibroblasts, § different from empty vector, and ¥ different from empty scaffold ($p < 0.05$)).

Histological analysis was conducted on explanted constructs after subcutaneous implantation for 28 days (Fig. 5.7). Significant remodeling/degradation of collagen scaffolds was apparent after 4 weeks *in vivo*; however, no marked difference in host inflammatory response was detected between cell-seeded and cell-free scaffolds. Hematoxylin-eosin staining revealed residual collagen fibers (S) and uniform distribution of infiltrating host cells throughout all constructs. After 4 weeks *in vivo*, punctate mineralized nodules (M) were detected by von Kossa staining only within Runx2-engineered constructs. Cells with osteoblast-like morphology were found adjacent to and embedded within mineralized matrix.

Genetically-engineered donor fibroblasts co-localize with mineralized matrix in vivo

Immunostaining for Runx2 and eGFP expression was performed on serial histological sections in order to assess the spatial distribution of Runx2-expressing fibroblasts and infiltrating host cells within collagen scaffolds *in vivo* (Fig. 5.8). Significant staining for both Runx2 and eGFP was visualized within the cytoplasm of cells adjacent to the newly formed mineral deposits. Minimal background staining for both proteins was observed in unmodified cell-seeded and cell-free scaffolds (data not shown). Interestingly, specific localized regions of Runx2-positive cells and mineralized matrix were detected which did not exhibit an eGFP-positive signal. Collectively, these results suggest that mineral deposition within collagen scaffolds *in vivo* is primarily of donor cell origin, but do not rule out contributions from recipient cells. Notably, Runx2 and eGFP expression was maintained throughout the 28 day subcutaneous implantation
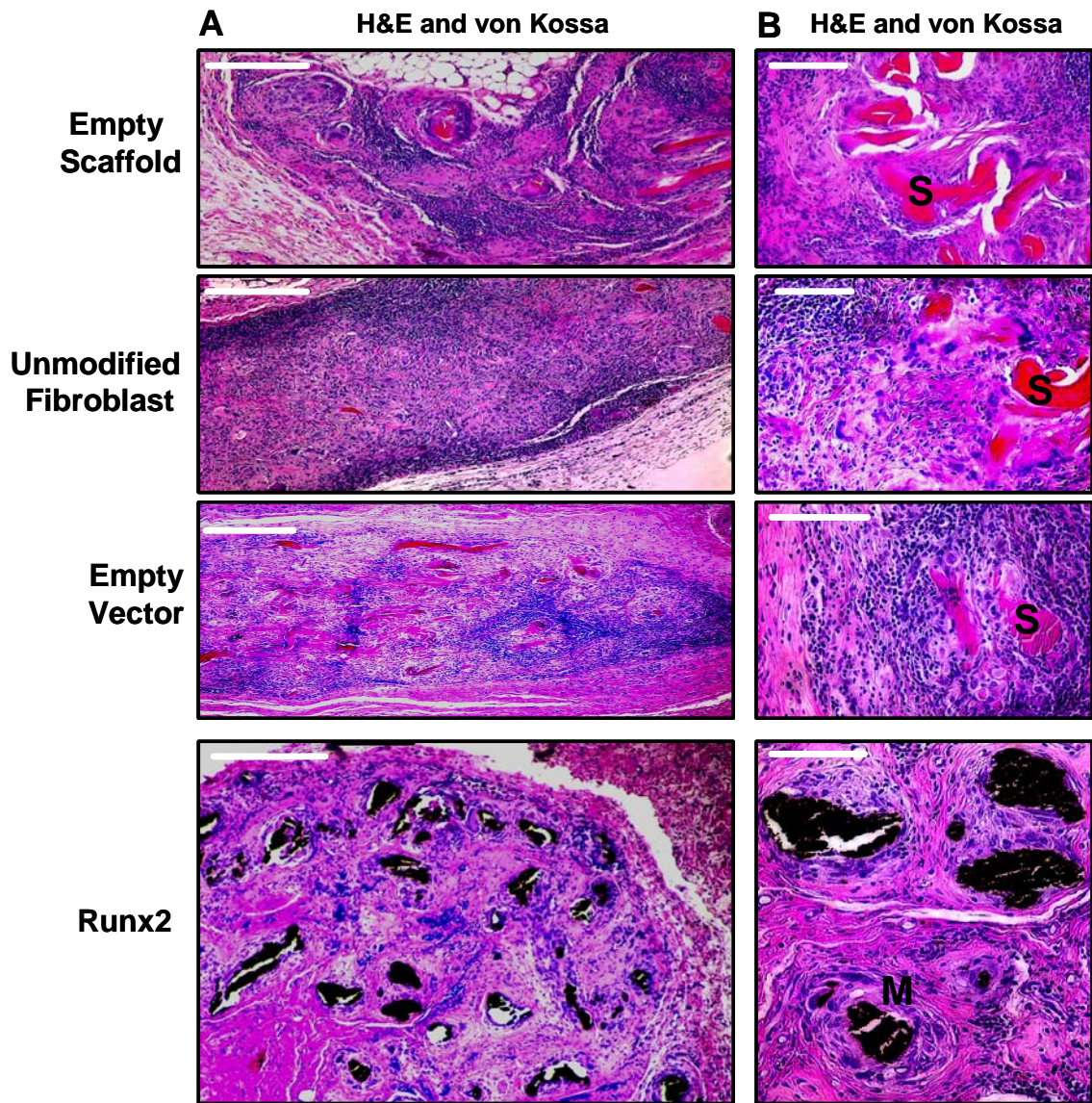
Figure 5.7. Donor fibroblasts, host cells, and matrix mineralization are uniformly distributed throughout Runx2-engineered constructs *in vivo*. Histological sections were stained with hematoxylin-eosin and von Kossa to observe cellular distribution and mineralization throughout cell-seeded and cell-free collagen scaffolds after 28 days *in vivo* (M = mineral and S = scaffold). (A) 4x micrographs. Scale bar indicates 1 mm. (B) 20x micrographs. Scale bar indicates 250 μm.

98

period, ruling out the possibility that exogenous transgene expression was inactivated *in vivo.*

Discussion

In the present study, we describe a hybrid *ex vivo* gene therapy/tissue engineering approach based on retroviral gene delivery of the osteogenic transcription factor Runx2 to primary dermal fibroblasts. Sustained expression of Runx2 induced osteogenic gene expression and mineralized matrix deposition in fibroblasts cultured on 3-D fibrous collagen disks *in vitro*. Scaffolds seeded with unmodified control cells showed an unexpected low level of radiopaque, von-Kossa positive material, as assessed by micro-CT imaging and histological analyses, respectively. However, analysis of the chemical composition of the mineral phase with FTIR spectroscopy revealed that Runx2-engineered scaffolds displayed bands characteristic of a biologically-equivalent, poorly crystalline, carbonate-containing hydroxyapatite, whereas this chemical signature was absent in control samples. Importantly, Runx2-transduced fibroblasts produced significant levels of matrix mineralization *in vivo* after 28 days implantation in a subcutaneous, heterotopic site, while negligible mineral deposits were evident in control constructs. Furthermore, immunohistochemical analysis revealed that Runx2-expressing cells co-localized with mineral deposits *in vivo*, suggesting that bone formation was primarily originated by transplanted donor cells. These results are significant toward the identification of a sustained mineralizing cell source for cell-based skeletal regeneration therapies.

99

Primary dermal fibroblasts have considerable potential as an autologous cell source for *ex vivo* gene therapy and bone tissue engineering applications, as they are easily obtained through minimally invasive skin biopsy and display a high capacity for *in vitro* expansion.   Conventional cell-based approaches typically involve the use of terminally differentiated osteoblasts,[102, 103] osteogenic cell lines,[105] unfractionated bone marrow stroma,[106, 107] or purified mesenchymal stem cells.[14] Immortalized osteogenic cell-lines are clonally-derived and well-characterized, but exhibit abnormal regulatory mechanisms that may lead to tumorigenic growth *in vivo*. Primary osteoblasts are difficult to isolate in sufficient quantities from trabecular bone and display a limited capacity for proliferation. Bone marrow-derived osteoprogenitors and purified MSCs show significant mineralization capacity *in vitro* and *in vivo*.[13, 17, 18] However, the widespread clinical success of these precursors remains limited by their complex and painful cell procurement process, potential for dedifferentiation during *in vitro* expansion, and reduced mineralization capacity associated with the age and disease-state of the donor.[292]   Because of these limitations, non-osteoblastic cell-types such as dermal fibroblasts, gingival fibroblasts, and skeletal myoblasts have been considered for their clinical relevance to bone repair applications.

Several growth and differentiation factor-based genetic engineering strategies have been employed for the induction of sustained osteogenesis in non-osteoblastic fibroblasts. Adenoviral-transduction of dermal fibroblasts with genes encoding BMP-2 or BMP-7 induces significant bone formation in both ectopic implantation sites and critical sized calvarial defects.[21, 24] BMP-7-expressing human gingival fibroblasts also deposit significant amounts of mineralized matrix *in vivo*.[25]   More recently, a

100
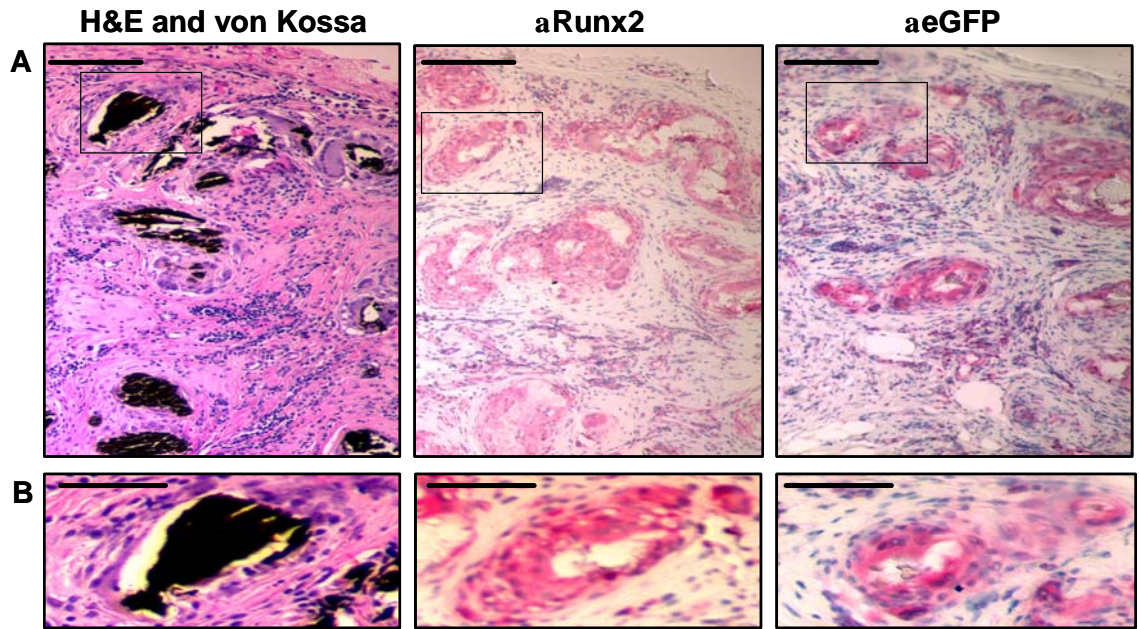
Figure 5.8. Genetically-engineered donor fibroblasts co-localize with mineralized matrix *in vivo*. The spatial localization of Runx2-expressing fibroblasts and mineral deposits within collagen scaffolds after 28 days subcutaneous implantation was investigated by immunohistochemical staining of serial histological sections for eGFP and Runx2 expression. (A) 10x micrographs. Scale bar indicates 500 μm. (B) 20x micrographs of inset in A. Scale bar indicates 250 μm.

combinatorial gene therapy approach based on co-transduction of BMP-2/BMP-7 in murine embryonic fibroblasts synergistically enhanced *in vivo* bone formation compared to transduction of individual molecules alone.[22]   Despite these advances, it is unlikely that one single strategy will be universally appropriate for the treatment of the numerous orthopedic conditions requiring bone grafting procedures.   Indeed, the potential for ectopic bone formation as a result of paracrine signaling to neighboring non-osseous tissues may limit the clinical application of growth factor-based approaches.[293, 294]   In the present study, we describe retroviral gene delivery of the osteogenic transcription factor Runx2 as a robust strategy for the conversion of primary dermal fibroblasts into a mineralizing osteoblastic phenotype. Runx2 is regulated at multiple levels by a complex cascade of soluble factors, hormones, and cell-matrix interactions and is a known downstream effector of BMP-2-activated signaling.[64, 221]   Thus, the use of a genetic engineering strategy which focuses on controlling expression of downstream transcriptional activator may avoid aberrant effects associated with unregulated secretion of soluble, osteoinductive factors.

It is well documented that adenoviral and retroviral gene delivery of Runx2 upregulates osteogenic gene expression in osteoblastic and non-osteoblastic cell types.[59, 66, 67, 137]   However, we and others have reported that forced Runx2 expression induces matrix mineralization in a cell type-dependent manner and is insufficient to direct significant *in vitro* nodule formation in NIH3T3 and IMR-90 fibroblasts, primary murine fibroblasts, and the C3H10T1/2 pluripotent fibroblastic cell-line.[23, 24, 66]   These results suggest that Runx2-mediated mineralization requires additional cofactors, which may not be endogenously expressed in certain nonosteoblastic cell-types.   Indeed, we have

recently reported that dexamethasone treatment is required for matrix mineralization in Runx2-expressing fibroblasts cultured in monolayer.[136] We applied these observations in the present work to demonstrate that primary dermal fibroblasts engineered to constitutively express Runx2 create mineralized templates *in vitro* when cultured on collagen scaffolds in osteogenic media supplemented with dexamethasone. Moreover, we also show that Runx2-expressing fibroblasts produced mineralized templates *in vivo* after implantation in a subcutaneous, heterotopic site. This finding is in contrast to previous reports indicating that transient adenoviral Runx2 expression is insufficient to produce significant levels of mineralization *in vivo*[23, 24] and suggests that sustained expression of this transcription factor is necessary for ectopic mineral deposition by transplanted fibroblastic cell-types. Notably, these results also indicate that *in vitro* pre-culture in osteogenic media supplemented with dexamethasone prior to implantation[138] is not necessary for the formation of robust mineralized templates by Runx2-expressing fibroblasts *in vivo*.

Bone formation within collagen scaffolds *in vivo* may be a result of several different mechanisms, including: (1) the direct deposition of mineralized matrix by Runx2-genetically engineered fibroblasts, (2) the secretion of soluble osteoinductive factors by Runx2-genetically engineered fibroblasts, which initiate osteogenic differentiation in recipient cells via paracrine signaling, and/or (3) the conversion of a specific population of recipient cells into a mineralizing osteoblast-like phenotype through the osteoinductive surface of collagen disks. Immunohistochemical analyses were performed to investigate the spatial distribution of Runx2-expressing fibroblasts and infiltrating host cells relative to mineral deposits within collagen scaffolds *in vivo*.

103

GFP+/Runx2+ cells co-localized with von Kossa-positive regions, suggesting that mineral formation primarily originates from genetically engineered donor fibroblasts. Interestingly, the presence of isolated mineralized nodules which spatially align with Runx2-expressing cells in the absence of GFP+ signal suggests that infiltrating host cells which endogenously express Runx2 may also contribute to *in vivo* mineral formation. Histological analyses revealed cells with osteoblast-like morphology adjacent to and embedded within mineralized matrix after 4 weeks *in vivo*. In contrast to previous reports,[23, 25] tissue morphology indicative of bone marrow, cortical bone, and/or cartilage was not observed, potentially because temporal changes in cellular differentiation throughout the implantation period (28 days) were not monitored in this work.

In the present study, unmodified control fibroblasts seeded on fibrous collagen disks displayed an unexpected upregulation of ALP and BSP gene expression and deposition of von Kossa-positive, radiodense plaques after 21-28 days *in vitro* culture in osteogenic media. Our observations are consistent with a recent report from Hee et al. demonstrating that scaffold architecture and chemical composition markedly influences osteoblastic gene expression in human dermal fibroblasts.[295] At first glance, these results suggest that the conversion of a non-osteoblastic cell source into a differentiated osteoblastic phenotype may be partially induced by scaffold-dependent effects. However, it has been well documented that *in vitro* culture conditions can lead to non-biologic mineral precipitation.[225, 289, 296, 297] Indeed, further investigation of the chemical composition of the mineral phase within control constructs by FTIR spectroscopy revealed the absence of the chemical signature characteristic of carbonate-containing, poorly crystalline hydroxyapatite.[227] Importantly, radiodense regions were not detected

104

on unmodified fibroblast-seeded control constructs implanted *in vivo*, confirming that the presence of non-biological mineral was an artifact of *in vitro* culture conditions. Finally, histological analyses showed that Runx2-expressing fibroblasts and mineral deposits were uniformly distributed throughout constructs implanted *in vivo*, but remained preferentially localized to the periphery of constructs cultured *in vitro*. Indeed, mass transport limitations associated with static culture are known to cause cell necrosis within the inner core of tissue engineered constructs[135, 138] and several groups have developed perfusion bioreactors to mimic the dynamic environment experienced by cells *in vivo*.[290, 291, 298] Collectively, these results highlight the limitations of *in vitro* pre-culture for tissue engineering applications and underscore the importance of rigorous characterization of *in vitro* mineral deposits,   particularly because the chemical composition of the hydroxyapatite mineral phase modulates osseointegration *in vivo*.[299-302]

In summary, we have demonstrated that sustained expression of Runx2 induces osteoblastic differentiation and biological mineral deposition in primary dermal fibroblasts cultured on fibrous collagen scaffolds *in vitro* and *in vivo*. The conversion of non-osteoblastic dermal fibroblasts into a sustained mineralizing cell source is significant toward the development of mechanically robust bone grafts which genetically match the patient and are capable of healing large, critical sized defects.

CHAPTER 6

MINERALIZATION CAPACITY OF RUNX2-GENETICALLY ENGINEERED FIBROBLASTS IS SCAFFOLD DEPENDENT*

Introduction

Conventional orthopaedic grafting templates based on autogenic bone, allogenic bone, or synthetic materials are widely utilized for the clinical treatment of non-healing skeletal defects. Although successful in many cases, these grafts remain limited by inadequate osseo-integration, donor site morbidity, poor mechanical properties, and/or the risk of disease transmission [3, 77-80, 303]. Bone tissue engineering has emerged as a promising strategy to overcome complications associated with these traditional skeletal repair therapies [9-12]. Tissue-engineered bone substitutes have been successfully developed through the integration of osteoinductive growth factors and/or osteogenic cells into an osteoconductive scaffolding matrix. Notably, several groups have demonstrated *in vitro* and *in vivo* mineralization and repair of bone defects by combining marrow-derived mesenchymal stem cells with three-dimensional scaffolds [13-18]. Despite these advances, the development of mechanically robust skeletal grafts which are immunoaccepted by the host and are capable of healing large, critical sized defects has not been realized.

Development of tissue-engineered constructs for skeletal regeneration of large critical-sized defects requires the identification of a sustained mineralizing cell source and careful optimization of scaffold architecture and surface properties. We have recently reported that Runx2-genetically engineered primary dermal fibroblasts express a mineralizing phenotype in monolayer culture, highlighting their potential as an autologous osteoblastic cell source which can be easily obtained in large quantities. One significant barrier toward the clinical application of tissue engineered bone grafts is the inadequate availability of a sustained mineralizing cell source. In order to address this limitation, genetic engineering strategies have been developed for the induction of osteoblastic differentiation in nonosteogenic cells [20-22, 67]. In particular, gene delivery of soluble factors, such as BMP-2 and BMP-7, or osteogenic transcription factors, such as Runx2/Cbfa1, has been investigated for the conversion of fibroblastic cell lines into an osteoblastic phenotype [23-25, 304]. We have recently demonstrated that retroviral Runx2 overexpression induces significant levels of mineral deposition by primary dermal fibroblasts cultured in monolayer [305]. These genetically modified fibroblasts have considerable potential as a cell source for bone tissue engineering applications because they are easily obtained from autologous donors through minimally invasive skin biopsy and have a high capacity for *in vitro* expansion.

In addition to the identification of an autologous mineralizing cell source, the successful development of bone grafting templates requires careful optimization of scaffold architecture and surface properties. Biomaterial scaffolds typically function as a three-dimensional structural support which promotes cell attachment, proliferation, and differentiation into functional osteoblasts and facilitates functional integration into the

107

defect site. Various classes of materials have been considered for skeletal grafting applications, including ceramics, natural and synthetic polymers, and their composites [306]. Among these, scaffolds based on naturally-derived collagen and synthetic polycaprolactone (PCL) and polylactide-co-glycolide (PLGA) polymers were selected for investigation in this study because of their widespread use in tissue engineering applications, well-documented biodegradation profile, FDA-approval, and commercial availability [307-310]. These scaffolds present a broad range of architectural and surface properties (e.g. topography, surface chemistry, roughness) that may potentially influence the biological response of seeded cells [311]. The objective of the present work is to evaluate the ability of three commonly utilized, commercially available scaffolds to support *in vitro* matrix mineralization when seeded with Runx2-expressing fibroblasts.

Materials and Methods

Cells and Culture Reagents

Primary fibroblasts were harvested from 8- to 16-week-old male Wistar rats by enzymatic digestion of the dermal skin layer [220]. Cells were expanded in growth media consisting of DMEM, 10% fetal bovine serum, and 1% penicillin-streptomycin. Antibiotics and cell culture media were obtained from Invitrogen (Carlsbad, CA), fetal bovine serum was purchased from Hyclone (Logan, UT), and all other cell culture supplements and reagents were acquired from Sigma (St. Louis, MO).

Retroviral Transduction

108

The Runx2 retroviral vector utilizes the promoter activity of a 5' long terminal repeat to express a single, bicistronic mRNA encoding the murine cDNA for the type II MASNSLF Runx2 isoform [221, 222], followed by an internal ribosomal entry site and a Zeocin resistance-enhanced green fluorescent fusion protein (eGFP)[66]. Empty vector control vector lacked the Runx2 insert. Plasmid DNA was purified from transformed *E. coli* using Megaprep kits from Qiagen (Valencia, CA). Retroviruses were packaged by transient transfection of helper-virus free ΦNX amphotropic producer cells with plasmid DNA as described elsewhere [66, 135].

Passage four primary fibroblasts were plated on tissue culture-grade polystyrene coated with 1 mg/ml type I collagen (Cohesion, Palo Alto, CA). Cells at 40-60% confluence were transduced with Runx2 or empty vector retroviral stocks and maintained in osteogenic growth media consisting of DMEM, 10% fetal bovine serum, 100 U/ml penicillin G sodium, and 100 μg/ml streptomycin sulfate. Runx2-transduced cells were analyzed for transduction efficiency by quantification of eGFP expression via flow cytometry with a Vantage SE cell sorter (Becton-Dickinson, San Jose, CA). High levels of eGFP were detected in ≥ 65% of primary dermal fibroblasts at 72 hours post-transduction. Transgene expression was still detectable at 21 days post-transduction (data not shown), demonstrating sustained and integrated expression of the target gene by the retroviral vector. Selection of Runx2/eGFP-positive cells was not performed.

Scaffold Seeding

The scaffolds investigated in this study were: (i) 75/25 PLGA (REGEN Biotech Inc., Korea, 8 mm diameter × 2 mm thick, 100-200 μm pore size, 85% porosity), (ii)

fused deposition-modeled PCL (8 mm diameter × 2 mm thick, 300-500 µm pore size, 66% porosity) [312], and (iii) and fibrous collagen disks (Kensey Nash, Exton, PA, 8 mm diameter x 2 mm thick, average pore size 61.7 µm, 93.7% pore volume). Scaffolds were coated with 20 µg/ml fibronectin in order to promote initial cell adhesion. At sixty hours post-infection, Runx2-transduced, empty vector-infected, and unmodified cells were trypsinized and seeded at $5x10^5$ cells/scaffold in DMEM supplemented with 10% fetal bovine serum, 100 U/ml penicillin G sodium, and 100 µg/ml streptomycin sulfate. Constructs were transferred twenty-four hours post-seeding to osteogenic differentiation media consisting of DMEM, 10% fetal bovine serum, 100 U/ml penicillin G sodium, 100 µg/ml streptomycin sulfate, 50 µg/ml L-ascorbic acid, 2.1 mM sodium β-glycerophosphate, and 10 nM dexamethasone. Culture media was changed every 2 days until end-point assay. No differences were observed between empty vector retrovirus (negative control) and unmodified cells in all experiments.

Cell Viability

Scaffolds were harvested at 1, 21, and 42 days post-seeding, rinsed in complete Dulbecco's phosphate buffered saline (PBS), and incubated in 4 µM calcein-AM and 4 µM ethidium homodimer-1 (Molecular Probes, Eugene, OR) in PBS for 30 minutes under gentle agitation. Constructs were then rinsed (3 x 10 minutes) in PBS and analyzed with a Zeiss LSM 510 Confocal Microscope using Ar and HeNe lasers and a 5x objective lens.

Cell Seeding Efficiency and DNA Content

110

Samples were harvested 24-hours post-seeding, rinsed with PBS, and frozen at -80°C. Scaffolds and serially diluted cell standards were thawed, lyophilized, and digested at 55°C in 500 μl of 0.25 mg/ml proteinase K (Fisher Scientific, Pittsburgh, PA) in 100 mM ammonium acetate (pH 7.0) for 24 hours. Digested samples were assessed for DNA content via the PicoGreen dsDNA Quantitation Kit (Molecular Probes, Eugene, OR). DNA data was converted to cell numbers using a linear standard curve and normalized by original seeding density (500,000 cells/scaffold) to determine cell seeding efficiency.

Real Time RT-PCR

Total RNA was isolated at 7 and 21 days post-seeding using the RNeasy RNA isolation kit with RNAlater stabilization reagent (Qiagen). cDNA synthesis was performed on DNaseI-treated (27 Kunitz units/sample) total RNA (0.25 μg) by oligo(dT) priming using the Superscript™ First Strand Synthesis System for RT-PCR (Invitrogen, Carlsbad, CA). Gene expression was assessed by quantitative RT-PCR using SYBR Green intercalating dye (Molecular Probes) and rat-specific primers [66, 137]. Primer specificity was confirmed by ABI Prism 7700 Dissociation Curve Software. Standards for each gene were amplified from cDNA using real-time oligonucleotides, purified using a Qiagen PCR Purification kit, and diluted over a functional range of concentrations. Transcript concentration in template cDNA solutions was quantified from a linear standard curve, normalized to total RNA (0.25 μg), and expressed as nanomoles of transcripts per μg of total RNA. Detection limits for each gene were determined by reactions without cDNA and fall below the y-axis intercept.

Microcomputed Tomography

High resolution X-ray microcomputed tomography (micro-CT) with a Scanco μCT Medical CT 40 imaging system (Bassersdorf, Switzerland) was used to quantify *in vitro* mineralization of 3-D scaffolds. Formalin-fixed specimens were scanned in 70% ethanol at 16 μm voxel resolution and evaluated at a threshold corresponding to a linear attenuation of 0.96 cm^{-1}, filter width of 1.2, and filter support of 2.0. Reconstructed and thresholded images were evaluated using direct distance transformation methods to calculate mineralized matrix volume within each construct [288].

FTIR Spectroscopy

Scaffolds at 42 days post-seeding were fixed in 100% ethanol and dried at 50ºC overnight. Bone samples were scraped from a lyophilized rat cranium and used as a positive control. Bulk samples were mixed with KBr (Sigma) and pressed into pellets with a custom built apparatus. Samples were analyzed with a Nicolet Nexus 470 FTIR spectrometer (ThermoNicolet, Madison, WI) equipped with a DTGS detector. Sixty-four scans were acquired at 4 cm^{-1} resolution under N_2 purge.

Histology

Formalin-fixed constructs were paraffin embedded and sectioned at 5 μm thickness. Sections were stained with hematoxylin-eosin and von Kossa to observe cellular distribution and matrix mineralization within 3-D constructs, respectively.

112

Data Analysis

All experiments were performed three times in triplicate, each with unique Runx2 retroviral supernatant preparations, and two independent isolates of primary dermal fibroblasts. Data are reported as mean ± standard error of the mean (SEM), and statistical comparisons using SYSTAT 8.0 were based on an analysis of variance (ANOVA) and Tukey's test for pairwise comparisons, with a p-value < 0.05 considered significant. In order to make the variance independent of the mean, statistical analysis of real-time PCR data was performed following logarithmic transformation of the raw data [66].

Results

Cellular Viability

Runx2-expressing and unmodified fibroblasts were seeded on collagen, PCL, and PLGA scaffolds at a density of 500,000 cells/construct and cultured *in vitro* under static conditions in osteogenic differentiation media. Scaffold colonization and cellular viability were assessed at 1, 21, and 42 days post-seeding by confocal microscopy and Live/Dead staining (Fig. 6.1). After 1 day in culture, cells displayed a fibroblastic morphology and were evenly distributed throughout all three scaffolds. Marked increases in green fluorescent intensity were observed at 21 and 42 days, indicating that cells remained viable and exhibited a time-dependent increase in construct colonization throughout the culture period. After 42 days in culture, confluent populations of viable cells and minimal necrotic regions (<5%) were observed at the periphery of all constructs. Cell viability did not appear to be dependent on scaffold properties. Nonetheless, differential patterns of cell localization were observed among collagen,

113
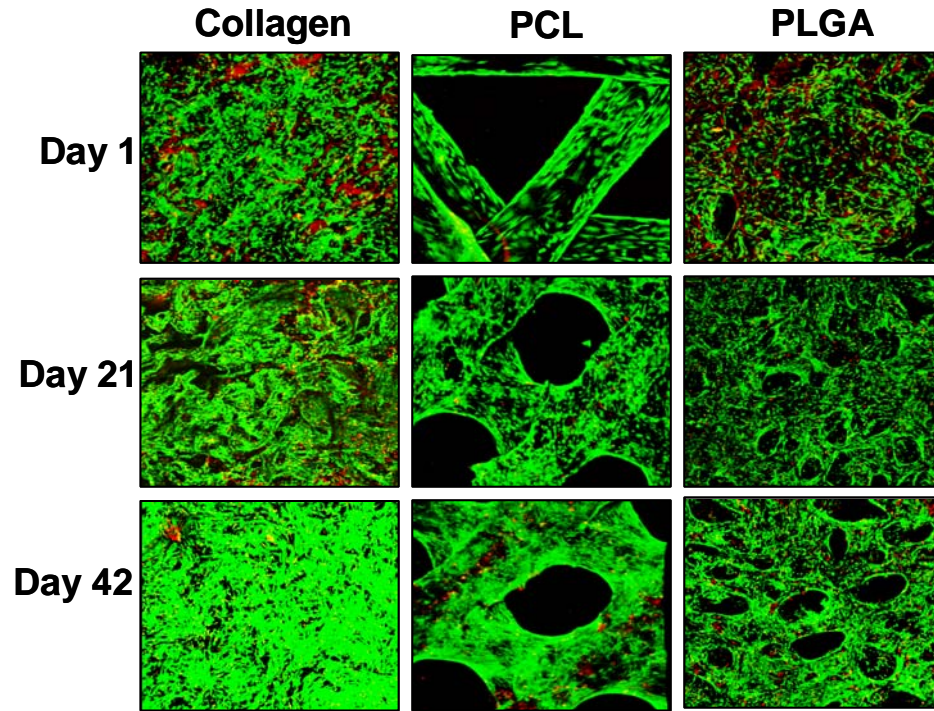
Figure 6.1. Runx2-transduced fibroblasts remain viable and populate polymeric scaffolds *in vitro*. Fibroblasts were transduced with Runx2 retrovirus, seeded on collagen, PLGA, or PCL scaffolds and cultured *in vitro* with osteogenic media. Cellular viability was assessed at 1, 21, and 42 days post-seeding by confocal microscopy and Live (green)/Dead (red) fluorescence staining. Scale bar indicates 1 mm.

PLGA, and PCL matrices, with construct colonization directed along the structural architecture of each scaffold.

Scaffold Colonization and Seeding Efficiency

Scaffold seeding efficiency and changes in cell number during *in vitro* culture were evaluated by quantification of DNA content at 1, 21, and 42 days post-seeding (Fig. 6.2A+B). After 1 day in culture, collagen scaffolds contained the greatest number of Runx2-expresing fibroblasts, corresponding to a seeding efficiency of $43.9 \pm 6.5\%$, while PCL and PLGA exhibited significantly lower seeding efficiencies of $11.1 \pm 1.9\%$ and $23.6 \pm 2.1\%$, respectively. After 21 days in culture, collagen and PLGA scaffolds showed a significant decrease in cell number, which leveled off at 42 days post-seeding. In contrast, Runx2-expressing fibroblasts seeded on PCL scaffolds exhibited a marked increase in cell number at 21 days post-seeding, which also leveled off at day 42. Because these trends are inconsistent with the increase in cell colonization observed at the periphery of fibrous collagen/PLGA sponges by fluorescence microscopy (Figure 1), we attribute the time-dependent reduction in DNA content to cell necrosis or lack of colonization within the inner core of these constructs. No differences in cell viability or colonization patterns were detected between Runx2-expressing and unmodified control cells at any time point (data not shown).

Osteoblastic Gene Expression

Osteogenic gene expression was investigated at 7 days post-seeding by quantitative RT-PCR (Fig. 6.3). Specifically, we examined expression of markers with a

115
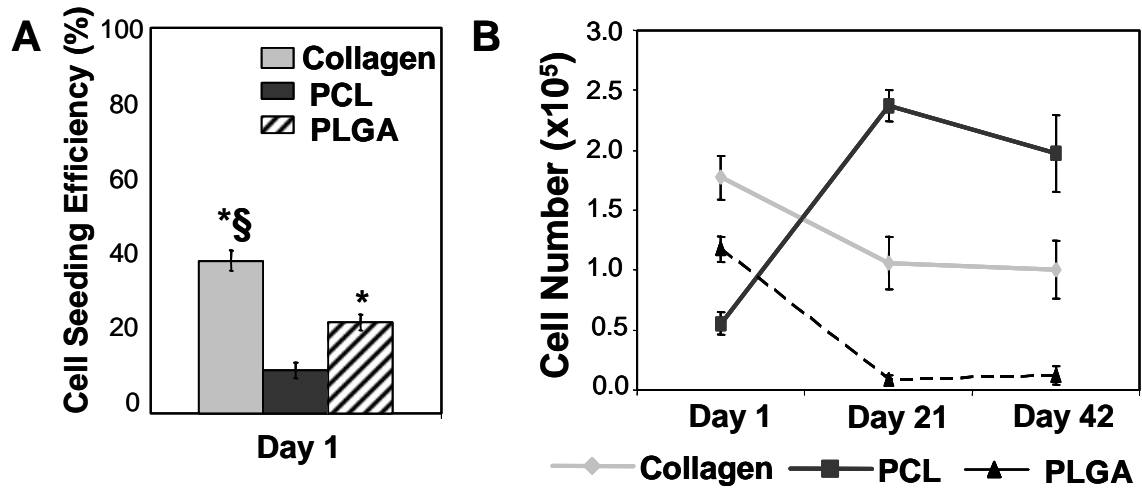
Figure 6.2.   Tissue-engineered constructs are differentially colonized by Runx2-expressing fibroblasts.   Fibroblasts were transduced with Runx2 retrovirus, seeded on collagen, PLGA, or PCL scaffolds and cultured *in vitro* with osteogenic media. (A) Cell seeding efficiency was determined by quantification of DNA content and cell number present in scaffolds at 1 day post-seeding (Mean ± SEM, n=6; ANOVA: p<0.002; *different from Runx2-PCL (p<0.05); § different from Runx2-PLGA (p<0.05)). (B) Cell numbers throughout culture period were evaluated by quantification of DNA content at 1, 21, and 42 days post-seeding (Mean ± SEM, n-3; ANOVA: p<0.05).
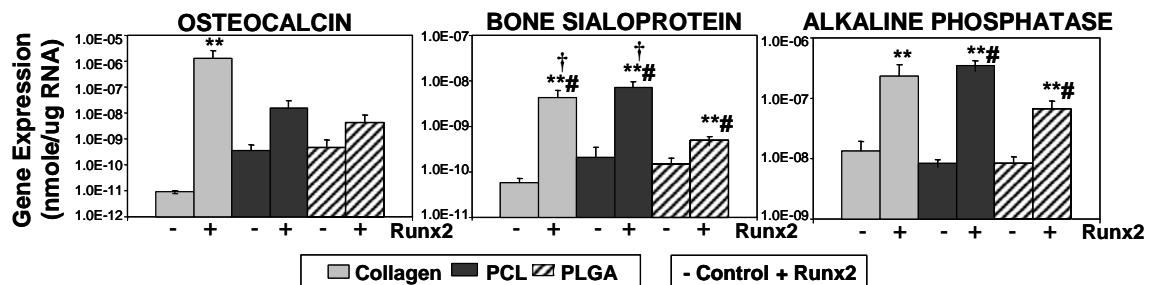
Figure 6.3. Runx2 upregulates osteoblastic gene expression in fibroblasts seeded on polymeric scaffolds. Fibroblasts were transduced with Runx2 retrovirus or left unmodified for controls, seeded on collagen, PLGA, or PCL scaffolds, and cultured *in vitro* with osteogenic media. mRNA transcript levels were investigated by quantitative RT-PCR at 7 days post-seeding (Mean + SEM, n=3; ANOVA: $p<1E-3$; * different from control-PCL only ($p<0.05$); **different from control-collagen and control-PCL ($p<0.05$); #different from control-PLGA ($p<0.05$); † different from Runx2-PLGA ($p<0.05$)).

well-documented role during the osteoblastic differentiation program, including: Runx2, alkaline phosphatase (ALP), osteocalcin (OCN), and bone sialoprotein (BSP) [224]. Runx2 mRNA was upregulated by at least one order-of-magnitude in Runx2-transduced fibroblasts seeded on all three scaffolds compared to unmodified control cells seeded on the same scaffolds (data not shown). Sustained expression of Runx2 significantly enhanced ALP and BSP expression in fibroblasts seeded on collagen, PLGA, and PCL scaffolds. Moreover, BSP gene expression was significantly higher on Runx2-engineered collagen and PCL constructs than on Runx2-engineered PLGA foams. OCN mRNA was upregulated in Runx2-engineered fibroblasts relative to unmodified control cells when seeded on fibrous collagen disks, but not when seeded on PCL or PLGA synthetic matrices. 18S gene expression was used as a loading control and remained unchanged for all treatment groups.

Mineral Deposition and Characterization

Mineralization within tissue-engineered constructs was quantified by micro-CT imaging at 28 and 42 days post-seeding (Fig. 6.4A+B). Runx2-expressing fibroblasts deposited significantly higher levels of mineralized matrix on collagen scaffolds cultured *in vitro* for 28 and 42 days compared to unmodified cells. Mineral deposition was also increased on Runx2-engineered PLGA foams relative to constructs containing control cells at 42 days post-seeding only. In contrast, Runx2-expressing fibroblasts seeded on PCL scaffolds showed no significant difference in mineral deposition compared to control cells at all time points. Importantly, genetically engineered cells displayed a significantly higher capacity for mineralization when seeded on collagen foams compared
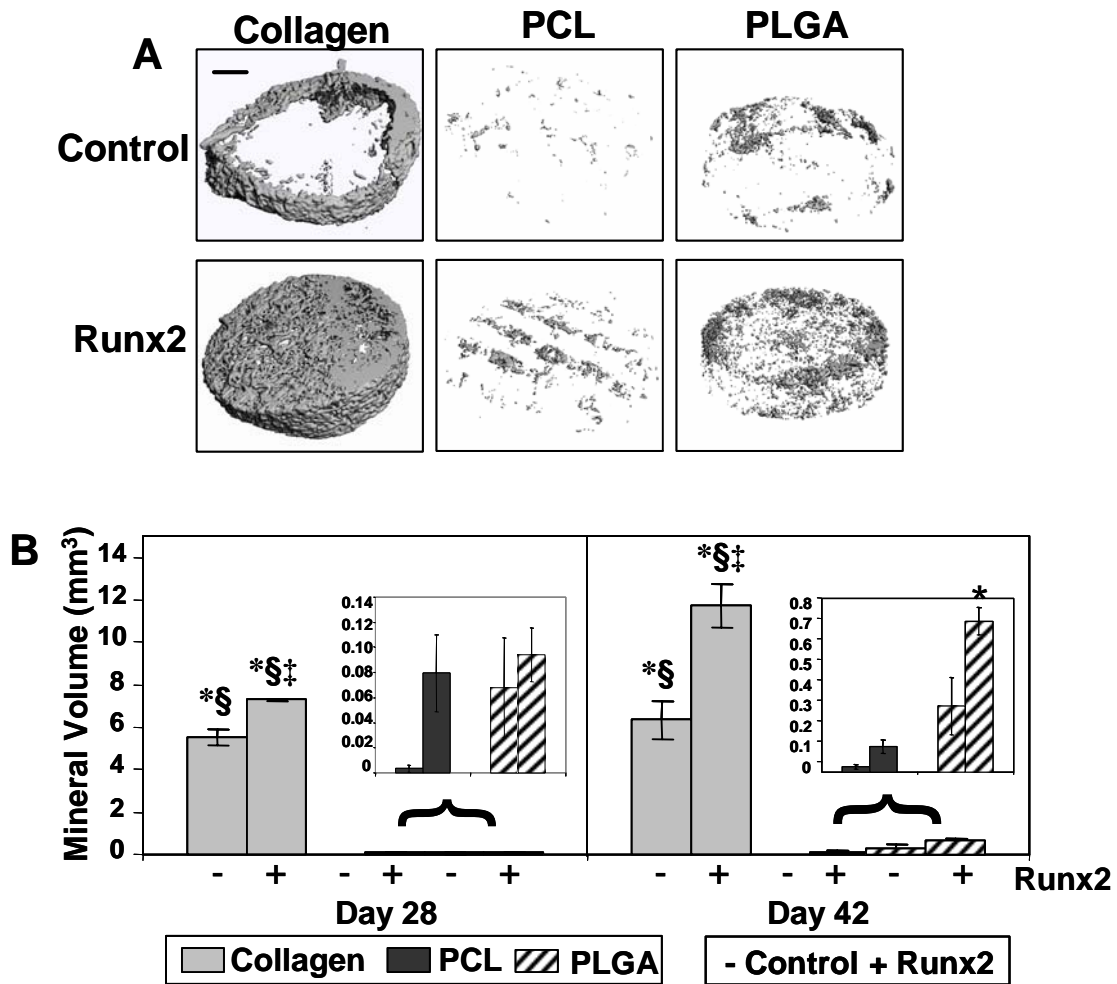
Figure 6.4. Mineralization capacity of Runx2-engineered fibroblasts is scaffold-dependent. (A) Representative micro-CT images of Runx2-expressing and unmodified fibroblasts seeded on collagen, PCL, and PLGA scaffolds and cultured in osteogenic media for 42 days. Scale bar indicates 1 mm. (B) Quantification of mineral volume by micro-CT image analysis of constructs after 28 and 42 days *in vitro* culture in osteogenic media (Mean + SEM, n=6; ANOVA: $p < 1E-11$; *different from control-PCL, Runx2-PCL, and control-PLGA ($p < 1E-5$); § different from Runx2-PLGA ($p < 1E-5$); ‡ different from control-collagen ($p < 0.05$)).

to PCL and PLGA synthetic matrices. A low level of radiopaque material was detected on all scaffolds seeded with unmodified control cells, with collagen showing significantly more background than PCL and PLGA. The presence of this radiodense material was dependent on the lot of serum (data not shown) and did not significantly increase with time in culture, suggesting that *in vitro* culture conditions may have led to amorphous calcium phosphate or non-biological mineral precipitation.

Fourier Transform Infrared spectroscopy (FTIR) was used to characterize the chemical composition of the mineral phase deposited within tissue-engineered constructs (Fig. 6.5). Constructs containing Runx2-engineered cells displayed amide I/II peaks at 1655 cm^{-1} and 1550 cm^{-1}, an enhanced phosphate peak at 1100 cm^{-1}, a doublet split phosphate peak at 560 and 605 cm^{-1}, and a carbonate peak at 870 cm^{-1}. This chemical signature is similar to the profile for cranial bone (positive control) and represents the characteristic bands of a carbonate-containing, poorly crystalline hydroxyapatite [227]. Deposition of biological mineral was observed on Runx2-engineered collagen, PCL and PLGA constructs. Importantly, the carbonate and phosphate doublet bands were absent in all three scaffolds seeded with control cells, suggesting that the radiopaque regions detected by micro-CT corresponded to non-biological mineral deposits. These observations are corroborated by reports from several other research groups that *in vitro* culture conditions can lead to non-biologic mineral precipitation [225, 289, 296, 297].

Cell and Mineral Distribution

The distribution of mineral within Runx2-engineered constructs was visualized by cross-sectional analysis of micro-CT images (Fig. 6.6A). Mineral deposits were

120
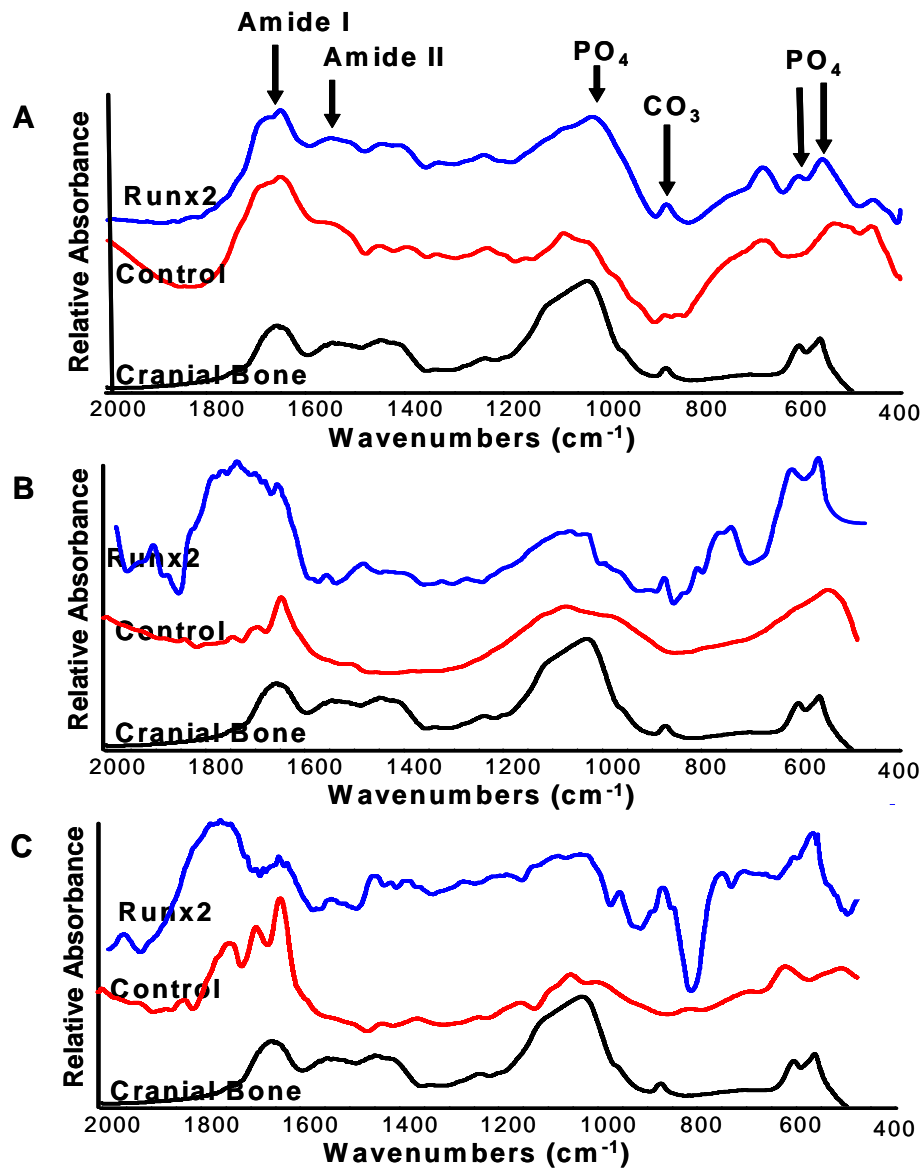
Figure 6.5. Runx2-engineered constructs display FTIR bands characteristic of carbonate-containing, poorly crystalline hydroxyapatite. Chemical composition of the mineral phase deposited on (A) collagen, (B) PCL, and (C) PLGA scaffolds was analyzed by Fourier transform infrared spectroscopy (FTIR) at 42 days post-seeding. All Runx2-engineered constructs and cranial bone samples displayed amide I and II peaks indicative of proteins, an enhanced phosphate peak at 1100 cm^{-1}, a doublet split phosphate peak at 560 and 605 cm^{-1}, and a carbonate peak at 870 cm^{-1}, which represent the characteristic bands of a carbonate-containing, poorly crystalline hydroxyapatite. Carbonate and phosphate doublet peaks were absent in all control constructs, indicating that the radiopaque regions observed on these scaffolds corresponded to non-biological mineral deposits.

confined to the outer 800 μm and 400 μm periphery of Runx2-engineered collagen and PLGA scaffolds, respectively. In contrast, mineral deposits were distributed throughout the interior of Runx2-engineered PCL scaffolds and remained confined to a 50-200 μm circumference surrounding polymeric struts. Cell and mineral distribution within tissue-engineered constructs was also examined by histological analyses (Fig. 6.6B). von Kossa staining for phosphate deposits confirmed the presence and orientation of mineral deposits observed by micro-CT imaging. All control scaffolds showed a low level of background von Kossa staining, likely caused by detection of the phosphate component within non-biological mineral deposits. Hematoxylin-eosin (H&E) staining revealed that cellular distribution was highly dependent on scaffold properties. Dense cell populations were confined to the outer face and edges of matrices with highly porous, sponge-like morphology (collagen and PLGA). Among these, a markedly thicker layer of cell growth was observed at the periphery of collagen compared to PLGA, and minimal cell growth was observed in the interior of both constructs. In contrast, a thin layer of cells were observed around all PCL microfilaments, including those within the construct interior. Notably, mineralization was co-localized with and adjacent to cell growth on all three scaffolds. No difference in cell distribution was detected in scaffolds seeded with control cells relative to Runx2 cells.

Discussion

We demonstrate that the osteogenic potential of Runx2-expressing fibroblasts is highly dependent on the architecture and surface properties of polymeric scaffolds. Micro-CT imaging revealed that genetically-modified fibroblasts deposit significantly
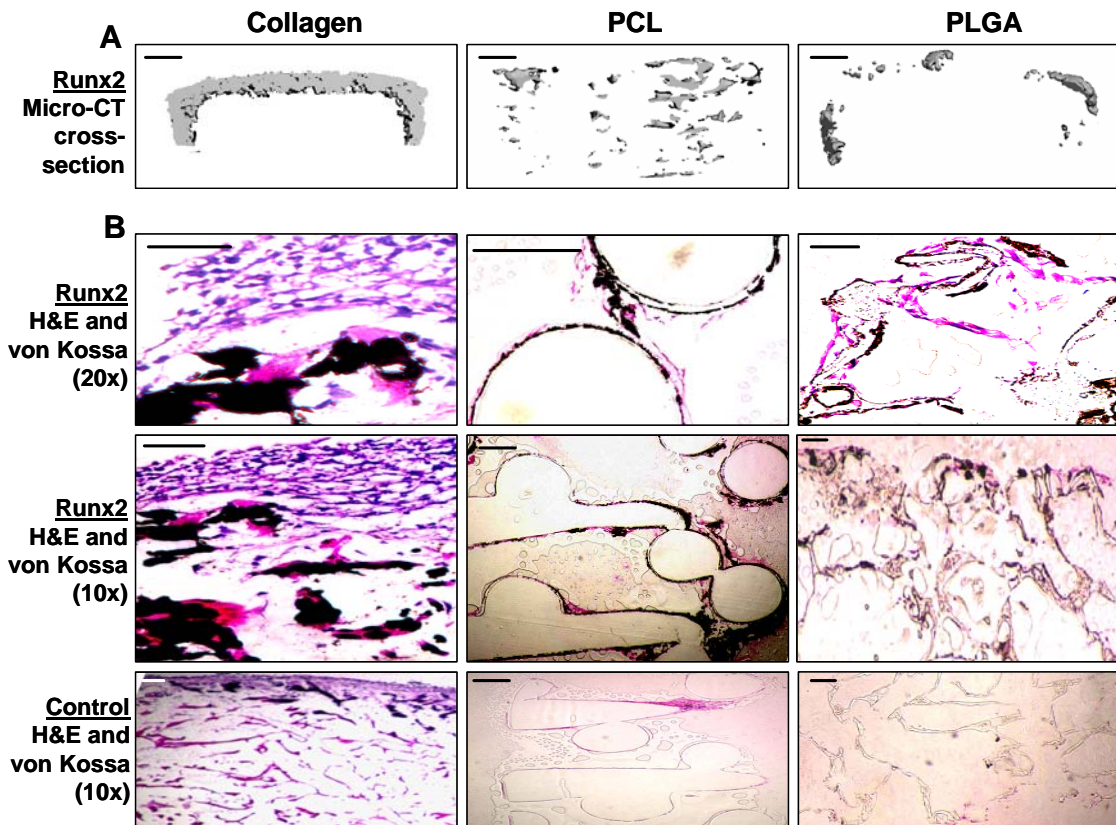
Figure 6.6. Scaffolds differentially modulate distribution of fibroblasts and matrix mineralization. (A) Cross-sectional micro-CT images depicting the distribution of mineralized matrix within Runx2-engineered constructs 42 days post-seeding. Scale bar indicates 1 mm. (B) Cellular distribution and mineral deposition within tissue-engineered constructs was visualized by staining histological sections with hematoxylin-eosin (H&E) and von Kossa, respectively. Scale bar indicates 200 μm.

123

higher levels of mineral on fibrous collagen disks relative to constructs based on PCL and PLGA. The chemical composition of the mineral phase on all three Runx2-engineered scaffolds was verified by FTIR spectroscopy to display the characteristic bands of carbonate-containing, poorly crystalline hydroxyapatite. This chemical signature was absent in control samples seeded with unmodified fibroblasts. Moreover, differential patterns of cell proliferation and gene expression were observed on tissue-engineered constructs, but these trends did not correlate with scaffold-directed mineral deposition. Histological analyses revealed that matrix mineralization co-localized with cellular distribution, which was confined to the periphery of fibrous collagen and PLGA sponges and around the circumference of PCL microfilaments. Collectively, this work underscores the importance of scaffold parameters on the capacity of Runx2-engineered primary dermal fibroblasts to differentiate into a mineralizing osteoblastic phenotype for bone tissue engineering applications.

An ideal biomaterial scaffold for bone grafting applications would satisfy several essential design criteria, including: (1) highly porous architecture to ensure cell survival and rapid vascular infiltration, (2) easily processed into anatomically-relevant shapes, (3) biocompatible to minimize host inflammatory response, (4) well-characterized biodegradation profile to enable persistence of bioactive factors at the implantation site, (5) surface chemistry/topography which promotes cell adhesion, proliferation, differentiation, and (6) mechanical properties which approximate native skeletal tissue and are tailored to the specific load-bearing application [313, 314]. A wide variety of polymers have been explored for their ability to satisfy these material requirements.

Among these, scaffolds manufactured from naturally-derived collagen and synthetic polymers, such as PLGA and PCL, have shown significant promise in numerous grafting and cell-transplantation applications [315]. Collagen is biodegradable, osteoconductive, and contains biological recognition sequences which may specifically influence cell behavior [316]. Yet, scaffolds produced with this natural polymer are limited by inadequate mechanical properties and batch-to-batch inconsistency. PCL and PLGA are aliphatic polyester polymers used to reproducibly manufacture scaffolds in large-scale with a highly controlled degradation profile and architecture [307, 317]. Despite these advantages, the hydrophobic surface chemistry and acidic by-products from the degradation of these synthetic polymers may create a microenvironment which is suboptimal for cell growth/differentiation. In addition, selection of a fabrication technique also plays an important role in defining the biological and mechanical properties of polymeric scaffolds. Conventional fabrication methods (solvent casting, melt molding, gas foaming) yield foam-like structures with variable control of pore size, distribution, and interconnectivity [314]. More recently, highly reproducible scaffolds with an interconnected network of honeycomb-like pores have been fabricated by fused deposition modeling [309, 310, 318-320]. Overall, it is clear that many of the specified design requirements for scaffold optimization are contradictory, making prioritization/reconciliation of these components a challenging step in the development of tissue-engineered bone grafts.

In the present work, we investigated the ability of three polymeric matrices with highly divergent properties to support osteoblastic differentiation and mineral deposition. The biological response of cells seeded within these matrices may be influenced by

125

scaffold architecture, surface properties (e.g. chemistry, roughness/topography), and/or surface chemistry-dependent differences in protein adsorption [311]. Numerous studies have shown that biomaterial surface properties, including chemistry and hydrophobicity, will modulate the type, quantity, conformation, and activity of adsorbed serum-derived proteins [321-325]. These substrate-dependent differences in protein adsorption have distinct effects on cellular adhesion and phenotype expression directed by biomaterial substrates [325-330]. All constructs in this study were pre-coated with the adhesive glycoprotein fibronectin and cultured for 42 days in osteogenic media containing serum. Thus, it is possible that scaffold surface chemistry modulated the conformation/activity of adsorbed fibronectin or other serum-derived proteins, which in turn may have regulated osteoblastic differentiation and mineralization [331, 332]. Furthermore, scaffold architecture (porosity, pore size, interconnectivity) has also shown a marked effect on bone formation and tissue in growth *in vivo* [333-336]. However, the effect of pore size on osteoblastic proliferation and function *in vitro* is highly variable depending on the substrate material, fabrication method, and the seeded osteogenic cell-type [309, 337-340]. Finally, biomaterial surface roughness has been reported to have a marked effect on proliferation, metabolism, and differentiation of osteoblastic cell-types [341, 342]. Overall, it is important to note that the optimization of scaffold architecture and surface properties would require the systematic isolation of each design parameter and the correlation of these parameters to osteogenic outcome variables. This work was intended to serve as a global assessment of the osteogenic capacity of Runx2-expressing fibroblasts when seeded on various scaffolds and cannot be used to draw direct correlations between individual construct parameters and osteogenic differentiation.

126

Scaffold-dependent modulation of cell numbers and colonization patterns within tissue-engineered constructs was observed in the present study. Runx2-expressing fibroblasts showed significantly higher seeding efficiency on fibrous collagen disks relative to PLGA and PCL matrices. Notably, this initial cell adhesion showed a strong inverse correlation with scaffold pore size (collagen (61.7um) > PLGA (100 um) > PCL (500um)), suggesting that a microporous architecture promotes better cell retention than an open macroporous network. Nevertheless, after 42 days in culture, DNA content decreased on collagen/PLGA foams and increased on PCL networks. We speculate that the time-dependent reduction in DNA content is due to cell necrosis within the inner core of constructs as a result of mass transport limitations associated with the porous, sponge-like architecture of collagen and PLGA foams [290, 291, 298]. This hypothesis is supported by the enhanced cell numbers observed on PCL, where the scaffold's macroporous, fully interconnected channel network may have led to improved diffusion of nutrients/oxygen and removal of waste products. Furthermore, histological analyses revealed that cell infiltration and mineral deposition was limited to the outer periphery of scaffolds with a fibrous foam-like geometry (collagen, PLGA). Despite similarities in geometry, collagen disks contained a markedly thicker cell layer than PLGA foams at the construct periphery, possibly because naturally-derived polymers more closely resemble the chemical composition of the cells' native environment. In contrast, tissue growth was directed along the circumference of interconnected microfilaments of PCL and distributed throughout the construct interior. Collectively, these results suggest that cell distribution is predominantly guided by scaffold architecture.

127

Runx2-expressing fibroblasts show the highest capacity for mineralization *in vitro* when seeded on fibrous collagen sponges. This enhanced cellular phenotype is likely a function of the porous scaffold architecture and the biological recognition sequences found within type I collagen, which are known to induce osteoblastic differentiation via $\alpha_2\beta_1$ integrin-mediated signaling cascades [80, 252, 343, 344]. Overall, trends in mineral density did not correlate with scaffold-dependent changes in DNA content, suggesting that enhanced mineral deposition is not a simple function of increased cell numbers. Indeed, minimal deposition of mineral was detected on PCL, despite the significant cell numbers within these scaffolds, highlighting the importance of the construct's material properties during osteoblastic differentiation. Runx2-engineered PLGA constructs showed significantly enhanced mineral deposition compared to PCL scaffolds containing Runx2-engineered fibroblasts, corroborating reports that PLGA-coated surfaces are more osteoconductive than those coated with PCL [345]. Finally, all constructs showed upregulation of osteoblastic genes when seeded with Runx2-transduced fibroblasts compared to unmodified control cells, but the magnitude of this expression was only slightly modulated by scaffold properties. Trends in gene expression also did not mirror mineral deposition, showing that cell function can be differentially modulated by scaffold properties despite minimal changes in early phenotypic markers. Further insights into the relative contributions of scaffold architecture and surface chemistry toward osteogenic differentiation would be obtained by culturing Runx2-expressing cells on collagen-, PLGA-, and PCL-coated two-dimensional surfaces.

In conclusion, we have demonstrated that the osteogenic potential of Runx2-expressing fibroblasts is highly dependent on scaffold properties, with fibrous collagen

128

disks exhibiting significantly higher mineral deposition than gas-foamed PLGA sponges and fused deposition modeled PCL. These results highlight the importance of scaffold optimization in the development of tissue engineered bone constructs.

CHAPTER 7

ENGINEERING HETEROGENEOUS BONE-LIGAMENT INTERFACES WITH A THREE-DIMENSIONAL SPATIAL DISTRIBUTION OF RUNX2 RETROVIRUS

Introduction

Interfacial zones between tissues provide specialized, transitional junctions central to normal tissue function. These interfaces usually consist of multiple cell-types and spatially-graded matrix components arranged in a complex hierarchical structure to fulfill specific functional roles. One example in human anatomy of this important structure-function relationship is found in the bone-soft tissue interfaces of the musculoskeletal system [346, 347]. In particular, the insertion site between the anterior cruciate ligament and the tibia consists of a heterogeneous interface with four distinct regions, including: ligament, fibrocartilage, calcified fibrocartilage, and bone [348-350]. This graded transitional zone facilitates the transmission of complex mechanical loads across the knee joint by minimizing stress concentrations at the junction of two tissue types [155, 351]. Conventional soft tissue autografts typically fail at this insertion site due to inadequate tissue integration, further highlighting the physiologic importance of these heterogeneous structures [149, 352, 353].

The lack of robust, functional interfaces between bone and soft tissues severely limits the functional integration and biological performance of conventional orthopaedic grafting strategies [156]. Tissue engineering principles have been pursued to create these heterogeneous interfaces [218]. The general paradigm for this approach, in which phenotype-specific cells and/or bioactive growth factors are integrated into polymeric

130

matrices, has been successfully applied in recent years toward the development of bone, ligament, and cartilage tissues in vitro and in vivo [142, 148, 156, 354]. Yet, beyond the basic evidence of tissue formation, the regeneration of complex tissue structures which recapitulate the microarchitecture and function of native tissue has not been realized. Overall, the development of graded/transitional interfacial tissue zones represents a significant challenge in current tissue engineering and regenerative medicine strategies.

Emerging themes in early embryonic development provide insights into natural biological mechanisms for complex tissue formation [355, 356]. One widely-accepted concept is that diffusion of small signaling molecules (i.e. morphogens) from a source to a sink leads to concentration gradients which specify spatial cues to specific cells [357]. Extracellular morphogen gradients often direct cell fate by activating intracellular transcription factors via concentration thresholds [358, 359]. Furthermore, the extracellular matrix has been found to aid in gradient formation by presenting binding sites for soluble morphogens via heparin sulfate proteoglycans [360]. Alternatively, morphogens can also be transcription factors with an intracellular mode of action [361-363]. Taken together, these principles suggest that the recapitulation of nature-inspired gradients may enable the organization of cell fates into specific three-dimensional patterns.

Current technologies to create gradients of bioactive molecules in vitro involve the encapsulation of growth factors within 3-D polymeric matrices or covalent/non-covalent immobilization of peptide sequences to patterned biomaterial surfaces [364-368]. These protein-based approaches are limited by suboptimal delivery vehicles, poor spatiotemporal dosage control, short protein half-life, and the cost-prohibitive supraphysiologic concentrations required to initiate a cellular response [369, 370]. In order to

131

circumvent these issues, we leveraged biomaterial-mediated retroviral gene transfer as a novel strategy to create a spatial distribution of genetic material encoding for a tissue-specific transcription factor within 3-D polymeric networks. We have previously reported that retroviral overexpression of the osteogenic transcription factor Runx2 using conventional *ex vivo* gene transfer techniques in fibroblasts will reprogram this non-osteoblastic cell into a mineralizing, osteoblastic phenotype in vitro and in vivo [131, 132, 136]. In the present study, we demonstrate that zonal organization of bone and soft tissue-mimetic tissue can be engineered by a simple, one step seeding of autologous fibroblasts onto polymeric scaffolds containing spatially-defined regions of the Runx2 retroviral vector. This approach is fundamentally different from current strategies used to create heterogeneous tissues, which use co-culture of multiple cellular phenotypes and/or multi-phase scaffolds with pore-size or compositional gradients [217, 371-373]. Overall, this research is significant toward the regeneration of transitional interfacial zones which mimic the cellular and micro-structural characteristics of native tissue. These strategies were developed in the context of the bone-ligament enthesis as a model system, but are broadly applicable to a wide variety of heterogeneous biological tissues.

Materials and Methods

Cell Culture and Reagents

Primary fibroblasts were harvested from 8- to 16-week-old male Wistar rats by enzymatic digestion of the dermal skin layer [220]. Cells were expanded in growth media consisting of DMEM, 10% fetal bovine serum, and 1% penicillin-streptomycin. Antibiotics and cell culture media were obtained from Invitrogen (Carlsbad, CA), fetal

bovine serum was purchased from Hyclone (Logan, UT), and all other cell culture supplements and reagents were acquired from Sigma (St. Louis, MO).

Retrovirus Production

The Runx2 retroviral vector utilizes the promoter activity of a 5' long terminal repeat to express a single, bicistronic mRNA encoding the murine cDNA for the type II MASNSLF Runx2 isoform,[221, 222] followed by an internal ribosomal entry site and a Zeocin resistance-enhanced green fluorescent fusion protein (Fig. 7.1A) [66]. Empty vector control plasmid lacked the Runx2 insert. Plasmid DNA was purified from transformed *E. coli* using Megaprep kits from Qiagen (Valencia, CA). Retroviruses were packaged by transient transfection of helper-virus free ΦNX amphotropic producer cells with plasmid DNA as described elsewhere [66].

Scaffold Coating and Seeding

Scaffolds were coated with 0.01% poly-L-lysine (70,000-150,000 MW), as this concentration and charge/molecule ratio has been shown to yield high levels of virus particle adsorption and transduction efficiency [374]. In order to test the feasibility of biomaterial-mediated retroviral gene transfer, rectangular fibrous collagen scaffolds (3 mm wide x 8 mm long x 2 mm thick, average pore size 61.7 μm, 93.7% pore volume, Kensey Nash, Exton, PA) were uniformly coated with poly-L-lysine (PLL) for 30 minutes followed by incubation in Runx2 or empty vector retroviral supernatant for 4.5 hours in a humidified 5% CO_2 atmosphere at 32 °C. Virus-only control scaffolds were uniformly coated with water followed by incubation in Runx2 retrovirus, while PLL-only

133

control scaffolds were uniformly coated with PLL followed by incubation in PBS supplemented with 10% fetal bovine serum. All constructs were washed 1-2x with PBS and seeded at a density of $2x10^5$ cells/scaffold in osteogenic growth media.

In order to generate constructs with a spatial distribution of retrovirus, collagen scaffolds (5 mm wide x 20 mm long x 2 mm thick) were partially coated on the proximal end with 0.01% PLL for 30 minutes and incubated in Runx2 or empty vector retroviral supernatant for 4.5 hours. Virus-only control scaffolds were partially coated with water followed by incubation in Runx2 retrovirus, while PLL-only control scaffolds were partially coated with PLL followed by incubation in PBS supplemented with 10% fetal bovine serum. These gradient constructs were washed 1-2x with PBS and seeded at a density of $1x10^6$ cells/scaffold in osteogenic growth media.

All constructs were transferred twenty-four hours post-seeding to osteogenic differentiation media consisting of DMEM, 10% fetal bovine serum, 100 U/ml penicillin G sodium, 100 µg/ml streptomycin sulfate, 50 µg/ml L-ascorbic acid, 2.1 mM sodium β-glycerophosphate, and 10 nM dexamethasone. Culture media was changed every 3 days until end-point assay. No differences were observed between empty vector retrovirus (negative control) and unmodified cells in all experiments.

Cell Viability

Scaffolds were harvested at 21 and 42 days post-seeding, rinsed in complete Dulbecco's phosphate buffered saline (PBS), and incubated in 4 µM calcein-AM and 4 µM ethidium homodimer-1 (Molecular Probes, Eugene, OR) in PBS for 30 minutes under

gentle agitation. Constructs were then rinsed (3 x 10 minutes) in PBS and analyzed with a Zeiss LSM 510 Confocal Microscope using Ar and HeNe lasers and a 5x objective lens.

DNA Content

Samples were harvested at 1, 21, and 42 days post-seeding, rinsed with PBS, and frozen at -80°C. Scaffolds and serially diluted cell standards were thawed, lyophilized, and digested at 55°C in 500 μl of 0.25 mg/ml proteinase K (Fisher Scientific, Pittsburgh, PA) in 100 mM ammonium acetate (pH 7.0) for 24 hours. Digested samples were assessed for DNA content via the PicoGreen dsDNA Quantitation Kit (Molecular Probes, Eugene, OR). Raw DNA data was converted to cell numbers using a linear standard curve.

Real time RT-PCR

Total RNA was isolated at 7 days post-seeding using the RNeasy RNA isolation kit with RNAlater stabilization reagent (Qiagen). cDNA synthesis was performed on DNaseI-treated (27 Kunitz units/sample) total RNA (0.25 μg) by oligo(dT) priming using the Superscript™ First Strand Synthesis System for RT-PCR (Invitrogen, Carlsbad, CA). Gene expression was assessed by quantitative RT-PCR using SYBR Green intercalating dye (Molecular Probes) and rat-specific primers as previously described [66, 137]. Primer specificity was confirmed by ABI Prism 7700 Dissociation Curve Software. Standards for each gene were amplified from cDNA using real-time oligonucleotides, purified using a Qiagen PCR Purification kit, and diluted over a functional range of concentrations. Transcript concentration in template cDNA solutions was quantified from a linear

standard curve, normalized to 0.25 µg of total RNA, and expressed as nanomoles of transcripts per µg of total RNA. Detection limits for each gene were determined by reactions without cDNA and fall below the y-axis minimum.

Microcomputed Tomography

High resolution X-ray microcomputed tomography (micro-CT) with a Scanco µCT Medical CT 40 imaging system (Bassersdorf, Switzerland) was used to quantify in vitro and in vivo mineralization of 3-D scaffolds. Formalin-fixed specimens were scanned at a 16 µm voxel resolution. Uniformly coated scaffolds cultured in vitro were evaluated at a threshold corresponding to a linear attenuation of 1.04 cm^{-1}, Gauss filter sigma of 1.2, and filter support of 2. The inner volume of partially coated scaffolds cultured in vitro was manually segmented to eliminate edge effects and evaluated between lower and upper thresholds corresponding to linear attenuations of 2.08 cm^{-1} and 3.2 cm^{-1}, respectively. Partially coated scaffolds implanted in vivo were evaluated at a threshold corresponding to a linear attenuation of 1.20 cm^{-1}. Reconstructed and thresholded images were evaluated using direct distance transformation methods to calculate mineralized matrix volume within each construct.

Mechanical Testing

Fresh specimens were washed in PBS, cut in half (gauge length and width of 10-mm and 5-mm, respectively), placed into soft-tissue clamps of an ELF 3200 mechanical testing system (EnduraTEC / Bose, Eden Prairie, MN), and pulled to failure at a rate of 0.2 mm/sec. Force was recorded using a 11-lb load cell (Interface, Scotsdale, AZ) and

136

displacement recorded via computer acquisition interface (WinTest, EnduraTEC). Stress and strain were calculated from the force and displacement data by adjusting for the tissue's cross-sectional area and gauge length, respectively.

Subcutaneous Implantation

Heterogeneous constructs were subcutaneously implanted into the backs of 7-week-old syngeneic rats after 24 hours culture in osteogenic growth media (n=3 for each treatment group). Two implants were placed in each animal, one on each side of a midline incision into subcutaneous pockets made by blunt dissection. Constructs were explanted after 2 weeks of implantation following euthanasia by CO_2 inhalation. All procedures were carried out according to an IACUC-approved protocol as previously described [131, 138].

Histology and Immunohistochemistry

Formalin-fixed constructs were paraffin embedded and sectioned at 5 μm thickness. Sections were stained with hematoxylin-eosin and von Kossa to observe cellular distribution and matrix mineralization within 3-D constructs, respectively. eGFP expression was observed by immunostaining using a colorimetric avidin-biotin kit (Vector Labs, Burlingame, CA). Sections were deparaffinized, rehydrated, and then pretreated using protease-induced antigen retrieval in 1 μg/mL proteinase K. After pretreatment, slides were incubated in a rabbit polyclonal primary antibody against eGFP (Molecular Probes) followed by sequential incubation in biotinylated anti-rabbit

137

secondary antibody and avidin-biotin linked alkaline phosphatase. Slides were then incubated in Vector Red substrate and counterstained with hematoxylin.

Data Analysis

Unless otherwise stated, all *in vitro* experiments were performed two times in triplicate, each with unique Runx2 retroviral supernatant preparations, and two independent isolates of primary dermal fibroblasts. Data are reported as mean ± standard error of the mean (SEM), and statistical comparisons using SYSTAT 8.0 were based on an analysis of variance (ANOVA) and Tukey's test for pairwise comparisons, with a p-value < 0.05 considered significant. In order to make the variance independent of the mean, statistical analysis of real-time PCR data was performed following logarithmic transformation of the raw data [66].

Results

Biomaterial-mediated retroviral gene transfer approach

As a first step toward creating a heterogeneous interface, we explored the feasibility of delivering genetic material to fibroblasts via a biomaterial-mediated retroviral gene transfer approach. We exploited the ability of cationic polymers (e.g. poly-L-lysine (PLL), polybrene) to neutralize charge and aggregate retroviral particles in order to immobilize retrovirus onto collagen scaffolds [374, 375]. Scaffolds were uniformly coated with 0.01% PLL incubated for 4.5 hours in retroviral supernatant, and seeded with primary dermal fibroblasts. Cells were enzymatically digested from collagen scaffolds and analyzed for transduction efficiency by quantification of eGFP expression via flow

138

cytometry with a Vantage SE cell sorter (Becton-Dickinson, San Jose, CA). eGFP expression was detected in $\geq$ 20% of primary dermal fibroblasts after 14 days in culture in osteogenic growth media, demonstrating sustained and integrated transgene expression by the retroviral vector (Fig. 7.1B). Quantitative RT-PCR analysis revealed that viral uptake of virus is dependent on pre-treating scaffolds with PLL, as eGFP gene expression was upregulated on PLL+R2RV-coated scaffolds compared to virus-only controls (Fig. 7.1C). These results were corroborated by immunohistochemical staining for eGFP expression. eGFP co-localized with fibroblasts only on scaffolds co-treated with PLL+R2RV (Fig. 7.1D, E). Finally, confocal image analysis of live/dead fluorescent staining (Fig. 7.1F) and quantification of DNA content (Fig. 7.1G) indicated that fibroblasts remain viable throughout the 42 day culture period and equivalently colonize collagen scaffolds independent of treatment group.

Biomaterial-mediated gene transfer of Runx2 retrovirus promotes osteogenesis in fibroblasts

Osteogenic gene expression within uniformly coated constructs was quantified by real time RT-PCR after 7 days culture in osteogenic differentiation media (Fig. 7.2A). Biomaterial-mediated delivery of the Runx2 retroviral vector upregulated osteoblastic gene expression compared to PLL-only and virus-only control constructs. This response was specific to osteogenic markers, as type II collagen expression remained unchanged. Mineral deposition within uniformly coated scaffolds was analyzed after 49 days culture in osteogenic differentiation media (Fig. 7.2B,C). Fibroblasts deposited a significant amount of mineralized matrix on collagen scaffolds coated with PLL+R2RV, while virus-

139
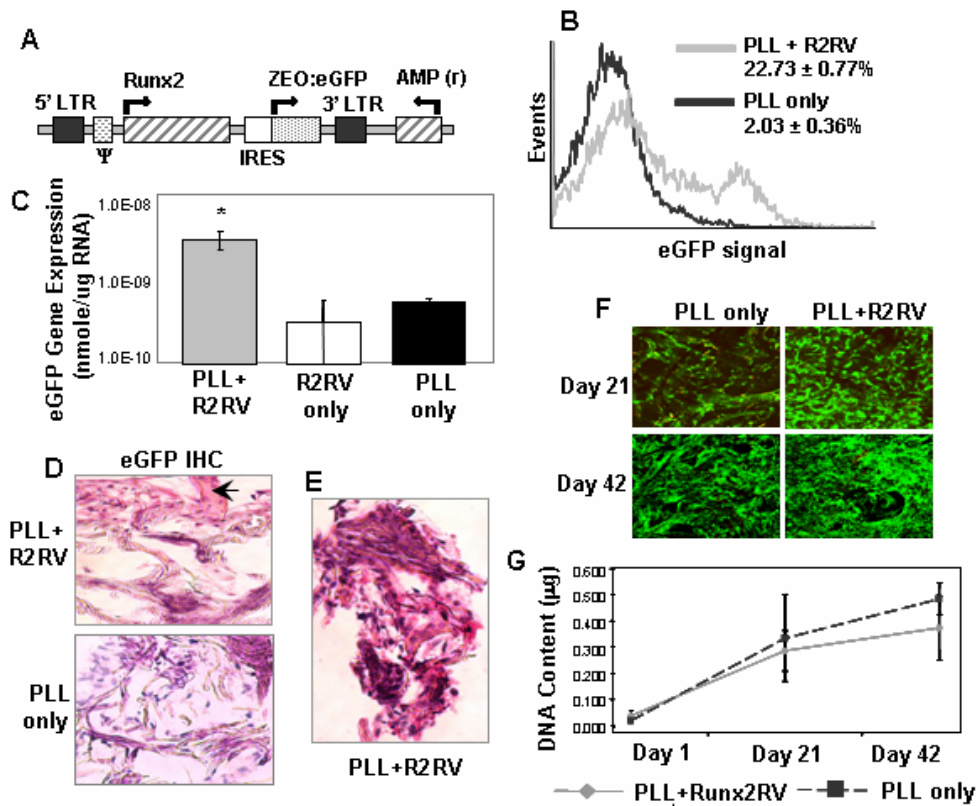
Figure 7.1: Biomaterial-mediated retroviral gene transfer results in efficient transduction and sustained transgene expression in fibroblasts. Negatively-charged Runx2 retrovirus (R2RV) was immobilized onto fibrous collagen scaffolds uniformly coated with the cationic poly-L-lysine (PLL). Primary dermal fibroblasts were then seeded onto these scaffolds and statically cultured *in vitro*. (A) The Runx2 retroviral vector expresses the type II Runx2 isoform and a Zeocin:eGFP selectable marker from a single bicistronic mRNA. (B) Detection of GFP expression by flow cytometry after enzymatic digestion of cells from collagen scaffolds demonstrated efficient fibroblast transduction at 14 days post-seeding. (C) eGFP mRNA levels were upregulated in PLL+R2RV-coated scaffolds compared to controls at 7 days post-seeding, demonstrating that viral uptake by fibroblasts is dependent on pre-coating scaffolds with poly-L-lysine (Mean + SEM, n=3; ANOVA: $p<0.05$; * different from R2RV only control ($p=0.05$)). (D) The spatial localization of eGFP expression and cell distribution was qualitatively observed within histological sections by immunohistochemical staining for eGFP (pink, arrow) and hematoxylin and eosin counterstain (blue), respectively. 10x micrographs. Scale bar=500 μm. (E) 20x micrograph of eGFP expression (pink) co-localizing with fibroblasts (blue) within a scaffold uniformly coated with PLL+R2RV after 21 days in culture. Scale bar=250 μm. (F) Uniform cellular colonization and viability throughout the 42 day culture period was confirmed by confocal microscopy image analysis of live (green)/dead (red) fluorescence staining and (G) quantification of DNA content (Mean + SEM, n=3; ANOVA: $p<0.05$).

140

only controls showed negligible mineral deposits. Notably, an unexpected low level of radiodense material was observed on PLL-only controls, suggesting that in vitro culture conditions may lead to precipitation of non-biological mineral. This possibility was further supported by FTIR analysis of the chemical composition of the mineral phase. Retrovirus-coated scaffolds and cranial bone samples displayed the characteristic bands of carbonate-containing, poorly crystalline hydroxyapatite, while this chemical signature was absent in control samples. In addition, immunohistochemical staining for eGFP expression was performed to assess the spatial distribution of transduced fibroblasts within uniformly coated constructs (Fig. 7.2D). eGFP-positive cells co-localized with von Kossa-positive mineral deposits, indicating that mineral deposition was primarily originated by fibroblasts which were susceptible to biomaterial-mediated viral gene delivery.

Importantly, histological and micro-CT analyses of cross-sectional images revealed that cell colonization and mineral deposition patterns are differentially modulated by the virus delivery strategy (Fig. 7.3A,B). Mineral deposits displayed a dense morphology and were confined to the periphery of scaffolds seeded with fibroblasts engineered with Runx2 retrovirus by conventional gene transfer techniques. In contrast, discrete mineralized nodules corresponding to transduced cell colonies were distributed throughout the interior of scaffolds that had been coated with PLL+R2RV prior to cell seeding. These results are important because the clinical application of current tissue engineering strategies to critical-sized bone defects is significantly limited by the formation of a mineralized shell around the scaffold periphery which, consequently, causes cell necrosis within the inner construct core [290, 298]. Taken together,
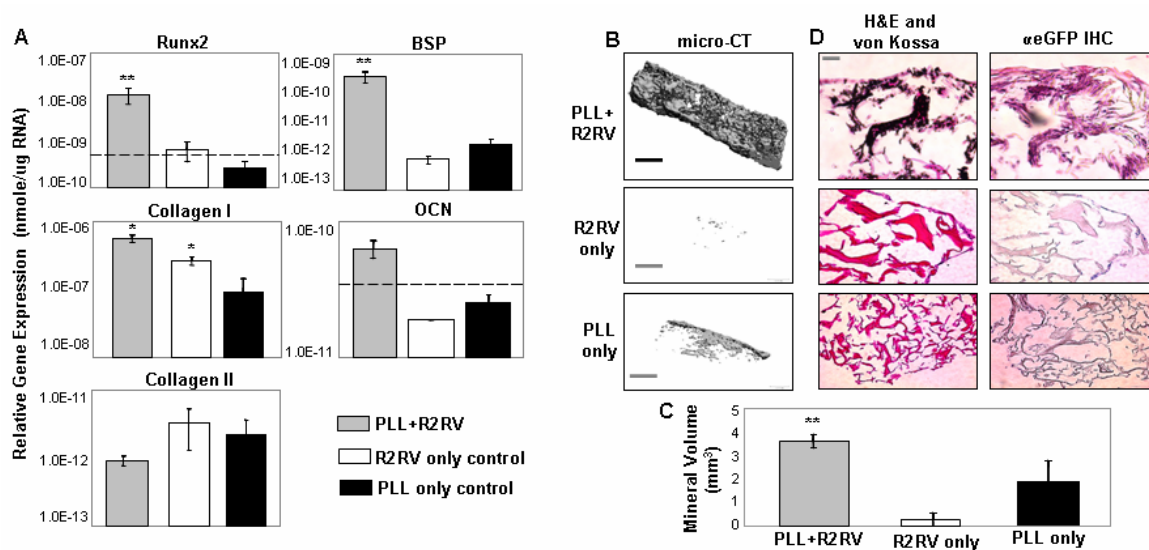
Figure 7.2: Biomaterial-mediated gene delivery of Runx2 retrovirus promotes osteoblastic differentiation in fibroblasts. Scaffolds were uniformly coated with poly-L-lysine (PLL) and incubated in retroviral supernatant (R2RV) prior to seeding with primary dermal fibroblasts. (A) Osteogenic gene expression was upregulated within constructs uniformly coated with PLL+R2RV compared to virus-only and PLL-only controls after 7 days in vitro culture in osteogenic media. (Mean + SEM, n=3; Runx2: ANOVA: p=0.002, ** different from both R2RV only (p=0.01) and PLL only (p=0.002) controls; BSP: ANOVA: p= 0.000066, ** different from both R2RV only (p=0.00009) and PLL only (p=0.00023) controls; CollagenI: ANOVA: p=0.017, * different from PLL only control (p=0.015). (B) Micro-CT images showing enhanced mineral deposition on scaffolds uniformly coated with PLL+R2RV compared to virus-only and PLL-only controls. Scale bar=1 mm. (C) Mineral deposition within uniformly coated scaffolds was quantified by micro-CT image analysis after 49 days in osteogenic media. (Mean + SEM, n≥4; ANOVA: p<0.0001; ** different from both R2RV only (p=0.00018) and PLL only (p=0.05) controls). (D) Histological analyses revealed that genetically-engineered eGFP-positive fibroblasts co-localized with mineral deposits, indicating that mineral deposition was primarily originated by fibroblasts which were susceptible to biomaterial-mediated viral gene delivery. Cell and mineralized matrix distribution was visualized by staining serial histological sections for eGFP expression (eGFP immunohistochemistry, pink), fibroblasts (H&E, blue), and phosphate deposits typically present within mineralized nodules (von Kossa, black). 10x micrographs. Scale bar indicates 500 μm.

142

Conventional *ex vivo* gene transfer | **Biomaterial-mediated viral delivery**

A — micro-CT

B — Histology (H&E and von Kossa)
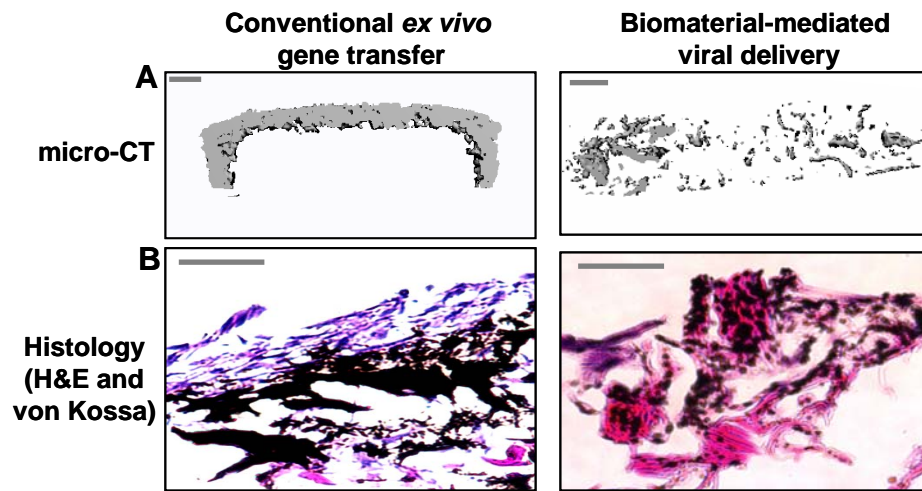
Figure 7.3. **Fibroblast colonization and mineral deposition patterns are differentially modulated by virus delivery strategy.** (A) Cross-sectional micro-CT images depicting the distribution of mineralized matrix within Runx2-engineered constructs. Scale bar indicates=1 mm. (B) Cell and mineral distribution within collagen disks was visualized by hematoxylin-eosin (H&E) and von Kossa staining, respectively. Scale bar=250 μm. Mineral deposits displayed a dense morphology and were confined to the periphery of scaffolds seeded with fibroblasts engineered by conventional ex vivo gene transfer techniques. In contrast, discrete mineralized nodules corresponding to individual transduced cells were distributed throughout the interior of scaffolds that had been coated with Runx2 retrovirus prior to fibroblast seeding.

143

these results indicate that biomaterial-mediated retroviral gene delivery is a feasible strategy for the genetic modification and differentiation of fibroblasts into a mineralizing osteoblastic phenotype within 3-D matrices.

Spatially-regulated genetic modification of fibroblasts in 3-D matrices

A spatial distribution of Runx2 retrovirus was created by partially coating the proximal end of scaffolds with PLL prior to incubation in retroviral supernatant (Fig. 7.4). These constructs were then seeded with primary dermal fibroblasts and cultured *in vitro* under static conditions in osteogenic media until endpoint assay. Immunohistochemical staining revealed the presence of a retrovirus-induced graded distribution of genetically engineered cells, with eGFP-expressing cells distributed throughout the scaffold interior on the proximal, PLL+R2RV-coated portion of constructs (Fig. 7.5B). These Runx2-expressing cells co-localized with a graded distribution of mineral deposition, further demonstrating that cellular uptake of the Runx2 retroviral vector is highly dependent on the adsorption of the retrovirus to positively-charged PLL prior to cell seeding (Fig. 7.5C). Confocal microscopy image analysis of live/dead fluorescent staining showed that cell distribution and viability were uniform throughout the scaffold, confirming that the spatial distribution of mineral was not due to differences in cell numbers (Fig. 7.5A).

144
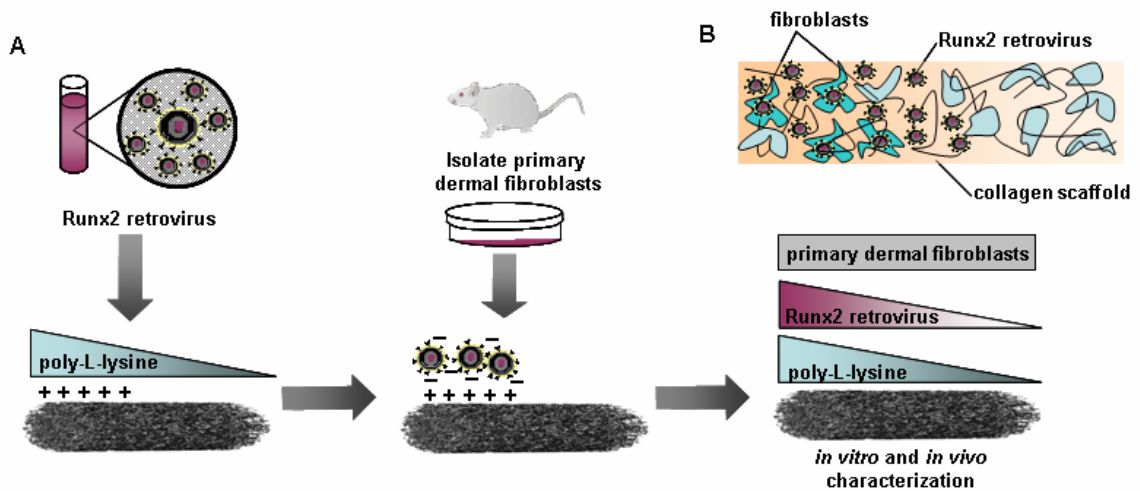
Figure 7.4. Biomaterial-mediated gene transfer approach used to spatially control genetic modification and differentiation of fibroblasts within 3-D matrices. (A) A spatial distribution of Runx2 retrovirus was created in 3-D by coating the proximal portion of fibrous collagen scaffolds with positively-charged poly-L-lysine prior to incubation in retroviral supernatant. These constructs were then seeded with primary dermal fibroblasts and cultured *in vitro* in osteogenic media or implanted *in vivo* into a subcutaneous, ectopic site until characterization with end point assays. (B) Schematic representation of cell-seeded constructs containing a spatial distribution of non-covalently immobilized retrovirus.

145
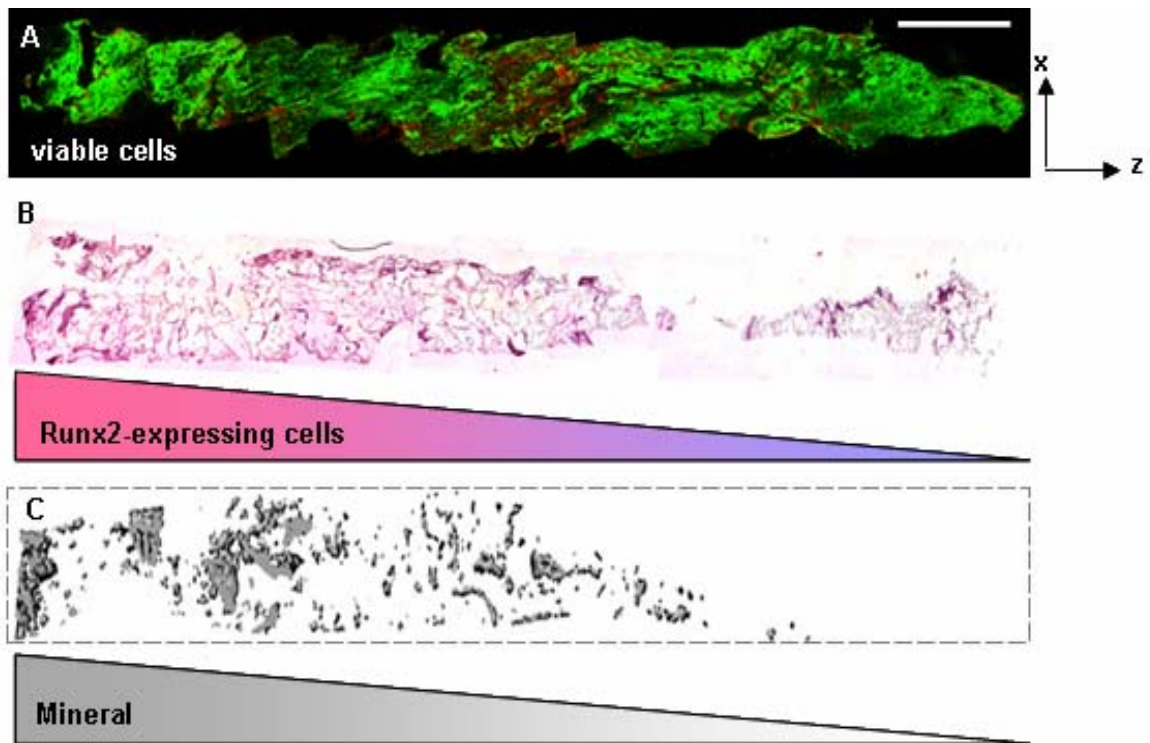
Figure 7.5. **Spatially regulated genetic modification of fibroblasts in 3-D matrices containing a graded distribution of Runx2 retrovirus.** A spatial distribution of Runx2 retrovirus was created by partially coating the proximal portion (left side) of fibrous collagen scaffolds with poly-L-lysine prior to incubation in retroviral supernatant. These constructs were then seeded with primary dermal fibroblasts and cultured *in vitro* in osteogenic media. (A) Confocal microscopy image of live (green)/dead (red) fluorescently-stained cells showing uniform fibroblast distribution. Scale bar=4 mm. (B) Immunohistochemical staining for eGFP counterstained with hematoxylin (blue) showing elevated eGFP expression (pink) on the region with immobilized Runx2 retrovirus. (C) Cross-sectional micro-CT image of mineral deposits showing transitional mineralized zone co-localizing with eGFP expression. Scaffold is outlined in dashed box.

Zonal organization of osteoblastic and fibroblastic phenotypes within 3-D matrices in vitro and in vivo

Gene expression within partially coated constructs was quantified by real time RT-PCR after 7 days in osteogenic differentiation media. Fibroblasts seeded on the proximal, PLL+R2RV-coated portion of collagen scaffolds (sideA) exhibited significant upregulation of osteoblastic genes, while cells seeded on the distal scaffold portion (sideB) incubated in retrovirus alone expressed background levels of these osteoblastic markers (Fig. 7.6A). This induction in osteoblastic differentiation was due the presence of immobilized Runx2 retrovirus as PLL-only treated scaffolds displayed background levels of osteoblastic markers.

Mineral deposition within partially coated constructs was evaluated with micro-CT image analysis after 42 days culture in osteogenic differentiation media. Remarkably, scaffolds containing a spatial distribution of immobilized retrovirus (PLL+R2RV) showed zonal organization of both mineral deposition and non-mineralized, fibroblastic extracellular matrix (Fig. 7.6B). The magnitude of the mineral volume fraction was highest on the proximal end of the scaffold and decreased gradually along the length of the construct toward the distal end (Fig. 7.6C). This mineral gradient was not detected on PLL-only and R2RV-only control constructs.

The biomechanical properties of these heterogeneous constructs were characterized with tensile testing at a strain rate of 0.2 mm/s (Fig. 7.6D). Construct stiffness (0.198 ± 0.038 N) and maximum force at failure (0.277 ± 0.04 N/mm) were significantly enhanced on the proximal, PLL-coated portion (side A) of R2RV-coated scaffolds when compared to control specimens. Furthermore, the material properties of

147

R2RV-coated constructs (Young's Modulus (0.16 ± 0.024) and maximum stress (0.03 ± 0.004)) were also significantly upregulated compared to control samples. Taken together, this data demonstrates that increases in both the structural and material mechanical properties of heterogeneous bone-ligament tissue constructs are localized to scaffold regions containing the highest amount of mineralized tissue.

Finally, engineered scaffolds were implanted into an ectopic, subcutaneous site in order to assess the capacity of these constructs to mature into a bone-ligament-mimetic tissue in vivo in the absence of osteoinductive cues and cell-types typically present in orthotopic defects. Micro-CT image analysis revealed spatial patterning of mineral deposition within constructs containing a graded distribution of the Runx2 retroviral vector after 14 days in vivo (Fig. 7.7A,B). Negligible mineral deposits were detected on control constructs coated with empty vector retrovirus.

Discussion

The ultimate goal of tissue engineering is the regeneration of complex tissues which mimic the cellular and micro-structural characteristics of native tissue to restore normal function. The objective of the present study was to engineer a heterogeneous bone-soft tissue interface by spatially regulating the expression of a tissue-specific transcription factor in fibroblasts within 3-D matrices. Toward this end, we first demonstrate that biomaterial-mediated retroviral gene transfer is a feasible strategy for the genetic modification and differentiation of fibroblasts into a mineralizing osteoblastic phenotype. We then leveraged the observation that retroviral uptake from tissue constructs was highly dependent on PLL to create a graded distribution of Runx2

148
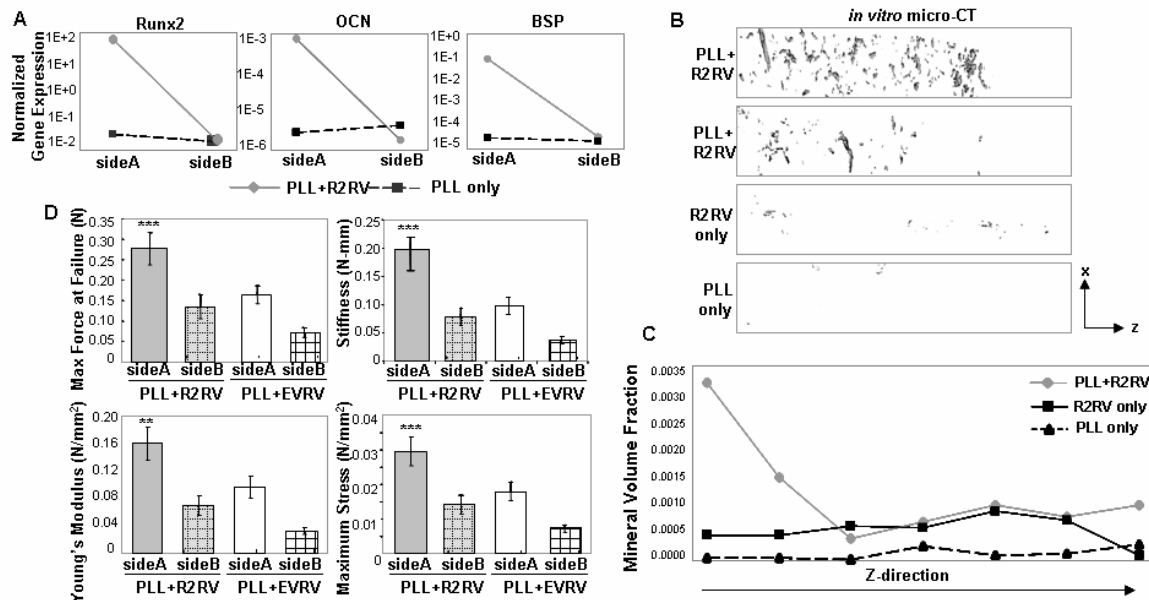
Figure 7.6. Zonal organization of osteoblastic and fibroblastic phenotypes created by 3-D retroviral gradients in vitro. A spatial distribution of Runx2 retrovirus was created by partially coating the proximal (left half, side A) portion of scaffolds with poly-L-lysine (PLL) prior to incubation in retroviral supernatant and cell seeding. (A) Osteogenic gene expression, including Runx2, osteocalcin, and bone sialoprotein, was upregulated by at least 2 orders-of-magnitude compared to controls on the proximal, PLL+R2RV-coated portion (side A) of a representative scaffold containing a virus gradient. (B) Micro-CT images showing spatial patterning of both mineral deposition and non-mineralized, fibroblastic extracellular matrix in tissue engineered constructs containing a spatial distribution of immobilized Runx2 retrovirus. This graded mineral distribution was not observed on virus-only or PLL-only controls. Scale bar=3.5mm. (C) Quantification of mineral volume in 2 mm segments moving lengthwise down the z-axis of representative constructs with micro-CT image analysis. (D) Tensile testing at a strain rate of 0.2 mm/s indicated that the structural and material mechanical properties were significantly enhanced on the proximal, PLL-coated portion (side A) of R2RV-coated scaffolds compared to control specimens. Notably, this increase in mechanical properties corresponding to the region of these constructs containing the highest content of mineral deposition. (Mean + SEM, n>10; Max Force at Failure: ANOVA: p=0.00012; *** ≠ EVRV sideB (p=0.000079), EVRV sideA (p=0.0437), and R2RV sideB (p=0.0089). Stiffness: ANOVA: p=0.0004; *** ≠ EVRV sideB (p=0.00034), EVRV sideA (p=0.035), and R2RV sideB (p=0.0122). Young's Modulus: ANOVA: p=0.000067; ** ≠ EVRV sideB (p=0.000047) and R2RV sideB (p=0.005). Maximum stress: ANOVA: p=0.000069; *** ≠ EVRV sideB (p=0.000044), EVRV sideA (p=0.049), and R2RV sideB (p=0.0065).

149

www.manaraa.com
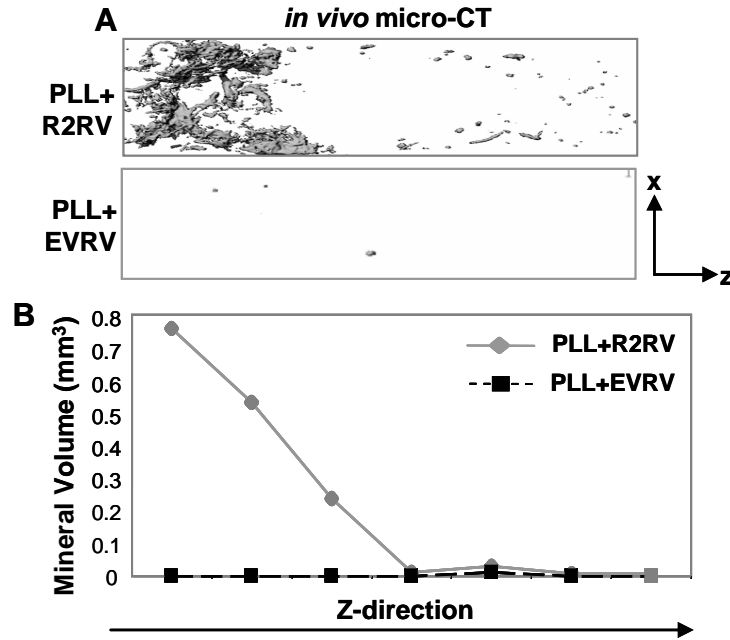
Figure 7.7. Runx2-induced spatial patterning of mineral deposition in vivo. Dermal fibroblasts were uniformly seeded on collagen scaffolds containing a spatial distribution of immobilized Runx2 retrovirus (left half of scaffold was coated with poly-L-lysine/Runx2 retrovirus). These heterogeneous tissue engineered constructs were implanted into a subcutaneous, ectopic site in order to assess the ability of these constructs to create a graded interface in the absence of an osteogenic environment. (A) Micro-CT images of explanted constructs after 14 days in vivo showing a spatial organization of mineral deposition. Scale bar=3mm. (B) Quantification of bone volume in 1 mm segments moving lengthwise down the z-axis of representative constructs by micro-CT image analysis. The magnitude of the mineral volume was highest on the proximal, PLL-coated portion of the scaffold and decreased gradually moving lengthwise down the z-axis of the construct toward the distal end. This positional mineral distribution was not observed on empty vector virus controls.

150

retrovirus within tissue engineered constructs. These 3-D retroviral gradients resulted in spatially regulated genetic modification of fibroblasts and, consequently, zonal organization of osteoblastic and fibroblastic cellular phenotypes in vitro. Furthermore, spatial patterns of mineral deposition and non-mineralized fibroblastic extracellular matrix were also observed after subcutaneous in vivo implantation. Taken together, these results indicate that a continuous, biphasic bone-soft tissue interface can be developed by a simple, one step seeding of fibroblasts into polymeric scaffolds containing a graded distribution of the Runx2 retroviral vector. Notably, the proposed work focuses on a single cell type to generate these heterogeneous tissue constructs; this aspect is fundamentally different from current approaches dealing with creating bi/tri-layered scaffolds via multiple steps and combining different cellular phenotypes (e.g., osteoblasts and fibroblasts) [217, 371, 372].

Concentration gradients of extracellular and intracellular morphogens play a central role in directing cell fate and establishing tissue axes during embryonic pattern formation [355, 356]. Remarkably, embryonic positional fields less than 30 cells wide can be organized into discrete domains of gene expression with crisp borders [376]. Mechanisms by which these gradients are translated into precise spatial control over cellular response are not fully understood. Yet, one predominant theme is that morphogen diffusion leads to the activation of downstream transcription factors via differential cell sensitivity to concentration thresholds [356, 358]. We hypothesize that precise and robust control over spatial patterns of tissue-specific transcription factor expression would be amenable to complex tissue formation. In support of this hypothesis, we provide evidence that a continuous, biphasic bone-soft tissue interface can be engineered with a 3-D gradient of

151

genetic material encoding for the osteogenic transcription factor Runx2. This result represents an important step toward the development of enabling technologies for precise and robust control over 3-D spatial cues. The degree to which a tissue engineered substitute must resemble native tissue in order to induce functional integration and regeneration has not been defined, but is likely dependent on the anatomic location of the defect. Ultimately, spatial control at the single-cell length scale (100 μm) may be required to engineer complex structures which recapitulate the precise architecture and biochemical properties of native tissue [359].

A central issue toward the creation of heterogeneous tissues is the development of technologies for spatiotemporal control over signaling molecule(s) to control cell phenotype. Attempts to create morphogen gradients in vitro have predominantly relied on the immobilization of growth factors within 3-D polymeric matrices or covalent/non-covalent tethering of peptide sequences to patterned biomaterial surfaces [365-368, 377]. These protein-based approaches are limited by suboptimal delivery vehicles, poor spatiotemporal dosage control, short protein half-life, and the cost-prohibitive supraphysiologic concentrations required to initiate a cellular response [370]. In addition, it is exceedingly difficult to engineer precise gradients of soluble bioactive factors in vivo due to the complex milieu [369]. Ultimately, it is unlikely that bolus delivery of a single protein gradient will supply sufficiently robust/precise spatiotemporal control to induce the formation of complex tissues which mimic native organ function. In this study, we explore the feasibility of biomaterial-mediated gene transfer to spatially pattern the genetic modification and subsequent differentiation of cells seeded within these constructs. In contrast to conventional gene therapy techniques, this approach promotes

152

gene delivery by co-localizing the cell adhesion substrate and gene delivery vehicle [378, 379]. This approach is more cost-effective than protein-based therapies and may allow for finer control over individual cell fate by providing graded positional cues within a 3-D substrate [380]. Furthermore, the selection of genetic material encoding for a tissue-specific transcription factor instead of a secreted, soluble factor, may offer more precise control over single-cell differentiation without dramatic consequences to the surrounding cells. Indeed, delivery of genes encoding for soluble factors has been problematic because cellular secretion of these proteins is poorly controlled and paracrine signaling to neighboring cells may induce undesired cellular effects[7, 8].

Gene carriers have been tethered to or encapsulated within biomaterial supports with a wide range of immobilization schemes [381]. These technologies have successfully facilitated the localized delivery of nonviral and viral vectors to cells seeded on 2-D biomaterial surfaces [379, 382, 383]. Furthermore, transient transfection of host cells in vivo was reported from 3-D scaffolds containing naked DNA plasmid and adenovirus [380, 384, 385]. More recently, the immobilization of adeno-associated virus to allogenic bone grafts has shown utility in bone healing [386]. Despite these advances, these technologies are limited in applications that require long-term transgene expression or spatial gradients of factor delivery. We expand upon these concepts with this work to create spatial gradients of retrovirus within three-dimensional polymeric networks. We develop a novel biomaterial-mediated method for retroviral gene delivery to fibroblasts by exploiting the ability of cationic polymers (e.g. PLL) to charge neutralize and aggregate retroviral particles [374, 375]. Importantly, retroviral particles immobilized within 3-D scaffolds retain the ability to transduce cells cultured on these matrices. Using this technique, we show

www.manaraa.com

that a homogeneous population of fibroblasts can be locally patterned into two different cell fates by seeding them on three-dimensional matrices containing defined spatial domains of immobilized retrovirus encoding for the osteogenic transcription factor Runx2.

Retroviral transduction of mammalian cells is a highly complex process which remains poorly understood. The general mechanism for viral attachment involves a three steps, including: (1) virus diffusion to the cell surface, (2) non-specific binding to the cell membrane, and (3) specific binding of viral envelope protein gp70 to its cognate cellular receptor [374]. Slow diffusion and rapid decay of retroviral particles have been identified as the primary factors limiting the efficiency of retroviral gene transfer [387]. Cationic polymers, such as polybrene and PLL, have been shown to enhance transduction efficiency by altering viral adsorption kinetics [374, 388]. These positively-charged polymers neutralize the negatively-charged retrovirus, thereby enhancing non-specific adsorption to target cell surface by reducing virus-cell electrostatic repulsion and enhancing viral aggregation [374]. In this study, we observed that biomaterial-mediated transduction is highly dependent on pre-coating these scaffolds with PLL prior to incubation in retroviral supernatant. We hypothesize that our approach may promote non-specific adsorption to target cell surface by overcoming diffusion limitations from conventional ex vivo techniques in suspension, enhancing virus aggregation, reducing viral degradation rate, and reducing cell-virus electrostatic repulsion.

Heterogeneous zones of ligament, fibrocartilage, mineralized fibrocartilage, and bone are found at the transitionary region between the anterior cruciate ligament and bone [348, 350, 389]. In the present work, we engineer a biphasic construct containing a

154

continuous interface of osteoblastic and fibroblastic tissue by using the bone-soft tissue interface as a model system. It is unlikely that static culture of these constructs in vitro will lead to the development of tissue that fully recapitulates the structure of this interface. However, we suggest that the interplay of these heterogeneous constructs with the mechanical forces and biochemical cues in an orthotopic in vivo environment may lead higher-order tissue organization [149, 352, 353]. More specifically, we hypothesize that the continuous interface between fibroblasts and mineralizing Runx2-expressing fibroblasts may lead to a cartilage intermediate. This hypothesis was formulated based on the fact that mesenchymal progenitor cells go through a highly complex, intermediate cartilaginous phase prior to mineralized matrix deposition during long-bone development and fracture healing in a process termed endochondral ossification [30, 31]. Further support for this idea is gathered by studies that provide evidence for a cartilage intermediate phase using fibroblast/osteoblast co-cultures [371].

In summary, we demonstrate that a biphasic construct containing a continuous interface of osteoblastic and fibroblastic tissue can be developed by a simple, one step seeding of autologous fibroblasts into polymeric scaffolds containing a graded distribution of the Runx2 retroviral vector. The concept of controlling expression of tissue-specific transcription factors to create spatial gradients of differential cell function within 3-D matrices may be applicable to the development of interfacial zones for a large number of tissue engineering applications. Overall, these results are significant toward the development of autologous grafting templates containing transitional interfacial zones for enhanced tissue integration and biological function.

CHAPTER 8

FUTURE CONSIDERATIONS

Significant progress has been attained toward the development of retroviral, adenoviral, and adeno-associated viral vectors for musculoskeletal tissue repair and regeneration. Recent studies in preclinical animal models suggest that virus-based genetic engineering strategies may provide enhanced in vivo bone formation compared to direct implantation of either osteogenic cells or recombinant protein therapy alone. Moreover, limitations associated with the administration of supraphysiologic recombinant protein doses may be circumvented by cells engineered to produce these factors in a continuous manner via natural cellular mechanisms. These advantages suggest that the additional complexity associated with genetic engineering strategies may be warranted for bone repair applications. However, before clinical application is realized, extensive preclinical studies, including experiments in larger animal models, will be necessary to address concerns that the therapeutic potential of targeted gene delivery will be counteracted by the safety risks associated with administration of viral vectors. Characterization of the safety profile of these vectors is particularly important for non-lethal bone repair applications that are meant to improve quality of life for the patient.

The optimal combination of gene transfer vector, regenerative molecule(s), and cell source for robust, yet highly controlled bone formation in immunocompetent patients has not been identified. Despite observed efficacy in animal models, the therapeutic dosage necessary to induce bone healing in humans without a significant humoral/cellular

immune response is still unknown. Characterization of the protein release profile and the threshold of factor delivery necessary to achieve efficacy will be necessary for each individual approach based on a different regenerative molecule or combination of molecules. Additional comparative studies will also be necessary to determine the relative potency as well as applicability of osteoblastic and nonosteoblastic cell-types in bone regeneration in order to select the appropriate cell source. Moreover, studies characterizing cell fate after implantation and the cellular origin of bone formation will become increasingly important in the clinical application of these strategies to human bone defects. A comparative analysis of the relative therapeutic merit of each genetic engineering strategy is challenging because independent investigators use a diverse range of vectors, cell-types, therapeutic transgenes, and in vivo animal models. Furthermore, it is difficult to draw conclusions even from studies which do attempt this comparison [390] because the mechanism of viral gene transfer is highly dependent on a number of variables which are difficult to control (e.g. transfection/transduction efficiency, vector exposure time during infection, virus titer, cell confluence, serum lot, cell proliferation rate, vector pseudotype, and/or infection procedure). Overall, the pursuit of many of these options in parallel is important because it is unlikely that one single strategy will be universally appropriate for the treatment of the diverse orthopaedic conditions requiring grafting procedures.

Significant progress has also been made in recent years toward the development of gene therapy-based strategies to improve the biochemical, mechanical, and histomorphological properties of healing ligament tissue. Nevertheless, this particular field is still in its infancy, largely because an incomplete understanding of the molecular

157

pathways involved in ligament development/healing has significantly hindered the development of novel strategies for ligament repair. The spatial and temporal cascade of factors that is necessary for the differentiation of stem cells into a ligament fibroblast-specific cellular phenotype has not been identified. In addition, no unique biochemical markers exist to distinguish ligament tissue from other fibroblastic tissue-types, making characterization difficult. Thus, future advances in ligament cell biology will likely enable development of genetic engineering strategies based on novel therapeutic molecules alone or in combination. Many more in vitro and in vivo studies will be necessary before a grafting template will be realized which recapitulates the precise architecture, biochemical composition, and mechanical properties of the native ligament tissue.

Numerous gene therapy strategies have successfully enhanced mineral deposition or soft tissue repair in vivo, but the development of grafts which fully recapitulate the three-dimensional structure and functional characteristics of bone and/or ligament tissue has not been realized. It is not currently well understood whether the optimal orthopaedic regenerative strategy must perfectly mimic the precise architecture and biochemical properties of native bone. Indeed, it is likely that the degree of native tissue recapitulation will be dependent on the anatomic location of the defect, the level of damage to vasculature and progenitor cell populations within the host tissue bed surrounding the repair site, and general health/age of the patient. Nevertheless, it is likely that the complex biomolecular organization of endogenous skeletal tissue cannot be achieved by the delivery of a single dose of recombinant protein to the repair site in a poorly-controlled manner. Future studies should aim to clarify how close to native tissue

is "close enough" to ubiquitously induce healing in variety of bone defects with varying severity. Current and emerging gene transfer technologies focusing on regulated expression systems (including inducible and tissue-specific systems) as well as combinatorial strategies may enable the design of therapies which more closely mimic the complex spatial and temporal cascade of proteins involved in bone formation. These strategies in combination with appropriate cell sources and engineered biomaterial matrices represent promising avenues to the generation of structural and functional regenerated bone and ligament tissue.

REFERENCES

1. Lane,J.M., Tomin,E., & Bostrom,M.P. Biosynthetic bone grafting. *Clin. Orthop. Relat Res.*S107-S117 (1999).

2. Bostrom,M.P., Saleh,K.J., & Einhorn,T.A. Osteoinductive growth factors in preclinical fracture and long bone defects models. *Orthop. Clin. North Am.* **30**, 647-658 (1999).

3. Bucholz,R.W. Nonallograft osteoconductive bone graft substitutes. *Clin. Orthop. Relat Res.*44-52 (2002).

4. Friedlaender,G.E. *et al.* Osteogenic protein-1 (bone morphogenetic protein-7) in the treatment of tibial nonunions. *J. Bone Joint Surg. Am.* **83-A Suppl 1**, S151-S158 (2001).

5. Geesink,R.G., Hoefnagels,N.H., & Bulstra,S.K. Osteogenic activity of OP-1 bone morphogenetic protein (BMP-7) in a human fibular defect. *J. Bone Joint Surg. Br.* **81**, 710-718 (1999).

6. Johnson,E.E., Urist,M.R., & Finerman,G.A. Bone morphogenetic protein augmentation grafting of resistant femoral nonunions. A preliminary report. *Clin. Orthop. Relat Res.*257-265 (1988).

7. Uludag,H., Gao,T., Porter,T.J., Friess,W., & Wozney,J.M. Delivery systems for BMPs: factors contributing to protein retention at an application site. *J. Bone Joint Surg. Am.* **83-A Suppl 1**, S128-S135 (2001).

8. Wozney,J.M. Overview of bone morphogenetic proteins. *Spine* **27**, S2-S8 (2002).

9. Bruder,S.P. & Fox,B.S. Tissue engineering of bone. Cell based strategies. *Clin. Orthop. Relat Res.*S68-S83 (1999).

10. Calvert,J.W., Weiss,L.E., & Sundine,M.J. New frontiers in bone tissue engineering. *Clin. Plast. Surg.* **30**, 641-8, x (2003).

11. Cowan,C.M., Soo,C., Ting,K., & Wu,B. Evolving concepts in bone tissue engineering. *Curr. Top. Dev. Biol.* **66**, 239-285 (2005).

12. Mistry,A.S. & Mikos,A.G. Tissue engineering strategies for bone regeneration. *Adv. Biochem. Eng Biotechnol.* **94**, 1-22 (2005).

13.   Arinzeh,T.L. *et al.* Allogeneic mesenchymal stem cells regenerate bone in a critical-sized canine segmental defect. *J. Bone Joint Surg. Am.* **85-A**, 1927-1935 (2003).

14.   Bruder,S.P., Fink,D.J., & Caplan,A.I. Mesenchymal stem cells in bone development, bone repair, and skeletal regeneration therapy. *J. Cell Biochem.* **56**, 283-294 (1994).

15.   Mauney,J.R., Volloch,V., & Kaplan,D.L. Role of adult mesenchymal stem cells in bone tissue engineering applications: current status and future prospects. *Tissue Eng* **11**, 787-802 (2005).

16.   Kahn,A., Gibbons,R., Perkins,S., & Gazit,D. Age-related bone loss. A hypothesis and initial assessment in mice. *Clin. Orthop. Relat Res.*69-75 (1995).

17.   Ohgushi,H., Goldberg,V.M., & Caplan,A.I. Repair of bone defects with marrow cells and porous ceramic. Experiments in rats. *Acta Orthop. Scand.* **60**, 334-339 (1989).

18.   Quarto,R. *et al.* Repair of large bone defects with the use of autologous bone marrow stromal cells. *N. Engl. J. Med.* **344**, 385-386 (2001).

19.   Quarto,R., Thomas,D., & Liang,C.T. Bone progenitor cell deficits and the age-associated decline in bone repair capacity. *Calcif. Tissue Int.* **56**, 123-129 (1995).

20.   Franceschi,R.T. *et al.* Gene therapy approaches for bone regeneration. *Cells Tissues. Organs* **176**, 95-108 (2004).

21.   Rutherford,R.B. *et al.* Bone morphogenetic protein-transduced human fibroblasts convert to osteoblasts and form bone in vivo. *Tissue Eng* **8**, 441-452 (2002).

22.   Zhao,M., Zhao,Z., Koh,J.T., Jin,T., & Franceschi,R.T. Combinatorial gene therapy for bone regeneration: cooperative interactions between adenovirus vectors expressing bone morphogenetic proteins 2, 4, and 7. *J. Cell Biochem.* **95**, 1-16 (2005).

23.   Yang,S. *et al.* In vitro and in vivo synergistic interactions between the Runx2/Cbfa1 transcription factor and bone morphogenetic protein-2 in stimulating osteoblast differentiation. *J. Bone Miner. Res.* **18**, 705-715 (2003).

24.   Hirata,K. *et al.* Transplantation of skin fibroblasts expressing BMP-2 promotes bone repair more effectively than those expressing Runx2. *Bone* **32**, 502-512 (2003).

161

25.   Krebsbach,P.H., Gu,K., Franceschi,R.T., & Rutherford,R.B. Gene therapy-directed osteogenesis: BMP-7-transduced human fibroblasts form bone in vivo. *Hum. Gene Ther.* **11**, 1201-1210 (2000).

26.   Winn,S.R., Hu,Y., Sfeir,C., & Hollinger,J.O. Gene therapy approaches for modulating bone regeneration. *Adv. Drug Deliv. Rev.* **42**, 121-138 (2000).

27.   Termaat,M.F., Den Boer,F.C., Bakker,F.C., Patka,P., & Haarman,H.J. Bone morphogenetic proteins. Development and clinical efficacy in the treatment of fractures and bone defects. *J. Bone Joint Surg. Am.* **87**, 1367-1378 (2005).

28.   Wozney,J.M. & Seeherman,H.J. Protein-based tissue engineering in bone and cartilage repair. *Curr. Opin. Biotechnol.* **15**, 392-398 (2004).

29.   Raisz,L.G. Physiology and pathophysiology of bone remodeling. *Clin. Chem.* **45**, 1353-1358 (1999).

30.   Cohen,M.M., Jr. Merging the old skeletal biology with the new. I. Intramembranous ossification, endochondral ossification, ectopic bone, secondary cartilage, and pathologic considerations. *J. Craniofac. Genet. Dev. Biol.* **20**, 84-93 (2000).

31.   Erlebacher,A., Filvaroff,E.H., Gitelman,S.E., & Derynck,R. Toward a molecular understanding of skeletal development. *Cell* **80**, 371-378 (1995).

32.   Reddi,A.H. Role of morphogenetic proteins in skeletal tissue engineering and regeneration. *Nat. Biotechnol.* **16**, 247-252 (1998).

33.   Lieberman,J.R., Daluiski,A., & Einhorn,T.A. The role of growth factors in the repair of bone. Biology and clinical applications. *J. Bone Joint Surg. Am.* **84-A**, 1032-1044 (2002).

34.   Lyons,K.M., Hogan,B.L., & Robertson,E.J. Colocalization of BMP 7 and BMP 2 RNAs suggests that these factors cooperatively mediate tissue interactions during murine development. *Mech. Dev.* **50**, 71-83 (1995).

35.   Nishimatsu,S. & Thomsen,G.H. Ventral mesoderm induction and patterning by bone morphogenetic protein heterodimers in Xenopus embryos. *Mech. Dev.* **74**, 75-88 (1998).

36.   Cho,T.J., Gerstenfeld,L.C., & Einhorn,T.A. Differential temporal expression of members of the transforming growth factor beta superfamily during murine fracture healing. *J. Bone Miner. Res.* **17**, 513-520 (2002).

37.   Cheng,H. *et al.* Osteogenic activity of the fourteen types of human bone morphogenetic proteins (BMPs). *J. Bone Joint Surg. Am.* **85-A**, 1544-1552 (2003).

162

38. Hassel,S. *et al.* Initiation of Smad-dependent and Smad-independent signaling via distinct BMP-receptor complexes. *J. Bone Joint Surg. Am.* **85-A Suppl 3**, 44-51 (2003).

39. Lee,K.S., Hong,S.H., & Bae,S.C. Both the Smad and p38 MAPK pathways play a crucial role in Runx2 expression following induction by transforming growth factor-beta and bone morphogenetic protein. *Oncogene* **21**, 7156-7163 (2002).

40. Nishimura,R., Hata,K., Harris,S.E., Ikeda,F., & Yoneda,T. Core-binding factor alpha 1 (Cbfa1) induces osteoblastic differentiation of C2C12 cells without interactions with Smad1 and Smad5. *Bone* **31**, 303-312 (2002).

41. Derynck,R. & Zhang,Y.E. Smad-dependent and Smad-independent pathways in TGF-beta family signalling. *Nature* **425**, 577-584 (2003).

42. Khan,S.N., Bostrom,M.P., & Lane,J.M. Bone growth factors. *Orthop. Clin. North Am.* **31**, 375-388 (2000).

43. Linkhart,T.A., Mohan,S., & Baylink,D.J. Growth factors for bone growth and repair: IGF, TGF beta and BMP. *Bone* **19**, 1S-12S (1996).

44. Thaller,S.R., Dart,A., & Tesluk,H. The effects of insulin-like growth factor-1 on critical-size calvarial defects in Sprague-Dawley rats. *Ann. Plast. Surg.* **31**, 429-433 (1993).

45. Carpenter,J.E. *et al.* Failure of growth hormone to alter the biomechanics of fracture-healing in a rabbit model. *J. Bone Joint Surg. Am.* **74**, 359-367 (1992).

46. Bonewald,L.F. & Dallas,S.L. Role of active and latent transforming growth factor beta in bone formation. *J. Cell Biochem.* **55**, 350-357 (1994).

47. Noda,M. & Camilliere,J.J. In vivo stimulation of bone formation by transforming growth factor-beta. *Endocrinology* **124**, 2991-2994 (1989).

48. Opperman,L.A., Chhabra,A., Cho,R.W., & Ogle,R.C. Cranial suture obliteration is induced by removal of transforming growth factor (TGF)-beta 3 activity and prevented by removal of TGF-beta 2 activity from fetal rat calvaria in vitro. *J. Craniofac. Genet. Dev. Biol.* **19**, 164-173 (1999).

49. Lind,M. *et al.* Transforming growth factor-beta enhances fracture healing in rabbit tibiae. *Acta Orthop. Scand.* **64**, 553-556 (1993).

50. Nielsen,H.M., Andreassen,T.T., Ledet,T., & Oxlund,H. Local injection of TGF-beta increases the strength of tibial fractures in the rat. *Acta Orthop. Scand.* **65**, 37-41 (1994).

51. Critchlow,M.A., Bland,Y.S., & Ashhurst,D.E. The effect of exogenous transforming growth factor-beta 2 on healing fractures in the rabbit. *Bone* **16**, 521-527 (1995).

52. Moore,R., Ferretti,P., Copp,A., & Thorogood,P. Blocking endogenous FGF-2 activity prevents cranial osteogenesis. *Dev. Biol.* **243**, 99-114 (2002).

53. Chen,L., Li,D., Li,C., Engel,A., & Deng,C.X. A Ser252Trp [corrected] substitution in mouse fibroblast growth factor receptor 2 (Fgfr2) results in craniosynostosis. *Bone* **33**, 169-178 (2003).

54. Chen,L. *et al.* Gly369Cys mutation in mouse FGFR3 causes achondroplasia by affecting both chondrogenesis and osteogenesis. *J. Clin. Invest* **104**, 1517-1525 (1999).

55. Kawaguchi,H. *et al.* Acceleration of fracture healing in nonhuman primates by fibroblast growth factor-2. *J. Clin. Endocrinol. Metab* **86**, 875-880 (2001).

56. Nakamura,K. *et al.* Local application of basic fibroblast growth factor into the bone increases bone mass at the applied site in rabbits. *Arch. Orthop. Trauma Surg.* **115**, 344-346 (1996).

57. Nakamura,T. *et al.* Stimulation of endosteal bone formation by systemic injections of recombinant basic fibroblast growth factor in rats. *Endocrinology* **136**, 1276-1284 (1995).

58. Harada,S. & Rodan,G.A. Control of osteoblast function and regulation of bone mass. *Nature* **423**, 349-355 (2003).

59. Ducy,P., Zhang,R., Geoffroy,V., Ridall,A.L., & Karsenty,G. Osf2/Cbfa1: a transcriptional activator of osteoblast differentiation. *Cell* **89**, 747-754 (1997).

60. Karsenty,G. *et al.* Cbfa1 as a regulator of osteoblast differentiation and function. *Bone* **25**, 107-108 (1999).

61. Komori,T. *et al.* Targeted disruption of Cbfa1 results in a complete lack of bone formation owing to maturational arrest of osteoblasts. *Cell* **89**, 755-764 (1997).

62. Mundlos,S. *et al.* Mutations involving the transcription factor CBFA1 cause cleidocranial dysplasia. *Cell* **89**, 773-779 (1997).

63. Otto,F. *et al.* Cbfa1, a candidate gene for cleidocranial dysplasia syndrome, is essential for osteoblast differentiation and bone development. *Cell* **89**, 765-771 (1997).

64.   Franceschi,R.T. & Xiao,G. Regulation of the osteoblast-specific transcription factor, Runx2: Responsiveness to multiple signal transduction pathways. *J. Cell Biochem.* **88**, 446-454 (2003).

65.   Franceschi,R.T. Functional cooperativity between osteoblast transcription factors: evidence for the importance of subnuclear macromolecular complexes? *Calcif. Tissue Int.* **72**, 638-642 (2003).

66.   Byers,B.A., Pavlath,G.K., Murphy,T.J., Karsenty,G., & Garcia,A.J. Cell-type-dependent up-regulation of in vitro mineralization after overexpression of the osteoblast-specific transcription factor Runx2/Cbfal. *J. Bone Miner. Res.* **17**, 1931-1944 (2002).

67.   Gersbach,C.A., Byers,B.A., Pavlath,G.K., & Garcia,A.J. Runx2/Cbfa1 stimulates transdifferentiation of primary skeletal myoblasts into a mineralizing osteoblastic phenotype. *Experimental Cell Research* **300**, 406-417 (2004).

68.   Ducy,P. *et al.* A Cbfa1-dependent genetic pathway controls bone formation beyond embryonic development. *Genes & Development* **13**, 1025-1036 (1999).

69.   Liu,W.G. *et al.* Overexpression of Cbfa1 in osteoblasts inhibits osteoblast maturation and causes osteopenia with multiple fractures. *Journal of Cell Biology* **155**, 157-166 (2001).

70.   Nakashima,K. *et al.* The novel zinc finger-containing transcription factor osterix is required for osteoblast differentiation and bone formation. *Cell* **108**, 17-29 (2002).

71.   Nishio,Y. *et al.* Runx2-mediated regulation of the zinc finger Osterix/Sp7 gene. *Gene* **372**, 62-70 (2006).

72.   Lee,M.H., Kwon,T.G., Park,H.S., Wozney,J.M., & Ryoo,H.M. BMP-2-induced Osterix expression is mediated by Dlx5 but is independent of Runx2. *Biochem. Biophys. Res. Commun.* **309**, 689-694 (2003).

73.   Yagi,K. *et al.* Bone morphogenetic protein-2 enhances osterix gene expression in chondrocytes. *J. Cell Biochem.* **88**, 1077-1083 (2003).

74.   Komori,T. [Functions of BMPs, Runx2, and osterix in the development of bone and cartilage]. *Nippon Rinsho* **63**, 1671-1677 (2005).

75.   Lee,M.H. *et al.* BMP-2-induced Runx2 expression is mediated by Dlx5, and TGF-beta 1 opposes the BMP-2-induced osteoblast differentiation by suppression of Dlx5 expression. *J. Biol. Chem.* **278**, 34387-34394 (2003).

76.   Lee,K.S. *et al.* Runx2 is a common target of transforming growth factor beta1 and bone morphogenetic protein 2, and cooperation between Runx2 and Smad5

165

induces osteoblast-specific gene expression in the pluripotent mesenchymal precursor cell line C2C12. *Mol. Cell Biol.* **20**, 8783-8792 (2000).

77. Finkemeier,C.G. Bone-grafting and bone-graft substitutes. *J. Bone Joint Surg. Am.* **84-A**, 454-464 (2002).

78. Khan,S.N., Tomin,E., & Lane,J.M. Clinical applications of bone graft substitutes. *Orthop. Clin. North Am.* **31**, 389-398 (2000).

79. Perry,C.R. Bone repair techniques, bone graft, and bone graft substitutes. *Clin. Orthop. Relat Res.*71-86 (1999).

80. Vaccaro,A.R. The role of the osteoconductive scaffold in synthetic bone graft. *Orthopedics* **25**, s571-s578 (2002).

81. Baltzer,A.W. & Lieberman,J.R. Regional gene therapy to enhance bone repair. *Gene Ther.* **11**, 344-350 (2004).

82. Alden,T.D. *et al.* In vivo endochondral bone formation using a bone morphogenetic protein 2 adenoviral vector. *Hum. Gene Ther.* **10**, 2245-2253 (1999).

83. Baltzer,A.W. *et al.* Genetic enhancement of fracture repair: healing of an experimental segmental defect by adenoviral transfer of the BMP-2 gene. *Gene Ther.* **7**, 734-739 (2000).

84. Baltzer,A.W. *et al.* Potential role of direct adenoviral gene transfer in enhancing fracture repair. *Clin. Orthop. Relat Res.*S120-S125 (2000).

85. Musgrave,D.S. *et al.* Adenovirus-mediated direct gene therapy with bone morphogenetic protein-2 produces bone. *Bone* **24**, 541-547 (1999).

86. Alden,T.D. *et al.* In vivo endochondral bone formation using a bone morphogenetic protein 2 adenoviral vector. *Hum. Gene Ther.* **10**, 2245-2253 (1999).

87. Christ,M. *et al.* Gene therapy with recombinant adenovirus vectors: evaluation of the host immune response. *Immunol. Lett.* **57**, 19-25 (1997).

88. Molinier-Frenkel,V. *et al.* Immune response to recombinant adenovirus in humans: capsid components from viral input are targets for vector-specific cytotoxic T lymphocytes. *J. Virol.* **74**, 7678-7682 (2000).

89. Rundle,C.H. *et al.* In vivo bone formation in fracture repair induced by direct retroviral-based gene therapy with bone morphogenetic protein-4. *Bone* **32**, 591-601 (2003).

90.   Wang,J.C. *et al.* Effect of regional gene therapy with bone morphogenetic protein-2-producing bone marrow cells on spinal fusion in rats. *J. Bone Joint Surg. Am.* **85-A**, 905-911 (2003).

91.   Lieberman,J.R. *et al.* Regional gene therapy with a BMP-2-producing murine stromal cell line induces heterotopic and orthotopic bone formation in rodents. *J. Orthop. Res.* **16**, 330-339 (1998).

92.   Lieberman,J.R. *et al.* The effect of regional gene therapy with bone morphogenetic protein-2-producing bone-marrow cells on the repair of segmental femoral defects in rats. *J. Bone Joint Surg. Am.* **81**, 905-917 (1999).

93.   Blum,J.S., Barry,M.A., Mikos,A.G., & Jansen,J.A. In vivo evaluation of gene therapy vectors in ex vivo-derived marrow stromal cells for bone regeneration in a rat critical-size calvarial defect model. *Hum. Gene Ther.* **14**, 1689-1701 (2003).

94.   Park,J. *et al.* Bone regeneration in critical size defects by cell-mediated BMP-2 gene transfer: a comparison of adenoviral vectors and liposomes. *Gene Ther.* **10**, 1089-1098 (2003).

95.   Chang,S.C. *et al.* Ex vivo gene therapy in autologous bone marrow stromal stem cells for tissue-engineered maxillofacial bone regeneration. *Gene Ther.* **10**, 2013-2019 (2003).

96.   Gysin,R. *et al.* Ex vivo gene therapy with stromal cells transduced with a retroviral vector containing the BMP4 gene completely heals critical size calvarial defect in rats. *Gene Ther.* **9**, 991-999 (2002).

97.   Tsuchida,H., Hashimoto,J., Crawford,E., Manske,P., & Lou,J. Engineered allogeneic mesenchymal stem cells repair femoral segmental defect in rats. *J. Orthop. Res.* **21**, 44-53 (2003).

98.   Bruder,S.P. & Fox,B.S. Tissue engineering of bone. Cell based strategies. *Clin. Orthop. Relat Res.*S68-S83 (1999).

99.   Mistry,A.S. & Mikos,A.G. Tissue engineering strategies for bone regeneration. *Adv. Biochem. Eng Biotechnol.* **94**, 1-22 (2005).

100.   Salgado,A.J., Coutinho,O.P., & Reis,R.L. Bone tissue engineering: state of the art and future trends. *Macromol. Biosci.* **4**, 743-765 (2004).

101.   Doll,B., Sfeir,C., Winn,S., Huard,J., & Hollinger,J. Critical aspects of tissue-engineered therapy for bone regeneration. *Crit Rev. Eukaryot. Gene Expr.* **11**, 173-198 (2001).

102.   Ishaug-Riley,S.L., Crane-Kruger,G.M., Yaszemski,M.J., & Mikos,A.G. Three-dimensional culture of rat calvarial osteoblasts in porous biodegradable polymers. *Biomaterials* **19**, 1405-1412 (1998).

103.   Yamanouchi,K. *et al.* Bone formation by transplanted human osteoblasts cultured within collagen sponge with dexamethasone in vitro. *J. Bone Miner. Res.* **16**, 857-867 (2001).

104.   Salgado,A.J., Coutinho,O.P., & Reis,R.L. Novel starch-based scaffolds for bone tissue engineering: cytotoxicity, cell culture, and protein expression. *Tissue Eng* **10**, 465-474 (2004).

105.   Shea,L.D., Wang,D., Franceschi,R.T., & Mooney,D.J. Engineered bone development from a pre-osteoblast cell line on three-dimensional scaffolds. *Tissue Eng* **6**, 605-617 (2000).

106.   Grundel,R.E., Chapman,M.W., Yee,T., & Moore,D.C. Autogeneic bone marrow and porous biphasic calcium phosphate ceramic for segmental bone defects in the canine ulna. *Clin. Orthop. Relat Res.*244-258 (1991).

107.   Ohgushi,H., Goldberg,V.M., & Caplan,A.I. Heterotopic osteogenesis in porous ceramics induced by marrow cells. *J. Orthop. Res.* **7**, 568-578 (1989).

108.   Horwitz,E.M. *et al.* Isolated allogeneic bone marrow-derived mesenchymal cells engraft and stimulate growth in children with osteogenesis imperfecta: Implications for cell therapy of bone. *Proc. Natl. Acad. Sci. U. S. A* **99**, 8932-8937 (2002).

109.   Pittenger,M.F. *et al.* Multilineage potential of adult human mesenchymal stem cells. *Science* **284**, 143-147 (1999).

110.   Mauney,J.R., Volloch,V., & Kaplan,D.L. Role of adult mesenchymal stem cells in bone tissue engineering applications: current status and future prospects. *Tissue Eng* **11**, 787-802 (2005).

111.   Bruder,S.P., Jaiswal,N., & Haynesworth,S.E. Growth kinetics, self-renewal, and the osteogenic potential of purified human mesenchymal stem cells during extensive subcultivation and following cryopreservation. *J. Cell Biochem.* **64**, 278-294 (1997).

112.   Dennis,J.E., Haynesworth,S.E., Young,R.G., & Caplan,A.I. Osteogenesis in marrow-derived mesenchymal cell porous ceramic composites transplanted subcutaneously: effect of fibronectin and laminin on cell retention and rate of osteogenic expression. *Cell Transplant.* **1**, 23-32 (1992).

113.   Mauney,J.R., Volloch,V., & Kaplan,D.L. Role of adult mesenchymal stem cells in bone tissue engineering applications: current status and future prospects. *Tissue Eng* **11**, 787-802 (2005).

168

114. Kon,E. *et al.* Autologous bone marrow stromal cells loaded onto porous hydroxyapatite ceramic accelerate bone repair in critical-size defects of sheep long bones. *J. Biomed. Mater. Res.* **49**, 328-337 (2000).

115. Bruder,S.P. & Fox,B.S. Tissue engineering of bone. Cell based strategies. *Clin. Orthop. Relat Res.*S68-S83 (1999).

116. Haynesworth,S.E., Goshima,J., Goldberg,V.M., & Caplan,A.I. Characterization of cells with osteogenic potential from human marrow. *Bone* **13**, 81-88 (1992).

117. Gersbach,C.A., Le Doux,J.M., Guldberg,R.E., & Garcia,A.J. Inducible regulation of Runx2-stimulated osteogenesis. *Gene Ther.*(2006).

118. Viggeswarapu,M. *et al.* Adenoviral delivery of LIM mineralization protein-1 induces new-bone formation in vitro and in vivo. *J. Bone Joint Surg. Am.* **83-A**, 364-376 (2001).

119. Lee,J.Y. *et al.* Clonal isolation of muscle-derived cells capable of enhancing muscle regeneration and bone healing. *J. Cell Biol.* **150**, 1085-1100 (2000).

120. Musgrave,D.S. *et al.* The effect of bone morphogenetic protein-2 expression on the early fate of skeletal muscle-derived cells. *Bone* **28**, 499-506 (2001).

121. Bosch,P. *et al.* Osteoprogenitor cells within skeletal muscle. *J. Orthop. Res.* **18**, 933-944 (2000).

122. Zuk,P.A. *et al.* Multilineage cells from human adipose tissue: implications for cell-based therapies. *Tissue Eng* **7**, 211-228 (2001).

123. De Ugarte,D.A. *et al.* Comparison of multi-lineage cells from human adipose tissue and bone marrow. *Cells Tissues. Organs* **174**, 101-109 (2003).

124. Wright,V. *et al.* BMP4-expressing muscle-derived stem cells differentiate into osteogenic lineage and improve bone healing in immunocompetent mice. *Mol. Ther.* **6**, 169-178 (2002).

125. Rose,T. *et al.* Gene therapy to improve osteogenesis in bone lesions with severe soft tissue damage. *Langenbecks Arch. Surg.* **388**, 356-365 (2003).

126. Dragoo,J.L. *et al.* Tissue-engineered bone from BMP-2-transduced stem cells derived from human fat. *Plast. Reconstr. Surg.* **115**, 1665-1673 (2005).

127. Peterson,B. *et al.* Healing of critically sized femoral defects, using genetically modified mesenchymal stem cells from human adipose tissue. *Tissue Eng* **11**, 120-129 (2005).

128.   Gugala,Z., Olmsted-Davis,E.A., Gannon,F.H., Lindsey,R.W., & Davis,A.R. Osteoinduction by ex vivo adenovirus-mediated BMP2 delivery is independent of cell type. *Gene Ther.* **10**, 1289-1296 (2003).

129.   Rose,T. *et al.* The role of cell type in bone healing mediated by ex vivo gene therapy. *Langenbecks Arch. Surg.* **388**, 347-355 (2003).

130.   Tu,Q., Valverde,P., & Chen,J. Osterix enhances proliferation and osteogenic potential of bone marrow stromal cells. *Biochem. Biophys. Res. Commun.* **341**, 1257-1265 (2006).

131.   Phillips,J.E., Guldberg,R.E., & Garcia,A.J. Dermal Fibroblasts Genetically Modified to Express Runx2/Cbfa1 as a Mineralizing Cell Source for Bone Tissue Engineering. *Tissue Eng* **13**, 2029-2040 (2007).

132.   Phillips,J.E., Hutmacher,D.W., Guldberg,R.E., & Garcia,A.J. Mineralization capacity of Runx2/Cbfa1-genetically engineered fibroblasts is scaffold dependent. *Biomaterials* **27**, 5535-5545 (2006).

133.   Minamide,A. *et al.* Mechanism of bone formation with gene transfer of the cDNA encoding for the intracellular protein LMP-1. *J. Bone Joint Surg. Am.* **85-A**, 1030-1039 (2003).

134.   Boden,S.D. *et al.* Lumbar spine fusion by local gene therapy with a cDNA encoding a novel osteoinductive protein (LMP-1). *Spine* **23**, 2486-2492 (1998).

135.   Gersbach,C.A., Byers,B.A., Pavlath,G.K., Guldberg,R.E., & Garcia,A.J. Runx2/Cbfa1-genetically engineered skeletal myoblasts mineralize collagen scaffolds in vitro. *Biotechnol. Bioeng.* **88**, 369-378 (2004).

136.   Phillips,J.E., Gersbach,C.A., Wojtowicz,A.M., & Garcia,A.J. Glucocorticoid-induced osteogenesis is negatively regulated by Runx2/Cbfa1 serine phosphorylation. *J. Cell Sci.* **119**, 581-591 (2006).

137.   Byers,B.A. & Garcia,A.J. Exogenous Runx2 Expression Enhances *in Vitro* Osteoblastic Differentiation and Mineralization in Primary Bone Marrow Stromal Cells. *Tissue Engineering* **10**, 1623-1632 (2004).

138.   Byers,B.A., Guldberg,R.E., & Garcia,A.J. Synergy between genetic and tissue engineering: Runx2 overexpression and in vitro construct development enhance in vivo mineralization. *Tissue Eng* **10**, 1757-1766 (2004).

139.   Zhao,Z., Zhao,M., Xiao,G., & Franceschi,R.T. Gene transfer of the Runx2 transcription factor enhances osteogenic activity of bone marrow stromal cells in vitro and in vivo. *Mol. Ther.* **12**, 247-253 (2005).

170

140.   Tu,Q., Valverde,P., & Chen,J. Osterix enhances proliferation and osteogenic potential of bone marrow stromal cells. *Biochem. Biophys. Res. Commun.* **341**, 1257-1265 (2006).

141.   Peng,H. *et al.* Synergistic enhancement of bone formation and healing by stem cell-expressed VEGF and bone morphogenetic protein-4. *J. Clin. Invest* **110**, 751-759 (2002).

142.   Huard,J., Li,Y., Peng,H., & Fu,F.H. Gene therapy and tissue engineering for sports medicine. *J. Gene Med.* **5**, 93-108 (2003).

143.   Miyasaka,K.C., Daniel,D.M., Stone,M.L., & Hirshman,P. The incidence of knee ligament injuries in the general population. American Journal of Knee Surgery4,3-8.(1991).

144.   Frank,C.B. & Jackson,D.W. The science of reconstruction of the anterior cruciate ligament. *J. Bone Joint Surg. Am.* **79**, 1556-1576 (1997).

145.   Kannus,P. Long-term results of conservatively treated medial collateral ligament injuries of the knee joint. *Clin. Orthop. Relat Res.*103-112 (1988).

146.   Loitz-Ramage,B.J., Frank,C.B., & Shrive,N.G. Injury size affects long-term strength of the rabbit medial collateral ligament. *Clin. Orthop. Relat Res.*272-280 (1997).

147.   Frank,C., McDonald,D., & Shrive,N. Collagen fibril diameters in the rabbit medial collateral ligament scar: a longer term assessment. *Connect. Tissue Res.* **36**, 261-269 (1997).

148.   Laurencin,C.T., Ambrosio,A.M., Borden,M.D., & Cooper,J.A., Jr. Tissue engineering: orthopedic applications. *Annu. Rev. Biomed. Eng* **1**, 19-46 (1999).

149.   Vunjak-Novakovic,G., Altman,G., Horan,R., & Kaplan,D.L. Tissue engineering of ligaments. *Annu. Rev. Biomed. Eng* **6**, 131-156 (2004).

150.   Cameron,M.L., Mizung,Y., & Cosgarea,A.J. Diagnosing and managing anterior cruciate ligament injuries. J Musculoskeletal Med 17, 47-53. 2000. Ref Type: Generic

151.   Fu,F.H., Bennett,C.H., Lattermann,C., & Ma,C.B. Current trends in anterior cruciate ligament reconstruction. Part 1: Biology and biomechanics of reconstruction. *Am. J Sports Med* **27**, 821-830 (1999).

152.   Poehling,G.G. *et al.* Analysis of outcomes of anterior cruciate ligament repair with 5-year follow-up: allograft versus autograft. *Arthroscopy* **21**, 774-785 (2005).

153.   Jackson,D.W., Heinrich,J.T., & Simon,T.M. Biologic and synthetic implants to replace the anterior cruciate ligament. *Arthroscopy* **10**, 442-452 (1994).

154.   Rougraff,B., Shelbourne,K.D., Gerth,P.K., & Warner,J. Arthroscopic and histologic analysis of human patellar tendon autografts used for anterior cruciate ligament reconstruction. *Am. J Sports Med* **21**, 277-284 (1993).

155.   Woo,S.L., Abramowitch,S.D., Kilger,R., & Liang,R. Biomechanics of knee ligaments: injury, healing, and repair. *J Biomech.* **39**, 1-20 (2006).

156.   Woo,S.L. *et al.* Tissue engineering of ligament and tendon healing. *Clin. Orthop. Relat Res.*S312-S323 (1999).

157.   Woo,S.L., Debski,R.E., Withrow,J.D., & Janaushek,M.A. Biomechanics of knee ligaments. *Am. J Sports Med* **27**, 533-543 (1999).

158.   Sciore,P., Boykiw,R., & Hart,D.A. Semiquantitative reverse transcription-polymerase chain reaction analysis of mRNA for growth factors and growth factor receptors from normal and healing rabbit medial collateral ligament tissue. *J Orthop. Res.* **16**, 429-437 (1998).

159.   Kofron,M.D. & Laurencin,C.T. Orthopaedic applications of gene therapy. *Curr. Gene Ther.* **5**, 37-61 (2005).

160.   Scherping,S.C., Jr. *et al.* Effect of growth factors on the proliferation of ligament fibroblasts from skeletally mature rabbits. *Connect. Tissue Res.* **36**, 1-8 (1997).

161.   Schmidt,C.C. *et al.* Effect of growth factors on the proliferation of fibroblasts from the medial collateral and anterior cruciate ligaments. *J Orthop. Res.* **13**, 184-190 (1995).

162.   Marui,T. *et al.* Effect of growth factors on matrix synthesis by ligament fibroblasts. *J Orthop. Res.* **15**, 18-23 (1997).

163.   Lee,J., Green,M.H., & Amiel,D. Synergistic effect of growth factors on cell outgrowth from explants of rabbit anterior cruciate and medial collateral ligaments. *J Orthop. Res.* **13**, 435-441 (1995).

164.   Hildebrand,K.A. *et al.* The effects of platelet-derived growth factor-BB on healing of the rabbit medial collateral ligament. An in vivo study. *Am. J Sports Med* **26**, 549-554 (1998).

165.   Hildebrand,K.A., Hiraoka,H., Hart,D.A., Shrive,N.G., & Frank,C.B. Exogenous transforming growth factor beta 1 alone does not improve early healing of medial collateral ligament in rabbits. *Can. J Surg.* **45**, 330-336 (2002).

166.   Spindler,K.P. *et al.* The biomechanical response to doses of TGF-beta 2 in the healing rabbit medial collateral ligament. *J Orthop. Res.* **21**, 245-249 (2003).

167.   Spindler,K.P., Dawson,J.M., Stahlman,G.C., Davidson,J.M., & Nanney,L.B. Collagen expression and biomechanical response to human recombinant transforming growth factor beta (rhTGF-beta2) in the healing rabbit MCL. *J Orthop. Res.* **20**, 318-324 (2002).

168.   Yasuda,K., Tomita,F., Yamazaki,S., Minami,A., & Tohyama,H. The effect of growth factors on biomechanical properties of the bone-patellar tendon-bone graft after anterior cruciate ligament reconstruction: a canine model study. *Am. J Sports Med* **32**, 870-880 (2004).

169.   Woo,S.L., Jia,F., Zou,L., & Gabriel,M.T. Functional tissue engineering for ligament healing: potential of antisense gene therapy. *Ann. Biomed. Eng* **32**, 342-351 (2004).

170.   Kofron,M.D. & Laurencin,C.T. Orthopaedic applications of gene therapy. *Curr. Gene Ther.* **5**, 37-61 (2005).

171.   Gerich,T.G., Kang,R., Fu,F.H., Robbins,P.D., & Evans,C.H. Gene transfer to the patellar tendon. *Knee. Surg. Sports Traumatol. Arthrosc.* **5**, 118-123 (1997).

172.   Gerich,T.G., Kang,R., Fu,F.H., Robbins,P.D., & Evans,C.H. Gene transfer to the rabbit patellar tendon: potential for genetic enhancement of tendon and ligament healing. *Gene Ther.* **3**, 1089-1093 (1996).

173.   Gerich,T.G., Kang,R., Fu,F.H., Robbins,P.D., & Evans,C.H. Gene transfer to the rabbit patellar tendon: potential for genetic enhancement of tendon and ligament healing. *Gene Ther.* **3**, 1089-1093 (1996).

174.   Martinek,V. *et al.* Enhancement of tendon-bone integration of anterior cruciate ligament grafts with bone morphogenetic protein-2 gene transfer: a histological and biomechanical study. *J Bone Joint Surg. Am.* **84-A**, 1123-1131 (2002).

175.   Martinek,V. *et al.* Enhancement of tendon-bone integration of anterior cruciate ligament grafts with bone morphogenetic protein-2 gene transfer: a histological and biomechanical study. *J Bone Joint Surg. Am.* **84-A**, 1123-1131 (2002).

176.   Lou,J. In vivo gene transfer into tendon by recombinant adenovirus. *Clin. Orthop. Relat Res.*S252-S255 (2000).

177.   Lou,J. In vivo gene transfer into tendon by recombinant adenovirus. *Clin. Orthop. Relat Res.*S252-S255 (2000).

178.   Menetrey,J. *et al.* Direct-, fibroblast- and myoblast-mediated gene transfer to the anterior cruciate ligament. *Tissue Eng* **5**, 435-442 (1999).

179.   Hildebrand,K.A. *et al.* Early expression of marker genes in the rabbit medial collateral and anterior cruciate ligaments: the use of different viral vectors and the effects of injury. *J Orthop. Res.* **17**, 37-42 (1999).

180.   Kofron,M.D. & Laurencin,C.T. Orthopaedic applications of gene therapy. *Curr. Gene Ther.* **5**, 37-61 (2005).

181.   Lou,J., Kubota,H., Hotokezaka,S., Ludwig,F.J., & Manske,P.R. In vivo gene transfer and overexpression of focal adhesion kinase (pp125 FAK) mediated by recombinant adenovirus-induced tendon adhesion formation and epitenon cell change. *J Orthop. Res.* **15**, 911-918 (1997).

182.   Lou,J., Tu,Y., Burns,M., Silva,M.J., & Manske,P. BMP-12 gene transfer augmentation of lacerated tendon repair. *J Orthop. Res.* **19**, 1199-1202 (2001).

183.   Lou,J., Tu,Y., Burns,M., Silva,M.J., & Manske,P. BMP-12 gene transfer augmentation of lacerated tendon repair. *J Orthop. Res.* **19**, 1199-1202 (2001).

184.   Nakamura,N. *et al.* Early biological effect of in vivo gene transfer of platelet-derived growth factor (PDGF)-B into healing patellar ligament. *Gene Ther.* **5**, 1165-1170 (1998).

185.   Nakamura,N. *et al.* Early biological effect of in vivo gene transfer of platelet-derived growth factor (PDGF)-B into healing patellar ligament. *Gene Ther.* **5**, 1165-1170 (1998).

186.   Hoffmann,A. *et al.* Neotendon formation induced by manipulation of the Smad8 signalling pathway in mesenchymal stem cells. *J Clin. Invest* **116**, 940-952 (2006).

187.   Hoffmann,A. *et al.* Neotendon formation induced by manipulation of the Smad8 signalling pathway in mesenchymal stem cells. *J Clin. Invest* **116**, 940-952 (2006).

188.   Frank,C. *et al.* Collagen fibril diameters in the healing adult rabbit medial collateral ligament. *Connect. Tissue Res.* **27**, 251-263 (1992).

189.   Woo,S.L., Chan,S.S., & Yamaji,T. Biomechanics of knee ligament healing, repair and reconstruction. *J Biomech.* **30**, 431-439 (1997).

190.   Woo,S.L. *et al.* Tissue engineering of ligament and tendon healing. *Clin. Orthop. Relat Res.*S312-S323 (1999).

191.   Woo,S.L., Jia,F., Zou,L., & Gabriel,M.T. Functional tissue engineering for ligament healing: potential of antisense gene therapy. *Ann. Biomed. Eng* **32**, 342-351 (2004).

192.   Frank,C., Schachar,N., & Dittrich,D. Natural history of healing in the repaired medial collateral ligament. *J Orthop. Res.* **1**, 179-188 (1983).

193.   Woo,S.L., Jia,F., Zou,L., & Gabriel,M.T. Functional tissue engineering for ligament healing: potential of antisense gene therapy. *Ann. Biomed. Eng* **32**, 342-351 (2004).

194.   Woo,S.L., Chan,S.S., & Yamaji,T. Biomechanics of knee ligament healing, repair and reconstruction. *J Biomech.* **30**, 431-439 (1997).

195.   Nakamura,N. *et al.* Decorin antisense gene therapy improves functional healing of early rabbit ligament scar with enhanced collagen fibrillogenesis in vivo. *J Orthop. Res.* **18**, 517-523 (2000).

196.   Hart,D.A. *et al.* Complexity of determining cause and effect in vivo after antisense gene therapy. *Clin. Orthop. Relat Res.*S242-S251 (2000).

197.   Nakamura,N. *et al.* A comparison of in vivo gene delivery methods for antisense therapy in ligament healing. *Gene Ther.* **5**, 1455-1461 (1998).

198.   Jia,F., Shimomura,T., Niyibizi,C., & Woo,S.L. Downregulation of human type III collagen gene expression by antisense oligodeoxynucleotide. *Tissue Eng* **11**, 1429-1435 (2005).

199.   Shimomura,T., Jia,F., Niyibizi,C., & Woo,S.L. Antisense oligonucleotides reduce synthesis of procollagen alpha1 (V) chain in human patellar tendon fibroblasts: potential application in healing ligaments and tendons. *Connect. Tissue Res.* **44**, 167-172 (2003).

200.   Woo,S.L., Jia,F., Zou,L., & Gabriel,M.T. Functional tissue engineering for ligament healing: potential of antisense gene therapy. *Ann. Biomed. Eng* **32**, 342-351 (2004).

201.   Altman,G.H. *et al.* Silk-based biomaterials. *Biomaterials* **24**, 401-416 (2003).

202.   Ge,Z., Yang,F., Goh,J.C., Ramakrishna,S., & Lee,E.H. Biomaterials and scaffolds for ligament tissue engineering. *J Biomed. Mater. Res. A* **77**, 639-652 (2006).

203.   Altman,G.H. *et al.* Silk-based biomaterials. *Biomaterials* **24**, 401-416 (2003).

204.   Altman,G.H. *et al.* Silk matrix for tissue engineered anterior cruciate ligaments. *Biomaterials* **23**, 4131-4141 (2002).

175

205.   Ge,Z., Goh,J.C., & Lee,E.H. Selection of cell source for ligament tissue engineering. *Cell Transplant.* **14**, 573-583 (2005).

206.   Petrigliano,F.A., McAllister,D.R., & Wu,B.M. Tissue engineering for anterior cruciate ligament reconstruction: a review of current strategies. *Arthroscopy* **22**, 441-451 (2006).

207.   Moreau,J.E., Chen,J., Horan,R.L., Kaplan,D.L., & Altman,G.H. Sequential growth factor application in bone marrow stromal cell ligament engineering. *Tissue Eng* **11**, 1887-1897 (2005).

208.   Wang,Y., Kim,H.J., Vunjak-Novakovic,G., & Kaplan,D.L. Stem cell-based tissue engineering with silk biomaterials. *Biomaterials* **27**, 6064-6082 (2006).

209.   Moreau,J.E. *et al.* Growth factor induced fibroblast differentiation from human bone marrow stromal cells in vitro. *J Orthop. Res.* **23**, 164-174 (2005).

210.   Chen,J. *et al.* Human bone marrow stromal cell and ligament fibroblast responses on RGD-modified silk fibers. *J Biomed. Mater. Res. A* **67**, 559-570 (2003).

211.   Altman,G.H. *et al.* Advanced bioreactor with controlled application of multi-dimensional strain for tissue engineering. *J Biomech. Eng* **124**, 742-749 (2002).

212.   Altman,G.H. *et al.* Cell differentiation by mechanical stress. *FASEB J* **16**, 270-272 (2002).

213.   Vunjak-Novakovic,G., Meinel,L., Altman,G., & Kaplan,D. Bioreactor cultivation of osteochondral grafts. *Orthod. Craniofac. Res.* **8**, 209-218 (2005).

214.   Altman,G.H. *et al.* Advanced bioreactor with controlled application of multi-dimensional strain for tissue engineering. *J Biomech. Eng* **124**, 742-749 (2002).

215.   Martinek,V. *et al.* Enhancement of tendon-bone integration of anterior cruciate ligament grafts with bone morphogenetic protein-2 gene transfer: a histological and biomechanical study. *J Bone Joint Surg. Am.* **84-A**, 1123-1131 (2002).

216.   Martinek,V. *et al.* Enhancement of tendon-bone integration of anterior cruciate ligament grafts with bone morphogenetic protein-2 gene transfer: a histological and biomechanical study. *J Bone Joint Surg. Am.* **84-A**, 1123-1131 (2002).

217.   Spalazzi,J.P., Doty,S.B., Moffat,K.L., Levine,W.N., & Lu,H.H. Development of controlled matrix heterogeneity on a triphasic scaffold for orthopedic interface tissue engineering. *Tissue Eng* **12**, 3497-3508 (2006).

218.   Mikos,A.G. *et al.* Engineering complex tissues. *Tissue Eng* **12**, 3307-3339 (2006).

219.   Sharma,B. *et al.* Designing zonal organization into tissue-engineered cartilage. *Tissue Eng* **13**, 405-414 (2007).

220.   Weinberg,W.C. *et al.* Reconstitution of Hair Follicle Development Invivo - Determination of Follicle Formation, Hair-Growth, and Hair Quality by Dermal Cells. *Journal of Investigative Dermatology* **100**, 229-236 (1993).

221.   Banerjee,C. *et al.* Differential regulation of the two principal Runx2/Cbfa1 N-terminal isoforms in response to bone morphogenetic protein-2 during development of the osteoblast phenotype. *Endocrinology* **142**, 4026-4039 (2001).

222.   Harada,H. *et al.* Cbfa1 isoforms exert functional differences in osteoblast differentiation. *J. Biol. Chem.* **274**, 6972-6978 (1999).

223.   Ducy,P., Boyce,B.F., Story,B., Dunstan,C., & Karsenty,G. Increased bone formation in osteocalcin-deficient mice without bone resorption defect. *Journal of Bone and Mineral Research* **11**, 43 (1996).

224.   Seibel,M.J. Molecular markers of bone turnover: biochemical, technical and analytical aspects. *Osteoporos. Int.* **11 Suppl 6**, S18-S29 (2000).

225.   Bonewald,L.F. *et al.* von Kossa staining alone is not sufficient to confirm that mineralization in vitro represents bone formation. *Calcif. Tissue Int.* **72**, 537-547 (2003).

226.   Boskey,A.L. *et al.* The mechanism of beta-glycerophosphate action in mineralizing chick limb-bud mesenchymal cell cultures. *Journal of Bone and Mineral Research* **11**, 1694-1702 (1996).

227.   Sauer,G.R. & Wuthier,R.E. Fourier transform infrared characterization of mineral phases formed during induction of mineralization by collagenase-released matrix vesicles in vitro. *J. Biol. Chem.* **263**, 13718-13724 (1988).

228.   Brann,D.W., Hendry,L.B., & Mahesh,V.B. Emerging Diversities in the Mechanism of Action of Steroid-Hormones. *Journal of Steroid Biochemistry and Molecular Biology* **52**, 113-133 (1995).

229.   Ishida,Y. & Heersche,J.N.M. Glucocorticoid-induced osteoporosis: Both in vivo and in vitro concentrations of glucocorticoids higher than physiological levels attenuate osteoblast differentiation. *Journal of Bone and Mineral Research* **13**, 1822-1826 (1998).

177

230.   Canalis,E. & Delany,A.M. Mechanisms of glucocorticoid action in bone. *Neuroendocrine Immune Basis of the Rheumatic Diseases Ii, Proceedings* **966**, 73-81 (2002).

231.   Shalhoub,V. *et al.* Effects of Glucocorticoids on Cell-Growth and Differentiation Gene-Expression in Mc3T3.E1 Cells - Inhibition of Cell-Growth and Mineralization by Dexamethasone. *Journal of Bone and Mineral Research* **10**, S291 (1995).

232.   Walsh,S., Jordan,G.R., Jefferiss,C., Stewart,K., & Beresford,J.N. High concentrations of dexamethasone suppress the proliferation but not the differentiation or further maturation of human osteoblast precursors in vitro: relevance to glucocorticoid-induced osteoporosis. *Rheumatology* **40**, 74-83 (2001).

233.   Delany,A.M., Gabbitas,B.Y., & Canalis,E. Cortisol Down-Regulates Osteoblast Alpha-1(I) Procollagen Messenger-Rna by Transcriptional and Posttranscriptional Mechanisms. *Journal of Cellular Biochemistry* **57**, 488-494 (1995).

234.   Weinstein,R.S., Jilka,R.L., Parfitt,A.M., & Manolagas,S.C. Inhibition of osteoblastogenesis and promotion of apoptosis of osteoblasts and osteocytes by glucocorticoids - Potential mechanisms of their deleterious effects on bone. *Journal of Clinical Investigation* **102**, 274-282 (1998).

235.   Chevalley,T., Strong,D.D., Mohan,S., Baylink,D.J., & Linkhart,T.A. Evidence for a role for insulin-like growth factor binding proteins in glucocorticoid inhibition of normal human osteoblast-like cell proliferation. *European Journal of Endocrinology* **134**, 591-601 (1996).

236.   Luppen,C.A., Smith,E., Spevak,L., Boskey,A.L., & Frenkel,B. Bone morphogenetic protein-2 restores mineralization in glucocorticoid-inhibited MC3T3-E1 osteoblast cultures. *Journal of Bone and Mineral Research* **18**, 1186-1197 (2003).

237.   Chang,D.J. *et al.* Reduction in transforming growth factor beta receptor I expression and transcription factor CBFa1 on bone cells by glucocorticoid. *Journal of Biological Chemistry* **273**, 4892-4896 (1998).

238.   Bellows,C.G., Aubin,J.E., & Heersche,J.N.M. Physiological Concentrations of Glucocorticoids Stimulate Formation of Bone Nodules from Isolated Rat Calvaria Cells-Invitro. *Endocrinology* **121**, 1985-1992 (1987).

239.   Cheng,S.L., Yang,J.W., Rifas,L., Zhang,S.F., & Avioli,L.V. Differentiation of Human Bone-Marrow Osteogenic Stromal Cells in Vitro - Induction of the Osteoblast Phenotype by Dexamethasone. *Endocrinology* **134**, 277-286 (1994).

178

240.   Sher,L.B. *et al.* Transgenic expression of 11 beta-hydroxysteroid dehydrogenase type 2 in osteoblasts reveals an anabolic role for endogenous glucocorticoids in bone. *Endocrinology* **145**, 922-929 (2004).

241.   Chen,T.L., Cone,C.M., & Feldman,D. Glucocorticoid Modulation of Cell-Proliferation in Cultured Osteoblast-Like Bone-Cells - Differences Between Rat and Mouse. *Endocrinology* **112**, 1739-1745 (1983).

242.   Rickard,D.J., Sullivan,T.A., Shenker,B.J., Leboy,P.S., & Kazhdan,I. Induction of Rapid Osteoblast Differentiation in Rat Bone-Marrow Stromal Cell-Cultures by Dexamethasone and Bmp-2. *Developmental Biology* **161**, 218-228 (1994).

243.   Prince,M. *et al.* Expression and regulation of Runx2/Cbfa1 and osteoblast phenotypic markers during the growth and differentiation of human osteoblasts. *J. Cell Biochem.* **80**, 424-440 (2001).

244.   Viereck,V. *et al.* Differential regulation of Cbfa1/Runx2 and osteocalcin gene expression by vitamin-D3, dexamethasone, and local growth factors in primary human osteoblasts. *Journal of Cellular Biochemistry* **86**, 348-356 (2002).

245.   Pei,W., Yoshimine,Y., & Heersche,J.N.M. Identification of dexamethasone-dependent osteoprogenitors in cell populations derived from adult human female bone. *Calcified Tissue International* **72**, 124-134 (2003).

246.   Shui,C.X., Spelsberg,T.C., Riggs,B.L., & Khosla,S. Changes in Runx2/Cbfa1 expression and activity during osteoblastic differentiation of human bone marrow stromal cells. *Journal of Bone and Mineral Research* **18**, 213-221 (2003).

247.   Komori,T. *et al.* Targeted disruption of Cbfa1 results in a complete lack of bone formation owing to maturational arrest of osteoblasts. *Cell* **89**, 755-764 (1997).

248.   Yang,S. *et al.* In vitro and in vivo synergistic interactions between the Runx2/Cbfa1 transcription factor and bone morphogenetic protein-2 in stimulating osteoblast differentiation. *J. Bone Miner. Res.* **18**, 705-715 (2003).

249.   Sudhakar,S., Li,Y., Katz,M.S., & Elango,N. Translational regulation is a control point in RUNX2/Cbfa1 gene expression. *Biochem. Biophys. Res. Commun.* **289**, 616-622 (2001).

250.   Lian,J.B. & Stein,G.S. The temporal and spatial subnuclear organization of skeletal gene regulatory machinery: Integrating multiple levels of transcriptional control. *Calcified Tissue International* **72**, 631-637 (2003).

251.   Xiao,G. *et al.* MAPK pathways activate and phosphorylate the osteoblast-specific transcription factor, Cbfa1. *J Biol. Chem.* **275**, 4453-4459 (2000).

179

252.   Xiao,G.Z., Wang,D., Benson,M.D., Karsenty,G., & Franceschi,R.T. Role of the alpha(2)-integrin in osteoblast-specific gene expression and activation of the Osf2 transcription factor. *Journal of Biological Chemistry* **273**, 32988-32994 (1998).

253.   Xiao,G., Jiang,D., Gopalakrishnan,R., & Franceschi,R.T. Fibroblast growth factor 2 induction of the osteocalcin gene requires MAPK activity and phosphorylation of the osteoblast transcription factor, Cbfa1/Runx2. *J. Biol. Chem.* **277**, 36181-36187 (2002).

254.   Wang,F.S. *et al.* Superoxide mediates shock wave induction of ERK-dependent osteogenic transcription factor (CBFA1) and mesenchymal cell differentiation toward osteoprogenitors. *Journal of Biological Chemistry* **277**, 10931-10937 (2002).

255.   Wee,H.J., Haung,G., Shigesada,K., & Ito,Y. Serine phosphorylation of RUNX2 with novel potential functions as negative regulatory mechanisms. *Embo Reports* **3**, 967-974 (2002).

256.   Quack,I. *et al.* Mutation analysis of cove binding factor A1 in patients with cleidocranial dysplasia. *American Journal of Human Genetics* **65**, 1268-1278 (1999).

257.   Whalen,S.G. *et al.* Phosphorylation within the transactivation domain of adenovirus E1A protein by mitogen-activated protein kinase regulates expression of early region 4. *Journal of Virology* **71**, 3545-3553 (1997).

258.   Sun,H., Charles,C.H., Lau,L.F., & Tonks,N.K. Mkp-1 (3Ch134), An Immediate-Early Gene-Product, Is A Dual-Specificity Phosphatase That Dephosphorylates Map Kinase In-Vivo. *Cell* **75**, 487-493 (1993).

259.   Liu,Y.S., Gorospe,M., Yang,C.L., & Holbrook,N.J. Role of Mitogen-Activated Protein-Kinase Phosphatase During the Cellular-Response to Genotoxic Stress - Inhibition of C-Jun N-Terminal Kinase-Activity and Ap-1-Dependent Gene Activation. *Journal of Biological Chemistry* **270**, 8377-8380 (1995).

260.   Imasato,A. *et al.* Inhibition of p38 MAPK by glucocorticoids via induction of MAPK phosphatase-1 enhances nontypeable Haemophilus influenzae-induced expression of toll-like receptor 2. *Journal of Biological Chemistry* **277**, 47444-47450 (2002).

261.   Lasa,M., Abraham,S.M., Boucheron,C., Saklatvala,J., & Clark,A.R. Dexamethasone causes sustained expression of mitogen-activated protein kinase (MAPK) phosphatase 1 and phosphatase-mediated inhibition of MAPK p38. *Molecular and Cellular Biology* **22**, 7802-7811 (2002).

262.   Kassel,O. *et al.* Glucocorticoids inhibit MAP kinase via increased expression and decreased degradation of MKP-1. *Embo Journal* **20**, 7108-7116 (2001).

263.   Engelbrecht,Y. *et al.* Glucocorticoids induce rapid up-regulation of mitogen-activated protein kinase phosphatase-1 and dephosphorylation of extracellular signal-regulated kinase and impair proliferation in human and mouse osteoblast cell lines. *Endocrinology* **144**, 412-422 (2003).

264.   Wu,W., Pew,T., Zou,M., Pang,D., & Conzen,S.D. Glucocorticoid receptor-induced MAPK phosphatase-1 (MPK-1) expression inhibits paclitaxel-associated MAPK activation and contributes to breast cancer cell survival. *Journal of Biological Chemistry* **280**, 4117-4124 (2005).

265.   Vogt,A. *et al.* The benzo[c] phenanthridine alkaloid, sanguinarine, is a selective, cell-active inhibitor of mitogen-activated protein kinase phosphatase-1. *Journal of Biological Chemistry* **280**, 19078-19086 (2005).

266.   Tenenbaum,H.C. & Heersche,J.N.M. Dexamethasone Stimulates Osteogenesis in Chick Periosteum Invitro. *Endocrinology* **117**, 2211-2217 (1985).

267.   Selvamurugan,N., Chou,W.Y., Pearman,A.T., Pulumati,M.R., & Partridge,N.C. Parathyroid hormone regulates the rat collagenase-3 promoter in osteoblastic cells through the cooperative interaction of the activator protein-1 site and the runt domain binding sequence. *Journal of Biological Chemistry* **273**, 10647-10657 (1998).

268.   Selvamurugan,N., Pulumati,M.R., Tyson,D.R., & Partridge,N.C. Parathyroid hormone regulation of the rat collagenase-3 promoter by protein kinase A-dependent transactivation of core binding factor alpha 1. *Journal of Biological Chemistry* **275**, 5037-5042 (2000).

269.   Zhang,Y., Biggs,J.R., & Kraft,A.S. Phorbol ester treatment of K562 cells regulates the transcriptional activity of AML1c through phosphorylation. *J Biol. Chem.* **279**, 53116-53125 (2004).

270.   Ducy,P. Cbfa1: A molecular switch in osteoblast biology. *Developmental Dynamics* **219**, 461-471 (2000).

271.   Thirunavukkarasu,K., Mahajan,M., McLarren,K.W., Stifani,S., & Karsenty,G. Two domains unique to osteoblast-specific transcription factor Osf2/Cbfa1 contribute to its transactivation function and its inability to heterodimerize with Cbf beta. *Molecular and Cellular Biology* **18**, 4197-4208 (1998).

272.   Ito,Y. Molecular basis of tissue-specific gene expression mediated by the Runt domain transcription factor PEBP2/CBF. *Genes to Cells* **4**, 685-696 (1999).

273. Kahler,R.A. & Westendorf,J.J. Lymphoid enhancer factor-1 and beta-catenin inhibit Runx2-dependent transcriptional activation of the osteocalcin promoter. *J. Biol. Chem.* **278**, 11937-11944 (2003).

274. Hess,J., Porte,D., Munz,C., & Angel,P. AP-1 and Cbfa/runt physically interact and regulate parathyroid hormone-dependent MMP13 expression in osteoblasts through a new osteoblast-specific element 2/AP-1 composite element. *Journal of Biological Chemistry* **276**, 20029-20038 (2001).

275. D'Alonzo,R.C., Selvamurugan,N., Karsenty,G., & Partridge,N.C. Physical interaction of the activator protein-1 factors c-Fos and c-Jun with Cbfa1 for collagenase-3 promoter activation. *J. Biol. Chem.* **277**, 816-822 (2002).

276. Hanai,J. *et al.* Interaction and functional cooperation of PEBP2/CBF with Smads - Synergistic induction of the immunoglobulin germline C alpha promoter. *Journal of Biological Chemistry* **274**, 31577-31582 (1999).

277. Zhang,Y.W. *et al.* A RUNX2/PEBP2 alpha A/CBFA1 mutation displaying impaired transactivation and Smad interaction in cleidocranial dysplasia. *Proceedings of the National Academy of Sciences of the United States of America* **97**, 10549-10554 (2000).

278. Gutierrez,S. *et al.* CCAAT/enhancer-binding proteins (C/EBP) beta and delta activate osteocalcin gene transcription and synergize with Runx2 at the C/EBP element to regulate bone-specific expression. *Journal of Biological Chemistry* **277**, 1316-1323 (2002).

279. McLarren,K.W. *et al.* The mammalian basic helix loop helix protein HES-1 binds to and modulates the transactivating function of the runt-related factor Cbfa1. *J. Biol. Chem.* **275**, 530-538 (2000).

280. Bruder,S.P. & Fox,B.S. Tissue engineering of bone. Cell based strategies. *Clin. Orthop. Relat Res.*S68-S83 (1999).

281. Salgado,A.J., Coutinho,O.P., & Reis,R.L. Bone tissue engineering: state of the art and future trends. *Macromol. Biosci.* **4**, 743-765 (2004).

282. Salgado,A.J., Coutinho,O.P., & Reis,R.L. Novel starch-based scaffolds for bone tissue engineering: cytotoxicity, cell culture, and protein expression. *Tissue Eng* **10**, 465-474 (2004).

283. Mauney,J.R., Volloch,V., & Kaplan,D.L. Role of adult mesenchymal stem cells in bone tissue engineering applications: current status and future prospects. *Tissue Eng* **11**, 787-802 (2005).

284. Bruder,S.P. & Fox,B.S. Tissue engineering of bone. Cell based strategies. *Clin. Orthop. Relat Res.*S68-S83 (1999).

182

285.   Wozney,J.M. & Seeherman,H.J. Protein-based tissue engineering in bone and cartilage repair. *Curr. Opin. Biotechnol.* **15**, 392-398 (2004).

286.   Zheng,H., Guo,Z., Ma,Q., Jia,H., & Dang,G. Cbfa1/osf2 transduced bone marrow stromal cells facilitate bone formation in vitro and in vivo. *Calcif. Tissue Int.* **74**, 194-203 (2004).

287.   Zhao,Z., Zhao,M., Xiao,G., & Franceschi,R.T. Gene transfer of the Runx2 transcription factor enhances osteogenic activity of bone marrow stromal cells in vitro and in vivo. *Mol. Ther.* **12**, 247-253 (2005).

288.   Hildebrand,T., Laib,A., Muller,R., Dequeker,J., & Ruegsegger,P. Direct three-dimensional morphometric analysis of human cancellous bone: microstructural data from spine, femur, iliac crest, and calcaneus. *J. Bone Miner. Res.* **14**, 1167-1174 (1999).

289.   Bonewald,L.F. *et al.* Comparison of mineralized matrix of fetal rat calvarial cells and MC-3T3-E1 osteoblast-like cells by Fourier transform infrared spectroscopy (FT-IR). *Journal of Bone and Mineral Research* **11**, S333 (1996).

290.   Glowacki,J., Mizuno,S., & Greenberger,J.S. Perfusion enhances functions of bone marrow stromal cells in three-dimensional culture. *Cell Transplant.* **7**, 319-326 (1998).

291.   Mueller,S.M., Mizuno,S., Gerstenfeld,L.C., & Glowacki,J. Medium perfusion enhances osteogenesis by murine osteosarcoma cells in three-dimensional collagen sponges. *J. Bone Miner. Res.* **14**, 2118-2126 (1999).

292.   Mauney,J.R., Volloch,V., & Kaplan,D.L. Role of adult mesenchymal stem cells in bone tissue engineering applications: current status and future prospects. *Tissue Eng* **11**, 787-802 (2005).

293.   Termaat,M.F., Den Boer,F.C., Bakker,F.C., Patka,P., & Haarman,H.J. Bone morphogenetic proteins. Development and clinical efficacy in the treatment of fractures and bone defects. *J. Bone Joint Surg. Am.* **87**, 1367-1378 (2005).

294.   Wozney,J.M. & Seeherman,H.J. Protein-based tissue engineering in bone and cartilage repair. *Curr. Opin. Biotechnol.* **15**, 392-398 (2004).

295.   Hee,C.K., Jonikas,M.A., & Nicoll,S.B. Influence of three-dimensional scaffold on the expression of osteogenic differentiation markers by human dermal fibroblasts. *Biomaterials* **27**, 875-884 (2006).

296.   Chung,C.H., Golub,E.E., Forbes,E., Tokuoka,T., & Shapiro,I.M. Mechanism of action of beta-glycerophosphate on bone cell mineralization. *Calcif. Tissue Int.* **51**, 305-311 (1992).

297.   Boyan,B.D., Schwartz,Z., & Boskey,A.L. The importance of mineral in bone and mineral research. *Bone* **27**, 341-342 (2000).

298.   Cartmell,S.H., Porter,B.D., Garcia,A.J., & Guldberg,R.E. Effects of medium perfusion rate on cell-seeded three-dimensional bone constructs in vitro. *Tissue Eng* **9**, 1197-1203 (2003).

299.   Porter,A. *et al.* Effect of carbonate substitution on the ultrastructural characteristics of hydroxyapatite implants. *J. Mater. Sci. Mater. Med.* **16**, 899-907 (2005).

300.   Patel,N. *et al.* A comparative study on the in vivo behavior of hydroxyapatite and silicon substituted hydroxyapatite granules. *J. Mater. Sci. Mater. Med.* **13**, 1199-1206 (2002).

301.   Schepers,E., de Clercq,M., Ducheyne,P., & Khan,S.N. Bioactive glass particulate material as a filler for bone lesions. J.Oral Rehabil. 18, 439. 1991. Ref Type: Generic

302.   Klein,C.P.A.T., Dreissen,A.A., de Groot,K., & van den Hooff,A. Biodegradation behavior of various calcium phosphate materials in bone tissue. J.Biomed.Mater.Res.17,769-784.(1983).

303.   Lane,J.M., Tomin,E., & Bostrom,M.P. Biosynthetic bone grafting. *Clin. Orthop. Relat Res.*S107-S117 (1999).

304.   Franceschi,R.T., Wang,D., Krebsbach,P.H., & Rutherford,R.B. Gene therapy for bone formation: in vitro and in vivo osteogenic activity of an adenovirus expressing BMP7. *J. Cell Biochem.* **78**, 476-486 (2000).

305.   Phillips,J.E., Gersbach,C.A., Wojtowicz,A.M., & Garcia,A.J. Glucocorticoid-induced osteogenesis is negatively regulated by Runx2/Cbfa1 serine phosphorylation. *J. Cell Sci.* **119**, 581-591 (2006).

306.   Liu,X. & Ma,P.X. Polymeric scaffolds for bone tissue engineering. *Ann. Biomed. Eng* **32**, 477-486 (2004).

307.   Hutmacher,D.W. Scaffolds in tissue engineering bone and cartilage. *Biomaterials* **21**, 2529-2543 (2000).

308.   Liu,X. & Ma,P.X. Polymeric scaffolds for bone tissue engineering. *Ann. Biomed. Eng* **32**, 477-486 (2004).

309.   Hutmacher,D.W. *et al.* Mechanical properties and cell cultural response of polycaprolactone scaffolds designed and fabricated via fused deposition modeling. *J. Biomed. Mater. Res.* **55**, 203-216 (2001).

310. Zein,I., Hutmacher,D.W., Tan,K.C., & Teoh,S.H. Fused deposition modeling of novel scaffold architectures for tissue engineering applications. *Biomaterials* **23**, 1169-1185 (2002).

311. Boyan,B.D., Hummert,T.W., Dean,D.D., & Schwartz,Z. Role of material surfaces in regulating bone and cartilage cell response. *Biomaterials* **17**, 137-146 (1996).

312. Byers,B.A., Guldberg,R.E., Hutmacher,D.W., & Garcia,A.J. Effects of Runx2 genetic engineering and in vitro maturation of tissue-engineered constructs on the repair of critical size bone defects. *J. Biomed. Mater. Res. A*(2005).

313. Hutmacher,D.W. Scaffold design and fabrication technologies for engineering tissues--state of the art and future perspectives. *J. Biomater. Sci. Polym. Ed* **12**, 107-124 (2001).

314. Sachlos,E. & Czernuszka,J.T. Making tissue engineering scaffolds work. Review: the application of solid freeform fabrication technology to the production of tissue engineering scaffolds. *Eur. Cell Mater.* **5**, 29-39 (2003).

315. Liu,X. & Ma,P.X. Polymeric scaffolds for bone tissue engineering. *Ann. Biomed. Eng* **32**, 477-486 (2004).

316. Chevallay,B. & Herbage,D. Collagen-based biomaterials as 3D scaffold for cell cultures: applications for tissue engineering and gene therapy. *Med. Biol. Eng Comput.* **38**, 211-218 (2000).

317. Peter,S.J., Miller,M.J., Yasko,A.W., Yaszemski,M.J., & Mikos,A.G. Polymer concepts in tissue engineering. *J. Biomed. Mater. Res.* **43**, 422-427 (1998).

318. Hollister,S.J. Porous scaffold design for tissue engineering. *Nat. Mater.* **4**, 518-524 (2005).

319. Lin,C.Y. *et al.* Functional bone engineering using ex vivo gene therapy and topology-optimized, biodegradable polymer composite scaffolds. *Tissue Eng* **11**, 1589-1598 (2005).

320. Hollister,S.J. Porous scaffold design for tissue engineering. *Nat. Mater.* **4**, 518-524 (2005).

321. McClary,K.B., Ugarova,T., & Grainger,D.W. Modulating fibroblast adhesion, spreading, and proliferation using self-assembled monolayer films of alkylthiolates on gold. *J. Biomed. Mater. Res.* **50**, 428-439 (2000).

322. Scotchford,C.A., Gilmore,C.P., Cooper,E., Leggett,G.J., & Downes,S. Protein adsorption and human osteoblast-like cell attachment and growth on alkylthiol on gold self-assembled monolayers. *J. Biomed. Mater. Res.* **59**, 84-99 (2002).

323. Mrksich,M. & Whitesides,G.M. Using self-assembled monolayers to understand the interactions of man-made surfaces with proteins and cells. *Annu. Rev. Biophys. Biomol. Struct.* **25**, 55-78 (1996).

324. Tengvall,P., Lundstrom,I., & Liedberg,B. Protein adsorption studies on model organic surfaces: an ellipsometric and infrared spectroscopic approach. *Biomaterials* **19**, 407-422 (1998).

325. Brash,J.L. Exploiting the current paradigm of blood-material interactions for the rational design of blood-compatible materials. *J. Biomater. Sci. Polym. Ed* **11**, 1135-1146 (2000).

326. Lan,M.A., Gersbach,C.A., Michael,K.E., Keselowsky,B.G., & Garcia,A.J. Myoblast proliferation and differentiation on fibronectin-coated self assembled monolayers presenting different surface chemistries. *Biomaterials* **26**, 4523-4531 (2005).

327. Keselowsky,B.G., Collard,D.M., & Garcia,A.J. Surface chemistry modulates focal adhesion composition and signaling through changes in integrin binding. *Biomaterials* **25**, 5947-5954 (2004).

328. Garcia,A.J., Vega,M.D., & Boettiger,D. Modulation of cell proliferation and differentiation through substrate-dependent changes in fibronectin conformation. *Mol. Biol. Cell* **10**, 785-798 (1999).

329. Tziampazis,E., Kohn,J., & Moghe,P.V. PEG-variant biomaterials as selectively adhesive protein templates: model surfaces for controlled cell adhesion and migration. *Biomaterials* **21**, 511-520 (2000).

330. Gorbet,M.B. & Sefton,M.V. Leukocyte activation and leukocyte procoagulant activities after blood contact with polystyrene and polyethylene glycol-immobilized polystyrene beads. *J. Lab Clin. Med.* **137**, 345-355 (2001).

331. Keselowsky,B.G., Collard,D.M., & Garcia,A.J. Integrin binding specificity regulates biomaterial surface chemistry effects on cell differentiation. *Proc. Natl. Acad. Sci. U. S. A* **102**, 5953-5957 (2005).

332. Keselowsky,B.G., Collard,D.M., & Garcia,A.J. Surface chemistry modulates fibronectin conformation and directs integrin binding and specificity to control cell adhesion. *J. Biomed. Mater. Res. A* **66**, 247-259 (2003).

333. Gauthier,O. *et al.* Macroporous biphasic calcium phosphate ceramics versus injectable bone substitute: a comparative study 3 and 8 weeks after implantation in rabbit bone. *J. Mater. Sci. Mater. Med.* **12**, 385-390 (2001).

334. Chang,B.S. *et al.* Osteoconduction at porous hydroxyapatite with various pore configurations. *Biomaterials* **21**, 1291-1298 (2000).

335.   Nishikawa,M. *et al.* Bone tissue engineering using novel interconnected porous hydroxyapatite ceramics combined with marrow mesenchymal cells: quantitative and three-dimensional image analysis. *Cell Transplant.* **13**, 367-376 (2004).

336.   Kruyt,M.C. *et al.* Optimization of bone-tissue engineering in goats. *J. Biomed. Mater. Res. B Appl. Biomater.* **69**, 113-120 (2004).

337.   Wu,Y.C., Shaw,S.Y., Lin,H.R., Lee,T.M., & Yang,C.Y. Bone tissue engineering evaluation based on rat calvaria stromal cells cultured on modified PLGA scaffolds. *Biomaterials* **27**, 896-904 (2006).

338.   Ishaug,S.L. *et al.* Bone formation by three-dimensional stromal osteoblast culture in biodegradable polymer scaffolds. *J. Biomed. Mater. Res.* **36**, 17-28 (1997).

339.   Mendes,S.C. *et al.* Evaluation of two biodegradable polymeric systems as substrates for bone tissue engineering. *Tissue Eng* **9 Suppl 1**, S91-101 (2003).

340.   Claase,M.B., Grijpma,D.W., Mendes,S.C., de Bruijn,J.D., & Feijen,J. Porous PEOT/PBT scaffolds for bone tissue engineering: preparation, characterization, and in vitro bone marrow cell culturing. *J. Biomed. Mater. Res. A* **64**, 291-300 (2003).

341.   Martin,J.Y. *et al.* Proliferation, differentiation, and protein synthesis of human osteoblast-like cells (MG63) cultured on previously used titanium surfaces. *Clin. Oral Implants. Res.* **7**, 27-37 (1996).

342.   Martin,J.Y. *et al.* Effect of titanium surface roughness on proliferation, differentiation, and protein synthesis of human osteoblast-like cells (MG63). *J. Biomed. Mater. Res.* **29**, 389-401 (1995).

343.   Lynch,M.P., Stein,J.L., Stein,G.S., & Lian,J.B. The influence of type I collagen on the development and maintenance of the osteoblast phenotype in primary and passaged rat calvarial osteoblasts: modification of expression of genes supporting cell growth, adhesion, and extracellular matrix mineralization. *Exp. Cell Res.* **216**, 35-45 (1995).

344.   Reyes,C.D. & Garcia,A.J. Alpha2beta1 integrin-specific collagen-mimetic surfaces supporting osteoblastic differentiation. *J. Biomed. Mater. Res. A* **69**, 591-600 (2004).

345.   Calvert,J.W. *et al.* Characterization of osteoblast-like behavior of cultured bone marrow stromal cells on various polymer surfaces. *J. Biomed. Mater. Res.* **52**, 279-284 (2000).

346.   Benjamin,M. *et al.* The skeletal attachment of tendons--tendon "entheses". *Comp Biochem. Physiol A Mol. Integr. Physiol* **133**, 931-945 (2002).

347. Thomopoulos,S., Williams,G.R., Gimbel,J.A., Favata,M., & Soslowsky,L.J. Variation of biomechanical, structural, and compositional properties along the tendon to bone insertion site. *J. Orthop. Res.* **21**, 413-419 (2003).

348. Wang,I.N., Mitroo,S., Chen,F.H., Lu,H.H., & Doty,S.B. Age-dependent changes in matrix composition and organization at the ligament-to-bone insertion. *J. Orthop. Res.* **24**, 1745-1755 (2006).

349. Mikos,A.G. *et al.* Engineering complex tissues. *Tissue Eng* **12**, 3307-3339 (2006).

350. Doschak,M.R. & Zernicke,R.F. Structure, function and adaptation of bone-tendon and bone-ligament complexes. *J. Musculoskelet. Neuronal. Interact.* **5**, 35-40 (2005).

351. Woo,S.L., Orlando,C.A., Gomez,M.A., Frank,C.B., & Akeson,W.H. Tensile properties of the medial collateral ligament as a function of age. *J. Orthop. Res.* **4**, 133-141 (1986).

352. Kurosaka,M., Yoshiya,S., & Andrish,J.T. A biomechanical comparison of different surgical techniques of graft fixation in anterior cruciate ligament reconstruction. *Am. J. Sports Med.* **15**, 225-229 (1987).

353. Friedman,M.J. *et al.* Autogeneic anterior cruciate ligament (ACL) anterior reconstruction of the knee. A review. *Clin. Orthop. Relat Res.*9-14 (1985).

354. Gersbach,C.A., Phillips,J.E., & Garcia,A.J. Genetic Engineering for Skeletal Regenerative Medicine. *Annu. Rev. Biomed. Eng* **9**, 87-119 (2007).

355. Lander,A.D. Morpheus unbound: reimagining the morphogen gradient. *Cell* **128**, 245-256 (2007).

356. Nusslein-Volhard,C. Gradients that organize embryo development. *Sci. Am.* **275**, 54-55 (1996).

357. Lander,A.D., Nie,Q., & Wan,F.Y. Do morphogen gradients arise by diffusion? *Dev. Cell* **2**, 785-796 (2002).

358. Affolter,M. & Basler,K. The Decapentaplegic morphogen gradient: from pattern formation to growth regulation. *Nat. Rev. Genet.* **8**, 663-674 (2007).

359. Kerszberg,M. & Wolpert,L. Specifying positional information in the embryo: looking beyond morphogens. *Cell* **130**, 205-209 (2007).

360. Zhu,A.J. & Scott,M.P. Incredible journey: how do developmental signals travel through tissue? *Genes Dev.* **18**, 2985-2997 (2004).

361.   Driever,W. & Nusslein-Volhard,C. The bicoid protein is a positive regulator of hunchback transcription in the early Drosophila embryo. *Nature* **337**, 138-143 (1989).

362.   Driever,W. & Nusslein-Volhard,C. The bicoid protein determines position in the Drosophila embryo in a concentration-dependent manner. *Cell* **54**, 95-104 (1988).

363.   Driever,W. & Nusslein-Volhard,C. A gradient of bicoid protein in Drosophila embryos. *Cell* **54**, 83-93 (1988).

364.   DeLong,S.A., Gobin,A.S., & West,J.L. Covalent immobilization of RGDS on hydrogel surfaces to direct cell alignment and migration. *J. Control Release* **109**, 139-148 (2005).

365.   DeLong,S.A., Moon,J.J., & West,J.L. Covalently immobilized gradients of bFGF on hydrogel scaffolds for directed cell migration. *Biomaterials* **26**, 3227-3234 (2005).

366.   Kang,C.E., Gemeinhart,E.J., & Gemeinhart,R.A. Cellular alignment by grafted adhesion peptide surface density gradients. *J. Biomed. Mater. Res. A* **71**, 403-411 (2004).

367.   Chen,R.R., Silva,E.A., Yuen,W.W., & Mooney,D.J. Spatio-temporal VEGF and PDGF delivery patterns blood vessel formation and maturation. *Pharm. Res.* **24**, 258-264 (2007).

368.   Luo,Y. & Shoichet,M.S. A photolabile hydrogel for guided three-dimensional cell growth and migration. *Nat. Mater.* **3**, 249-253 (2004).

369.   Chen,R.R. & Mooney,D.J. Polymeric growth factor delivery strategies for tissue engineering. *Pharm. Res.* **20**, 1103-1112 (2003).

370.   Langer,R. Drug delivery and targeting. *Nature* **392**, 5-10 (1998).

371.   Wang,I.N. *et al.* Role of osteoblast-fibroblast interactions in the formation of the ligament-to-bone interface. *J. Orthop. Res.*(2007).

372.   Sharma,B. & Elisseeff,J.H. Engineering structurally organized cartilage and bone tissues. *Ann. Biomed. Eng* **32**, 148-159 (2004).

373.   Sharma,B. *et al.* Designing zonal organization into tissue-engineered cartilage. *Tissue Eng* **13**, 405-414 (2007).

374.   Davis,H.E., Rosinski,M., Morgan,J.R., & Yarmush,M.L. Charged polymers modulate retrovirus transduction via membrane charge neutralization and virus aggregation. *Biophys. J.* **86**, 1234-1242 (2004).

189

375.	Le Doux,J.M., Landazuri,N., Yarmush,M.L., & Morgan,J.R. Complexation of retrovirus with cationic and anionic polymers increases the efficiency of gene transfer. *Hum. Gene Ther.* **12**, 1611-1621 (2001).

376.	Irvine,K.D. & Rauskolb,C. Boundaries in development: formation and function. *Annu. Rev. Cell Dev. Biol.* **17**, 189-214 (2001).

377.	DeLong,S.A., Gobin,A.S., & West,J.L. Covalent immobilization of RGDS on hydrogel surfaces to direct cell alignment and migration. *J. Control Release* **109**, 139-148 (2005).

378.	De Laporte,L. & Shea,L.D. Matrices and scaffolds for DNA delivery in tissue engineering. *Adv. Drug Deliv. Rev.* **59**, 292-307 (2007).

379.	Pannier,A.K. & Shea,L.D. Controlled release systems for DNA delivery. *Mol. Ther.* **10**, 19-26 (2004).

380.	Storrie,H. & Mooney,D.J. Sustained delivery of plasmid DNA from polymeric scaffolds for tissue engineering. *Adv. Drug Deliv. Rev.* **58**, 500-514 (2006).

381.	Park,T.G., Jeong,J.H., & Kim,S.W. Current status of polymeric gene delivery systems. *Adv. Drug Deliv. Rev.* **58**, 467-486 (2006).

382.	Pannier,A.K., Anderson,B.C., & Shea,L.D. Substrate-mediated delivery from self-assembled monolayers: effect of surface ionization, hydrophilicity, and patterning. *Acta Biomater.* **1**, 511-522 (2005).

383.	Gersbach,C.A., Coyer,S.R., Le Doux,J.M., & Garcia,A.J. Biomaterial-mediated retroviral gene transfer using self-assembled monolayers. *Biomaterials*(2007).

384.	Jang,J.H., Houchin,T.L., & Shea,L.D. Gene delivery from polymer scaffolds for tissue engineering. *Expert Rev. Med. Devices* **1**, 127-138 (2004).

385.	Bonadio,J., Smiley,E., Patil,P., & Goldstein,S. Localized, direct plasmid gene delivery in vivo: prolonged therapy results in reproducible tissue regeneration. *Nat. Med.* **5**, 753-759 (1999).

386.	Ito,H. *et al.* Remodeling of cortical bone allografts mediated by adherent rAAV-RANKL and VEGF gene therapy. *Nat. Med.* **11**, 291-297 (2005).

387.	Le Doux,J.M., Davis,H.E., Morgan,J.R., & Yarmush,M.L. Kinetics of retrovirus production and decay. *Biotechnol. Bioeng.* **63**, 654-662 (1999).

388.	Davis,H.E., Morgan,J.R., & Yarmush,M.L. Polybrene increases retrovirus gene transfer efficiency by enhancing receptor-independent virus adsorption on target cell membranes. *Biophys. Chem.* **97**, 159-172 (2002).

389.   Mikos,A.G. *et al.* Engineering complex tissues. *Tissue Eng* **12**, 3307-3339 (2006).

390.   Blum,J.S., Barry,M.A., Mikos,A.G., & Jansen,J.A. In vivo evaluation of gene therapy vectors in ex vivo-derived marrow stromal cells for bone regeneration in a rat critical-size calvarial defect model. *Hum. Gene Ther.* **14**, 1689-1701 (2003).